ABSTRACT

Title of Dissertation:

CHARACTERIZATION OF LEACHABLE DISSOLVED ORGANIC MATTER FROM BIOSOLIDS AND IMPLICATIONS FOR NUTRIENT RELEASES, MODELING, AND EMERGING CONTAMINANTS

Sarah Fischer, Doctor of Philosophy, 2019

Dissertation directed by: Professor Alba Torrents, Civil and Environmental Engineering Department

Treated wastewater residuals are utilized as a soil amendment to recycle nutrients to agricultural soils. Due to international application, biosolids are also a significant source of anthropogenic dissolved organic matter (DOM) to the environment.

The first research contribution characterized DOM and nitrogen mineralization rates of anaerobically digested (AnD) biosolids with variable pre-treatments, such as the thermal hydrolysis pretreatment coupled to anaerobic digestion (THP-AnD). There was not strong evidence that differently pretreated-AnD material had largely different aerobic inorganic nitrogen releases when incubated in a sandy loam soil. Variable pools of DOM decayed in soil treatments over time. Biosolids-DOM was then characterized from a greater representation of full-scale stabilization processes including limed stabilization (LT), aerobic digestion (AeD), and anaerobic digestion (AnD). These different final

stabilization processes produced substantially different leachates characterized by organic carbon content, size-exclusion chromatography, and fluorescence spectroscopy. Traditional optical metrics previously defined for aquatic DOM did not consistently capture fluorescence maxima of the anthropogenic material. Therefore, boundary-based excitation emission matrix (EEM) analyses were re-defined based on local fluorescence maxima. Novel parallel factor analysis (PARAFAC) and spectral database comparisons confirmed that biosolids-DOM contain both common high energy stimulated components and low energy stimulated components that are unique to digested leachates.

The third research contribution applied fluorescence suppression experiments to measure interactions of halogenated ECs with contrasting biosolids-DOM types. Despite digested biosolids-DOM containing different humic acid-like or fulvic acid-like signatures than limed leachates, antimicrobial triclocarban and industrial compound 2-4 dichlorophenol suppressed similar high energy fluorescent signatures in all biosolids-DOM. This suggests TCC and 2-4 DCP electronically interacts with smaller aromatic compounds, such as amino acids, and this interaction is not unique to DOM from different waste stabilizations. This study contributes to future bioavailability assays modeling complex effects of leachate quality on halogenated contaminants.

This thesis also confirmed the presence of dehalogenating microbes in the anaerobic microbial community structure of a THP-AD system. These results contribute to work assessing solids treatments, where halogenated emerging contaminants can be dehalogenated before land application. This dissertation advances understanding of biosolids DOM leachates, modeling EEM data, and fate of ECs during full-scale solids treatment processes.

Acknowledgements

Thank you to my adviser, committee, friends, and family for making this doctorate a reality. This experience has challenged me to rise to an incredible opportunity. Thank you to my Ph.D. adviser Alba Torrents for trusting me and supporting me through great experiences at DC Water, the USDA, and in teaching in the engineering department. I feel more confident for the next steps. Thank you to Birthe Kjellerup for welcoming me into a wonderful world of microbiology and for your inclusive mentorship. Thank you to Michael Gonsior for your help with dissolve organic matter chemistry, interest in the subject matter, and opportunity for Amanda and I to work at the Chesapeake Biological Laboratory. Thank you to Greg McCarty for the opportunity to work at the USDA-ARS, to set up some challenging experiments, and for giving me ideas on how to improve my writing. Thank you to Dr. Lance Yonkos for always being a fun and excited presence in research and giving me the opportunity to think a bit about toxicology. I'm grateful for my committee's commitment to research and education. I look forward to keeping their influence on my research and professional growth in my future career.

Thank you to Sandra Davis and the Marine, Estuarine, and Environmental Sciences program for supporting me throughout this experience. Thank you to the Menzer family for the Summer Doctoral Fellowship Award. I loved being a part of the Civil and Environmental Engineering Department as well and to have had the opportunity to be supported by and work with so many talented and hardworking individuals.

Thank you to Mark Ramirez at DC Water for his help with research and being interested in my professional growth. I am grateful to the scientists at the University of Arizona for the opportunity to work at the Arizona Lab for Emerging Contaminants. These individuals include Dr. Jon Chorover, Dr. Leif Abrell, and Dr. Ray Runyon.

Thank you to the fantastic set of women who helped me with data collection and interest in education. These individuals include Sarah Castro, Emily Healey, Amanda Hamilton, Taylor Motley, and Tianyin Ouyang. Thank you for your hard work and smiles. I'm so grateful for my graduate school friends and colleagues from many wonderful backgrounds and diverse interests. They have been amazing people to be around. Thank you to my best friends outside of graduate school: Rachel, Jenny, Becca, and Ben.

Thank you to my wonderful family. You are my role models. Thank you for being loving and supportive.

Table of Contents

Acknowledgements ii
Table of Contents iii
List of Tables vi
Chapter 1 viii
Chapter 2 viii
Chapter 3 ix
Chapter 4 xi
Chapter 5 xii
Chapter 1: Introduction 1
1.1 Biosolids Management and Treatment Monitoring 1
1.2 Dissolved Organic Matter Terminology, Debate, and Compound Classes 5
1.3 Optical Properties Analyses of Dissolved Organic Matter 7
1.3 Contaminants of concern in biosolids 11
Chapter 2: Nitrogen release and dissolved organic matter (DOM) decomposition of anaerobically digested biosolids with variable pre-treatments in aerobic sandy loam soil 13
Abstract 13
1. Introduction 14
2. Materials and Methods 19
2.1 Biosolids Collection 19
2.2 Organic Matter and Dissolved Organic Matter (DOM) Characterization 19
2.3 Nitrogen Mineralization Rate Experiments 22
2.4. Fluorescence Changes of Biosolids-DOM in during aerobic soil mineralization 25
3. Results 25
3.1.1. Geochemical Characteristics of Biosolids and DOM 25
3.1.2. DOM Fluorescence characteristics 26
3.1.3. FTIR spectral characteristics of DOM 28
3.1.4. High Performance Size Exclusion Chromatography of DOM 29
3.2. Nitrogen releases in biosolids-soil mesocosms 30
3.3. Transformation of biosolids-DOM in biosolids-soil mesocosms over time 32
4. Conclusions 37
5. Figures – Chapter 2 39
Chapter 3: Biosolids stabilization processes produce substantially different leachable DOM and complicates traditional fluorescence analysis for characterization 57
Abstract 57
1. Introduction 58
2. Materials and Methods 62
2.1 Biosolids and Sludge Collection 62
2.1 Total and Volatile Solids, Dissolved Organic Matter (DOM) Extraction, DOC, and pH measurement 63
2.2 High Performance Size-Exclusion Chromatography of Biosolids Extracts 64
2.3 Fluorescence Measurements 65
2.4 Excitation Emission Matrix Quantitation and Analysis 66

2.5 Fluorescence Regional Integration (FRI) 66
2.6 Local Maxima Analysis and Previously Described Peak Regions 67
2.7 Optical Properties Calculations and Visualization 67
2.8 Parallel Factor Analysis (PARAFAC) 68
3. Results 69
3.1 Total Solids, Volatile Solids, Water-Extractable Dissolved Organic Carbon Content, and pH of Extracts 69
3.2 High Performance Size Exclusion Chromatography of Biosolids-DOM 70
3.3 Biosolids-DOM Fluorescence Spectroscopy 71
3.4 Quantitative Analysis: Classic and Adapted Fluorescence Regional Integration (FRI) 72
3.5 Peak Area Assessment 74
3.6 Optical Properties-derived Indices 76
3.7 PARAFAC Models and Comparisons to the OpenFluor Database 77
3.8 Additional Fluorescence Spectroscopy on DOM across Solid Stabilization trains 79
4. Discussion 81
4.1 Implications for Biosolids Residuals Management 81
4.2 Recommendations for Quantitative Analysis of Anthropogenic DOM Pools 82
5. Figures – Chapter 3 86
6. Supporting Information 94
Chapter 4: Fluorescence Suppression Experiments to understand interactions of halogenated antimicrobials with contrasting biosolids-DOM pools 105
Abstract 106
1. Introduction 107
2. Material and Methods 110
3. Results and Discussion 112
4. Conclusions 118
5. Figures: Chapter 4 119
Chapter 5: Dehalogenating microbes and anaerobic community structure across thermal hydrolysis and anaerobic digestion systems 130
Abstract 130
1. Introduction 131
2. Material and Methods 134
2.1 Sludge Collection and DNA Extraction 134
2.2 Polymerase Chain Reaction (PCR) and Quantitative Polymerase Chain Reaction (qPCR) for dehalorespirating bacteria in full-scale digesters 134
2.2 THP-AD Mesocosm Experiment Amplicon sequencing and sequence processing 135
2.3. Statistical Community Analysis 136
3. Results and Discussion 137
3.3 Targeted Halorespiring Primer Survey 137
3.3 Abundance of *Chloroflexi Dehalogenimonas* across DC Water Blue Plains 137
3.3 THP-AD versus non-THP-AD substrate Mesocosm Community Analysis 138
4. Conclusions 141
5. Figures for Chapter: 142

Chapter 6: Dissertation Conclusions..... 150
Bibliography 155

List of Tables

Chapter 1: Introduction

Table 1: Common descriptors dissolved organic matter from operationally-defined substances to functional group categories.

Chapter 2

Table 1: Details of three RRFs with anaerobic digestion (AD) and dewatered biosolids collected for experiments. Reported RRF information was obtained through personal correspondence with RRF supervisors. Total solids, volatile solids, and pH of solids and DOM represent the average of three collection dates for each RRF.

Table 2: Biosolids-DOM Fluorophore Maxima in soil incubations over time.

SI Table 1: Biosolids and soil collection dates. Asterisk (*) indicates biosolid sample date used for N mineralization experiments.

SI Table 2a: Excitation and emission (Ex/Em) wavelength boundaries applied for classically defined fluorescence regional integration (FRI) analysis of biosolids-dissolved organic matter extracts. Based on Chen et al. (2003).

SI Figure 2b. Modified FRI Regions for Biosolids-DOM Leachates:

SI Table 3: Fluorescent (FDOM) Component Peaks proposed by Stedman et al. 2003 and Coble et al. 2007:

SI Table 4: Peak Intensities and assignments of Biosolids-DOM presented in Figure 3, with FRI.

SI Table 5: Standard and Smith model results for Potential N Mineralization (PMN) and rate k determined by (1972) for biosolids-amended soil.

Chapter 3

Table 1: Description of waste stabilizations and resource recovery facilities (RRF) sampled for this study. Total and volatile solids are also reported.

Table 2: Determination A:C and T:C Peak ratios by classically defined boundaries and adapted for proximal maxima of biosolids DOM, peak T:C ratio and was also computed.

SI Table 1: Excitation and emission (Ex/Em) wavelength boundaries applied for fluorescence regional integration (FRI) analysis of biosolids-dissolved organic matter extracts. Based on Chen et al. (2003).

SI Table 2: Adapted Ex/Em wavelength boundaries applied for fluorescence regional integration (FRI) analysis of biosolids-dissolved organic matter extracts.

SI Table 3: Fluorescent (FDOM) Component Peaks areas summarized in Stedman et al. 2003, Coble et al. (2007), and Gabor et al. (2014)

SI Table 4: Results of Fluorescence Index Computation. Indices were computed on individual EEMs and averaged by treatment type. Standard deviation of averages of treatment type are also reported.

Chapter 4

Table 1: Chemical properties of EC quenchers used in fluorescence interaction measurements.

Table 2: Summary of 2nd residual computation results with the Ex_{max}:Em_{max} and peak intensity of quenching of DOM are indicated. Quenching of the contaminant was removed from the 1st residual.

Chapter 5

Table 2: Results of 16S rRNA Dehalorespirer Primer Survey on anaerobic digest sludge. Samples collected June, 2016.

Chapter 1

Figure 1: Example of gel chromatography with UV absorbance at 254 nm of DOM extracted from biosolids samples in during 100 days of composting from Wang et al. (2013).

Figure 2: Jablonski diagram of electron transitions, from Hudson et al. (2007).

Figure 3: Theoretical examples of DOM constituents can exhibit an absorbance and fluorescence response Hudson et al. (2007)

Chapter 2

Figure 1: a) Organic carbon and total nitrogen (TN) of dewatered biosolids and soil before mesocosm experiments. b) Leachable dissolved organic N in itinial biosolids extracts for RRFs on a dry weight basis. Error bars represent standard deviation of three averaged collection dates. * Indicates significant difference ($p < 0.05$) in average relative other samples in set (n=3 sample dates) by a one-way ANOVA with *post-hoc* Tukey HSD test.

Figure 2: Fluorescence characterization of biosolids-DOM extracts at dewatering facilities. Each excitation-emission matrix represents the average of n=3 sampling dates. A) Fluorescence Regional Integration boundaries on EEMs and %*P* results according to classically defined regions published in Chen et al. (2003). B) Adapted FRI boundaries for biosolids-DOM that encapsulates fluorescence beyond ex: 400 nm and combines bisected fluorescence maxima of region I and II.

Figure 3: FTIR spectra of extracted biosolids-DOM (top panel) and DOM reference materials (lower panel). Distinct peaks (cm-1) are noted above peaks.

Figure 4: Mineral NH_4^+ (a.) and NO_3^- (b.) development in biosolids-soil incubations.

Figure 5: First-order kinetic fit of net mineral N (NO_3^- and NH_4^+) produced from aerobic incubation of biosolids treatments with confidence band shaded in grey. The fractions of nitrogen mineralized (K_{min}) per treatment are indicated below model fits and are based on the first order kinetic model (Eqn. 1, Figure 5) and initial biosolids organic N supplied to soil mesocosms (eqn. 2).

Figure 6: Fluorescence changes in Biosolids DOM transformations over time in aerobic soil incubations mesocosms (a,c,and e). The fluorescence spectra of soil incubations (g.) were subtracted from biosolids-soil mixtures to isolate biosolids DOM decomposition. Differences in biosolids DOM from day 45 to 105 are indicated (b.,d., f.).

Chapter 2: Supporting Information

SI Figure 1: Field work and mesocosm set-up photos. Photos a.) and b) are soil collection at 5 – 15 cm depth of fine sandy loam soil from a historic A_p horizon at University of Maryland's Hayden Farm, 10 feet away from crop. Initial inorganic N in soil was determined and accounted for (subtracted) in N mineralization rate determinations. Photo c.) shows the destructively sampled mesocosms of soil and biosolids mixtures in temperature (20◦C) and humidity-controlled dark growing chamber. Photo d.) shows the water extraction of dissolved organic matter from biosolids samples before amendent to soil mesocosms and DOM characterization.

SI Figure 2: HPLC-SEC chromatographs for anaerobically-digested (AD) biosolids DOM for three sample dates per WWTP.
Date of biosolids collection DD-MM-YY format. a) DOM from WWTP with THP-AD system. B) Biosolids-DOM from RRF without pretreatment and c) fermentation prior to anaerobic digestion (AD) exhibited similar molar mass distributions and polydispersity as THP-AD biosolids-DOM. Reference material D.) SROM contrasted the sludge-DOM chromatographs while the waste-actived sludge product e) Milorganite DOM exhibit similar molar mass distributions to AD Materials. The apparent molar mass of peak locations (Mp) based on PSS polymer standards are indicated.

SI Figure 3: Excitation and emission loadings of 4 and 5 component EEM-PARAFAC models generated during preliminary analysis. Loadings were appraised for the following features (Murphy et al. 2013): (i) minimal overlap between the excitation and emission spectra, (ii) excitation spectra that may have multiple peaks, but emission spectra exhibit a single distinct peak, (iii) excitation spectrum has two or more peaks indicating consecutive excited state absorption bands, some absorption (excitation) occurs between these peaks, and (iv) excitation and emission spectra do not exhibit abrupt changes over very short wavelength distances.

Chapter 3

Figure 1: Extractable DOC (mg) per kilogram biosolid, on a dry weight basis. The average pH of water-soluble organic matter extracts is listed above each type. Limed biosolids DOC was not corrected for weight due to lime addition to solids. Denotation (**) represent a significant difference in extractable DOC/kg d.w. solid observed for aerobically digested material compared to the two other treatments, by a one-way ANOVA and unpaired t test between types.

Figure 2: HP-SEC Chromatographs of biosolids-DOM from a) limed, b) anaerobically-digested, and c) aerobically digested waste stabilization classes pH ~7.4 for multiple resource recovery facilities. The apparent molar mass (Mp) of eluted DOM peaks are indicated on chromatographs.

Figure 3: Excitation emission matrices (EEMs) of biosolids-DOM from multiple RRFs and stabilization. A., c., and e.) Averaged EEMs of all biosolids-DOM by LT, AnD, and

AeD stabilizations with fluorescence maxima indicated. B.,d., and f.) EEMs of DOMs extracted (n=3) from final biosolids collected at individual RRFs with LT, AnD, and AeD. Local maxima are indicated with numbers.

Figure 4: Visualization of three classically defined quantitative methods for averaged EEMs applied to biosolids-DOM averaged by treatment types of LT (n=12), AnD (n=12), and AeD (n=11) biosolids DOM. A-c) FRI regions, d.) results of FRI. error bars represent standard deviation of P% for multiple EEMs per RRF solid, e-h) previously defined peak A, C, B, and T boundaries and local maxima (white circle) of underlying EEM, i-l) Fluorescence indices HIX, BIX, and FI denoted on biosolids-DOM and SRNOM EEMs. Additional description and results of FRI, Peak A:C boundaries and index computation are summarized in SI Tables 1-3.

Figure 5: Boundaries and results of fluorescence regional integration (FRI) adapted for biosolids-DOM fluorescence maxima.

Figure 6: Biosolids-DOM EEM-PARAFAC model fingerprints of a) LT-biosolids-DOM, b) AeD biosolids, and c) AnD biosolids-DOM. D. Table of maximum excitation and emission Exmax, Emmax (nm) and average Fmax of each component. Further details of models are presented in the supplementary information.

Figure 7: Excitation-emission matrices (EEMs) and evolution of multiple Ex/Em maxima on sludge-DOM across full-scale anaerobic digestion treatment trains. EEMs of additional treatment trains are presented in SI Figure 5.

Chapter 3: Supporting Information

SI Figure 1: a. SEC chromatograph for 67K-182 Da standards, retention times (min) labeled above peaks. Standards were injected in triplicate. b. Resulting calibration curve of PSS Standards Retention times versus Log(Molar Mass). The linear relationship between standards log molar mass (MM) and retention time was Log(MM) = -0.57264(min) + 13.44113 ± 0.45004, with an adj. R-square = 0.972. Error bars represent average RT of triplicate injections per molar mass standard; error bar magnitude was smaller than the point size displayed. c. Chromatograph of SROM. Apparent molar mass of peak (M_p) locations are indicated in daltons (Da) . Majority of SROM corresponded to an M_p of 2020 Da with small signal corresponding to 188 daltons. d. Full chromatograph of AeD-biosolids DOM and evidence of particulates, polymer, and/or supramolecular assembly.

SI Figure 2: Xenochemical influence on biosolids-DOM. **(**a) Biosolids-DOM Extracts. Extracts from the Worton, MD facility were blue in color, (b) EEM of proprietary dewatering polymer added to sludge before final dewatering. Fluorescence was assessed at 7.5 mg C/L and contained minimal fluorescence contribution (>0.08 RU) to biosolids-FDOM.

SI Figure 3: Excitation and emission loadings of 4 and 5 component EEM-PARAFAC models generated during preliminary analysis. Loadings were appraised for the following features (Murphy et al. 2013): (i) minimal overlap between the excitation and emission spectra, (ii) excitation spectra that may have multiple peaks, but emission spectra exhibit a single distinct peak, (iii) excitation spectrum has two or more peaks indicating consecutive excited state absorption bands, some absorption (excitation) occurs between these peaks, and (iv) excitation and emission spectra do not exhibit abrupt changes over very short wavelength distances.

SI Figure 4: Split Half Validations of PARAFAC Models

SI Figure 5: Component comparisons at a 0.97 threshold for three biosolids-DOM PARAFAC models deposited to the OpenFluor plugin for OpenChrom.

Chapter 4

Figure 1: Absorbance plots of AnD Sod Run Biosolids-DOM blue) with and without TCC, with blanked with the absorbance of TCC (orange). TCC in 0.1% acetone and high purity water only (grey) had high absorbance at 259 nm. The overlay of AnD-DOM only and AnD-DOM with TCC confirm that the TCC spectra is effectively blanked and has a simple additive effect on the absorbance spectra.

Figure 2: Absorbance plots of AeD Tolchester (Tolc) Biosolids-DOM with and without TCC (blue) and with TCC blanked (orange). The lack of significant variance in absorbance confirm the superposition model held and that added TCC was effectively blanked from AeD biosolids DOM

Figure 3: Individual EEMs TCC and 2-4 DCP in 0.1% acetone and high purity water.

Figure 4: Fluorescence Quenching EEM of Lime Treated (LT) Little Patuxent (LLP) DOM and Triclocarban (TCC). EEMs from left to right: A) individual EEMs TCC in 0.1% acetone and high purity water, and LLP-DOM in 0.1% acetone. B) Theoretically constructed and experimental mixture EEMs pf TCC and LLP (all blanked with acetone), followed by residual. C) Experimental mixtures blanked against TCC, first residual of theoretical and experimental mixtures, and 2nd residual of mixtures and TCC spectra.

Figure 5: EEMs of LT Laurel Biosolids DOM. Theoretical construction of TCC and LT Laurel DOM is not shown. A) LLaurel DOM only (0.1% acetone), b) 1st residual of theoretical and experimental mixture (blanked against TCC) indicating combined quenching of TCC and and DOM and c) 2nd residual removing quenching of TCC, indicating quenching of DOM only.

Figure 6: EEMs of AnD DCW (THP-AD) biosolids-DOM Quenching. Theoretical Construction of TCC & DCW THP-AD DOM Only. Experimental TCC + DCW with TCC Blank.

Figure 7: EEMs of AnD Sod Run biosolids-DOM Quenching. Theoretical construction of TCC & Sod Run DOM Only, experimental TCC + Sod Run with TCC Blank, and residual spectra.

Figure 8: EEMs of AeD Tolchester -DOM Quenching.

Figure 9: EEMs of Suwannee River Natural Organic Matter and 2-4 DCP Quenching

Chapter 5

Figure 1: Abundance of obligate dehalorespirer *Chloroflexi Dehalogenimonas* in sludge across DC Water, Blue Plains wastewater treatment facility. Quantitative polymerase chain reaction indicated log(2) to log (3) fold greater abundance of *Dehalogenimonas* in anaerobic digesters for two sampling events.

Figure 2: Rarefaction analysis confirm sufficient sampling depth for bioinformatic analyses on selected mesocosm sequenced timepoints. Sufficient sampling depth was marginally achieved for "THP Sludge Influent" and not achieved for "THP Effluent" samples, likely due to poor DNA quality. These samples were excluded from select statistical analyses.

Figure 3: Relative Abundance and Taxonomic Assignment for Community structure at different Phylogenetic levels across anaerobic mesocosm with THP substrate and without THP substrate. Several phylogenetic levels are indicated.

Figure 4: Alpha Diversity analysis across mesocosm experiment with THP substrate and without. Computation of alpha diversity by several sub-tests are indicated. A) Limited differences in alpha diversity as a function of treatment type or b) time.

Figure 5: Statistical Community Differences as a function of i) substrate treatment ("With THP", "Without THP", AD Inoculum only) or ii) time (days) was assessed by several ordination methods applying Bray-Curtis dissimilarity estimates within the function options for ordinate in phyloseq. THP Influent and Effluent samples were removed for additional ordinations.

Figure 6: Ordination of treatment and time effects were also appraised utilizing envfit {vegan} and metaMDS {phyloseq} assignment.

Chapter 1: Introduction

1.1 Biosolids Management and Treatment Monitoring

Recycling of municipal solid wastes to agricultural lands or gardening products is emphasized in countries that have industrialized wastewater treatment, growing quantities of material, and decreasing availability or high costs associated to landfilling solids (Olk et al. 2019). Both on-site resource recovery facility (RRF) treatments or post-facility composting of solids reduces odors and pathogens and can reduce mass and volume by approximately 50% (He et al., 1992). Treated solids are also often dewatered or air-dried to reduce bulk before distribution. Biosolids treatment may be through one or a combination of stabilization methods, including (1) biological processes via anaerobic or aerobic digestion and aerobic composting, (2) physical processes such as thermal hydrolysis (high heat and pressure), pasteurization (minimum heat), thermal drying, or air and solar drying, and (3) chemical processes such as caustic lime treatment (Rigby et al. 2016). United States Environmental Protection Agency (US EPA) Part 503 of biosolids regulations defines effective anaerobic digestion as the biological decomposition of solids for a minimum of 15 days at 35°C to 55°C or 60 days at 20°C in the absence of oxygen. Aerobic digestion is biological decomposition of sludge in the presence of oxygen for 40 days at 20°C or 60 days at 15°C. Sufficient lime stabilization raises the pH of biosolids to 12 after 2 hours of contact. The stabilizations are designed and regulated for the ability to effectively reduce pathogens and vector attractiveness. In the US, an EPA Class A designated biosolid appropriate for lawns, home garden, and commercial sales has pathogen densities reduced below detection limits defined as less than 3 most probable

number (MPN) of *Salmonella sp*, less than 1 plaque forming units (PFUs) per 4 grams biosolids (d.w. basis) for enteric viruses, and less than 1 viable helminth ova, all per 4 grams biosolids (d.w. basis) (Lu et al. 2012). Class B solids of restricted use requires fecal coliform densities of less than 2 million MPN or CFU per gram of total biosolids, dry weight basis (US EPA, 1995).

Beyond pathogen treatment and limits on heavy metal loadings, biosolids are managed to ensure solids are transformed to a stable, well-characterized form with predictable nutrient releases, low odors or noxious qualities, and ease of handling (Lu et al. 2012). Transformations of sludge and biosolids have been monitored by a number of parameters including C:N ratios, CO_2 respiration rates (Gilmour and Skinner, 1999), BOD and COD of leachates (Wang et al. 2013), nutrient speciation and nutrient release rates (Rigby et al. 2016), odor measurements (Romero-Flores et al. 2017, 2018) or by spectrometric methods of UV-visible, fluorescence, Nuclear Magnetic Resonance (NMR), or Fourier-transform infrared spectroscopy (FTIR) (Wang et al. 2014, Fels et al. 2014, Sun et al. 2016). El Fels (2014) monitored aerobic co-composting of sludge and lignocellulosic palm tree waste by nutrient development, lipid content, spectroscopic analyses, and phytotoxicity. Phytotoxicity, or the inability of a seed to germinate, decreased significantly over months of composting. This was correlated to a decrease in NH_4^+ and an increase in stability and presence of oxidized functional groups inferred by spectroscopic analyses. A decrease in extractable lipid content co-occurred with an increase in aromatic structures measured by FTIR spectroscopy.

Spectroscopic analyses of organic residue quality can be applied to the solid fraction directly by ^{13}C-NMR and FTIR (Piterina et al. 2009, Purusottam, 2015) or to

leachate quality with solution-based UV-visible absorbance and fluorescence spectroscopy, and lyophilized leachate powders for FTIR and ^{1}C-NMR. These tools provide information on morphology of biomolecules over time, including release, production, or degradation of polymers, lipids, small molecules such as amino acids, operationally-defined materials of humic acids or fulvic acids, and information about chemical bounds – aliphatic, aromatic, or functional group information that may transform during engineered or composting processes (Wang et al. 2013).

Leachates of residues are also commonly analyzed for molecular weight distributions (Olk et al. 2019). Molecular weight distributions can be determined by colligative methods of cryoscopy and vapor pressure osmometry. Non colligative methods, or methods without the use of solvent, include UV-scanning ultracentrifugation, field-flow fractionation, gel chromatography, and size exclusion chromatography (SEC). Wang et al. (2013) measured that that the molecular weight of water-extractable DOM of biosolids increased during aerobic composting, as indicated by longer elution times of DOM via gel chromatography (Figure 1). Development of higher weight molecular material (also associated with "humic acids") during stabilization has been termed "humification" and is a debated issue in soil science (Lehmann and Kleber, 2015). Lehmann and Kleber (2015) discussed the counter concept of "humification" and that organic matter is a continuum of decomposing organic compounds to more soluble forms. Smaller dissolved monomers may be first to decompose as complex larger organics are released. This topic is further discussed in the following section. Light absorbance at 254 nm has been previously associate to unsaturated and aromatic components in DOM that form during oxidation of carbon (Thomas et al. 2017).

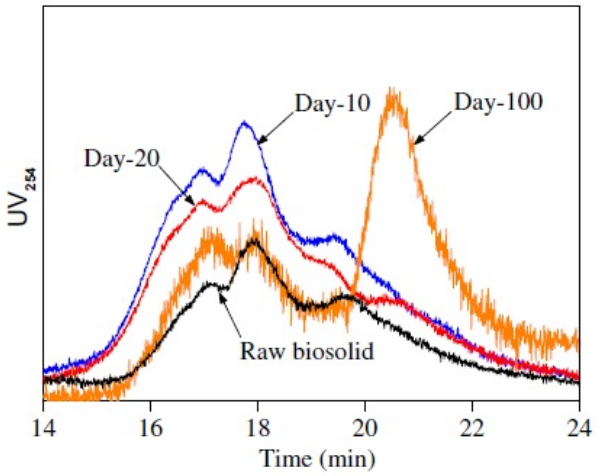

Figure 1: Example of gel chromatography with UV absorbance at 254 nm of DOM extracted from biosolids samples in during 100 days of composting with aeration and pumice from Wang et al (2013). Molecular weight of DOM leachates absorbing 254 nm increased in samples over time.

1.2 Dissolved Organic Matter Terminology, Debate, and Compound Classes

The focus of this dissertation is water-soluble organic matter from biosolids. Dissolved organic material (DOM) is a complex, heterogeneous mixture of biological organic compounds that can pass through ≤ 0.45 μm filter, derived from plant litter, algal decomposition, soil, animal manures, biosolid leachates, and microbial exudates (Leenheer and Croué, 2003). DOM is measured in aquatic, marine, terrestrial, wastewater and solids treatments under a range of biogeochemical scenarios. A 'battery' of analytical approaches can applied to evaluate used to assess the complex mixtures to ascertain structural information: resin-based fractionation (XAD-8/DAX-8) for acidic or basic properties, pyrolysis-mass spectrometry, ultrahigh-resolution mass spectrometry, electron spin resonance spectroscopy, acidimetric titrations, electrochemistry, or Nuclear Magnetic Resonance (NMR) (Sharpless and Blough, 2014). Accordingly, discussion of DOM ranges from broad operational-defined groups (humic and fulvic acids, Table 1) to more specific compound classes defined by functional groups (quinones, indoles), or biomolecules (amino acids, carbohydrates, lignin, cellulose, lipids). Humic and fulvic acids are simply defined based on pH solubility below and above pH 1 and thus they can consist of thousands of not hundreds of thousand possible organic compounds (Olk et al. 2019).

Table 1: Common descriptors of DOM from operationally-defined substances to functional group categories.

	Formal Definitions and examples	**Broader Community Understanding or Implications (Olk et al. 2019, Minor et al. 2014)**
Humic acids (HAs)	• Precipitates at pH ≤ 1 • Adsorb to a nonionic resin with hydrophobic qualities • Assumed to have a larger carbon backbone relative to fulvic acids • Some acidic functional groups	• Associated with aged soils and composts, and stable manures • Color causing fraction of dissolved OM and soil OM • Brown to black color Associated with polymeric aromatic carbon moieties such as polyphenols
Fulvic Acids (FAs)	• Soluble in both alkali and acidic conditions but adsorb to a nonionic resin when protonated, distinguishing it from organic matter fractions that are very hydrophilic. • Soluble at all pH levels.	• Yellow to brown in color • Color causing fraction of dissolved OM and soil OM (chromophoric) • Presumably smaller carbon backbone than HA and less aromatic and/or increased carboxylic acid functional groups
Biomolecules	• Amino acids (AA) such as tyrosine, tryptophan, and phenylalanine • Cellulose and lignin	• Amino acid detection was associated to wastewater or animal manure impacted environments (Baker et al. 2002) • Lignin, tannins and cellulose are associated with breakdown products of plants
Functional groups abundant in DOM	• Indoles, quinones, hydroxylated phenols • Saturated and unsaturated C-C • Carbonyl and carboxyl bonds	• Electron donating/accepting dynamics play a role in redox and photochemistry • Increase in unsaturated bonds and carboxylation indicate more oxidized material

Aging of organic matter in sediments, soil, manures, and biosolids has *historically been* referred to as "humification" (Gabor et al. 2014). The term "humification" is actively debated and even cited as a contentious, dated word because it is derived from strong alkaline-extract soil materials that are argued to have abstracted to limited environmental significance (Kleber and Jenner et al. 2019). Alkaline extractions were originally developed to remove all soil organic carbon from the mineral phase. The term humification has, however, been tied to detection of higher molecular weight, aromatic compounds as material ages (Olk et al. 2019). In biosolids stabilization literature, many studies report on the trend that polyaromatic, higher molecular weight material, or material previously associated to "humic acid"-like or "fulvic acid"-like dissolved signatures are developing with maturation or age (Wang et al. 2014).

One framework to explain this phenomenon is that higher molecular weight, less soluble material are released during breakdown of stable, refractory cellulose or lignin from solid phases, while there may be consumption of small molecular weight material. A counter theory is microbially-driven polymerization of organic matter where low molecular weight is synthesized to high molecular weight carbon. DOM polymerization is a strongly disputed process (Kleber and Lehmann, 2019) but it seems the most feasible process in anaerobic reducing environments if at all (Hebting et al. 2003).

1.3 Optical Properties Analyses of Dissolved Organic Matter

This thesis has significant focus on the optical properties of DOM and draws in complementary analyses of Fourier Transform Infrared (FTIR) spectroscopy and size-exclusion chromatography (SEC). The optical properties of DOM, including both

absorbance and fluorescence spectroscopy, is based on the ability of molecules to absorb light and potentially re-emit that energy as fluorescence. Compounds that absorb light are called chromophores, and DOM may be colored yellow to brown as they absorb UV and blue range visible light (Minor et al. 2014). Compounds that re-emit light energy are called fluorophores (Mopper et al., 1996). Fluorescence occurs when electrons in a molecule are excited to a higher energy level by the absorption of photons and then return to its lower energy ground state by emitting energy as a quantum of light (Hudson et al. 2007). The Jablonski diagram (Figure 2) is a means to represent electronic transitions involved in absorption and fluorescence of energy by molecules. Some excitation energy is always due to collision, non-radiative decay and other processes such that energy of an emitted photon during fluorescence is always lower than the excitation energy. The difference between excitation and emission energy or wavelength is known as the Stokes' Shift (Lakowicz, 2006). Fluorescence of conjugated aromatic organic compounds (when stimulated) is common due to the energy sharing π orbitals.

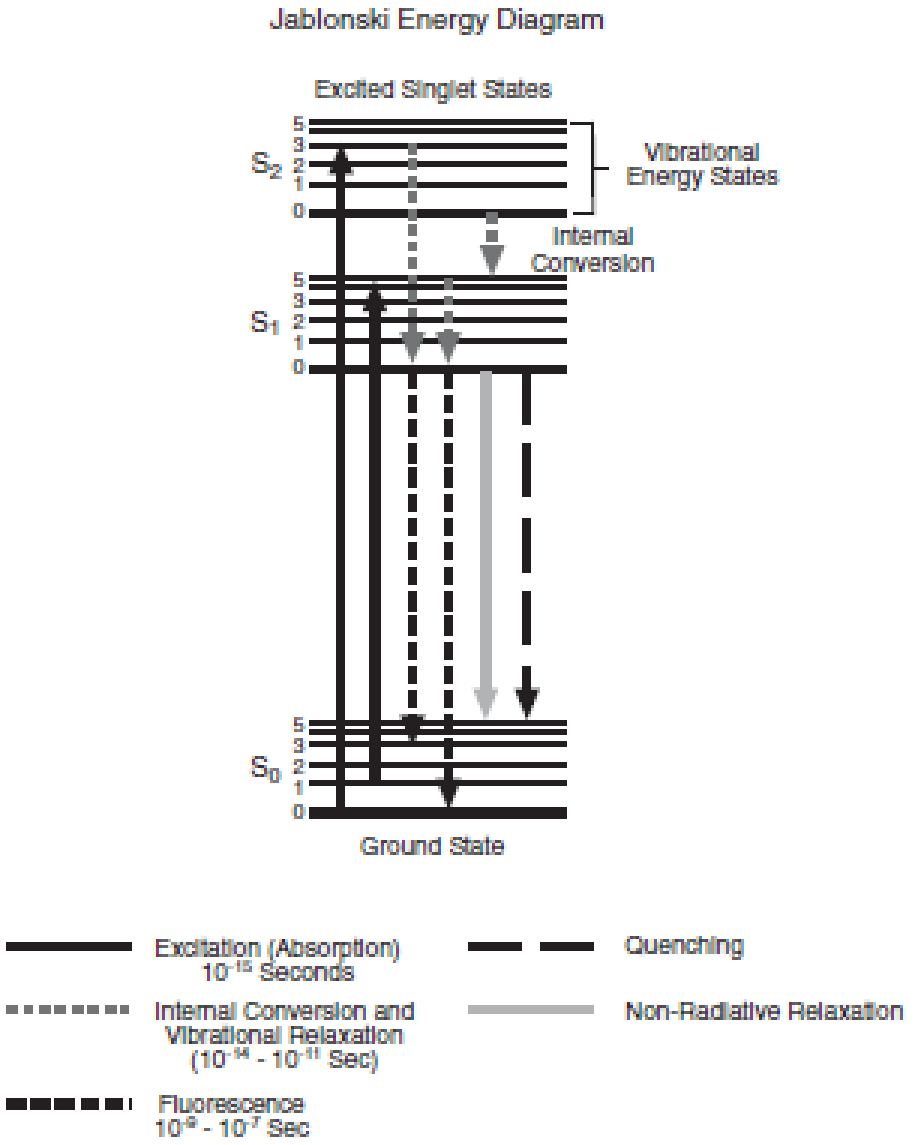

Figure 2: Jablonski diagram from Hudson et al. (2007). A number of electronic transitions occur in conjugated molecules when excited by light and determine local maxima within a fluorescence spectrum.

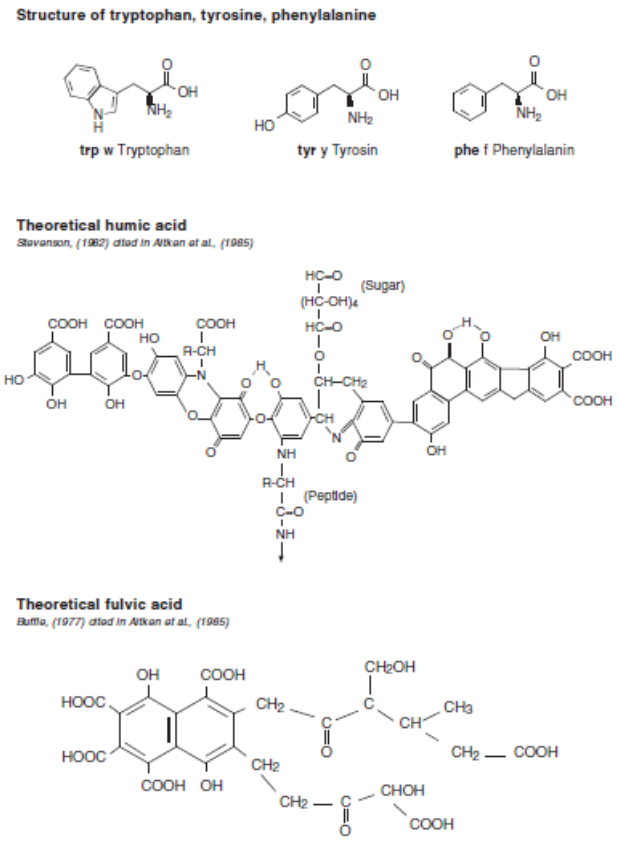

Figure 3: Examples of DOM constituents that could exhibit an absorbance and fluorescence response. Adapted from Hudson et al. (2007)

Amino acids tyrosine and tryptophan are examples of DOM biomolecules that exhibit a fluorescence response (Figure 3). Fulvic and humic acids (Table 1) also contain conjugated aromatic systems that fluorescence. Because humic and fulvic acids were originally operationally-defined by pH solubility and not fluorescence, actual fluorophores within these very complex pools remain unknown. Similarly, complex charge transfer interactions between molecules may alter the fluorescence response so that it cannot be simply used to quantify fluorophores in DOM.

1.3 Contaminants of concern in biosolids

Biosolids are a well-documented source of contaminants of emerging concern (CECs) from consumer products (McClellan et al. 2010). The US EPA regulates biosolids for ceiling concentrations of nine heavy metals and one class of industrial organic contaminants, polychlorinated biphenyls (PCBs) at a total mass of at 50 µg/kg d.w. basis (EPA Clean Water Act, Rule 503). Beyond this, a wide range of emerging contaminants (ECs) are detected in solids and remain unregulated (US EPA National Sludge Survey, 2009). Halogenated ECs persist in biosolids and soil (Andrade et al. 2010) and can be taken up by edible crops (Vrkoslavová et al. 2010). In the 2001 EPA National Sewage Sludge Survey for Pharmaceuticals and Personal Care Products (PPCPs) of 110 biosolids samples collected nationally, halogenated antimicrobials triclocarban (TCC) and triclosan (TCS) are examples of the most abundant analytes of thirty-eight pharmaceutical and personal care products (PPCPs) detected, accounting for 65% of the total PPCP mass, and are resistant to wastewater treatment processes (McClellan et al. 2010). Halogenated ECs have also been detected in runoff from land receiving biosolid (Topp et al., 2008; Edwards et al., 2009; Sabourin et al., 2009). Brominated flame retardants such as

polybrominated diphenyl ethers (PBDEs) are also examples of halogenated organic contaminants in biosolids distributed to agricultural lands (Andrade et al. 2010).

These compounds are considered CECs because of their prevalence in society and mounting evidence for human and ecological risk (Ogunyoku et al. 2014). These compounds demonstrate endocrine disrupting activity in mammals (Zorrilla et al. 2009). Halogenated ECs are also toxic to aquatic organisms at environmentally relevant concentrations (Brausch and Rand 2011). Because halogenated compounds such as PBDEs and antimicrobials are hydrophobic (logKow > 2), a significant fraction of halogenated EC compounds partition to the treated solids at wastewater treatment facilities, resulting in accumulation in the final biosolids (Lozano et al. 2010).

While CECs are consistently measured in biosolids, the US EPA (2018) determined that a lack of data exists for risk assessment, bioavailability, and mobility assessment of 352 pollutants deriving from biosolids. DOM in soil and aquatic systems has a broadly demonstrated role in the movement and bioavailability of metals, nanoparticles, and organic contaminants (Kalbitz et al. 1998, Chefetz et al. 2008, Delgado-Moreno et al. 2010, Chen et al. 2015). The role of biosolids-specific DOM on chemical interactions and bioavailability of halogenated emerging contaminants has not yet been extensively evaluated. To this end, this dissertation also investigated interactions of leachable organic matter and with two organic contaminants triclocarban and 2-4 dichlorophenol in fluorescence quenching experiments.

Chapter 2: Nitrogen release and dissolved organic matter (DOM) decomposition of anaerobically digested biosolids with variable pre-treatments in aerobic sandy loam soil

Abstract

Advanced thermal hydrolysis pretreatment (THP) coupled to anaerobic digestion (AD) systems are increasingly implemented to treat municipal solids, but limited study indicates whether THP-AD materials merit different land application rates than other AD biosolids. Three AD biosolids collected from full-scale treatment facilities with contrasting pre-treatments were evaluated for differences in dissolved organic matter (DOM) quality and nitrogen mineralization. Several DOM characterization techniques reflected similarities in FTIR spectra and humic acid-like fluorescence maxima at Ex_{max}:Em_{max} 415:480 nm among AD leachates not present in the waste activated sludge product Milorganite. AD biosolids were then incubated in aerobic sandy loam soil for 3 months. The 105-day net inorganic N produced was 155.3 ± 12.1 mg N/kg for AD biosolids with no pretreatment, 148.5 ± 18.2 mg N/kg for fermentation-AD biosolids, 139.7 ± 17.4 mg N/kg for THP-AD biosolids, and 353.68 ± 15.1 mg N/kg for Milorganite (dry weight basis). Mineral N releases modeled by first order kinetics also indicated variable kinetics for AD solids during the first 20 days due to NH_4^+ releases, but similar overall mineralized N after 105 days for AD treatments. Excitation emission matrix (EEM) spectra of leachable DOM from biosolids-soil mixtures indicated that the humic acid-like fluorophore of Ex_{max}:Em_{max} at 415 nm:480 nm initially present in dewatered leachates decayed by day 45, suggesting that larger, complex carbon sources liberated during solids stabilization may decompose first in soils. In summary, other variables

(source material, AD operation) may have a greater influence on final agronomic decomposition than full-scale pretreatments to AD alone.

1. Introduction

In recent decades, many wastewater treatment plants have been re-engineered their processes to better serve society as resource recovery facilities (RRF) that provide treated water and nutrients-rich biosolids, valued by industries and society (Daigger 2009). Treated biosolids are valued as a soil amendment because they can enhance nutrient availability, soil structure, and bulk density of agricultural soils (Singh et al. 2008). Through treatment and land-application programs, biosolids reduce reliance on inorganic fertilizers (Lagae et al. 2009).

After RRF treatment, land-applied biosolids are aerobically mineralized by soil microorganisms, releasing organically bound nitrogen (N) to the plant available nitrogen (PAN) forms NO_3^- and NH_4^+. Federal United States application guidelines mandate biosolids be applied on the fraction of organic N that will be converted to PAN during the first year of application and anticipated crop demand. This fraction of mineral N released is also termed K_{min}, which is the mineralization rate constant (Part 503 USEPA, 1994). Solids from different waste stabilization practices are applied according to their K_{min} constants, ranging from 0.4 or a 40% PAN release for unstabilized or waste activated sludge to 0.1 or a 10% PAN release expected for composted solids in the first year (USEPA 1994). Underestimation of N release can result in the over-application of biosolids and cause leaching of excess N and eutrophication (Meyer et al. 2001, Lapen et al. 2008, Fischer et al. 2017). Conversely, overestimation of mineralization rates can lead

to underapplication of biosolids and lower than optimal crop yields (Henry, 1991; Cogger et al., 2004). Due to the range of potential mineral N releases, the US EPA recommends laboratory-based incubation tests for new or blended biosolids products (US EPA 1995, Kumar et al. 2014).

Recently, a large and advanced metropolitan RRF installed a thermal hydrolysis processing (THP) system prior to mesophilic anaerobic digestion (AD) for the enhanced stabilization of final wastewater residuals. The THP pre-treatment heats sludge to 165°C and pressurizes the material to 55 - 138 PSI at a solids retention time of 30 minutes, akin to autoclaving solids before digestion (Wang et al. 2018). The THP pre-treatment hydrolyzes macromolecular compounds such as proteins, lipids, and polysaccharides in sludge (Wilson and Novak 2009) to enhance downstream methane production during anaerobic digestion (Xue et al. 2015). Because of the additional benefits of pathogen destruction, biogas production, and total solids reduction, full-scale versions of THP coupled with anaerobic digestion are increasingly being implemented at RRFs internationally (Chauzy et al. 2014, Barber et al. 2012, Oosterhuis et al. 2014). Although significant research has examined the impacts of the THP process on anaerobic digestion at RRFs, limited studies have considered the behavior of the combined THP-AD treated material in final land-application scenarios in detail (Morris et al. 2003). With the increased implementation of THP-AD worldwide, additional studies are needed to understand how the physical and biological combination of the THP-AD process may alter the agronomic behavior of biosolids, as well as the quality of dissolved organic matter (DOM) introduced to the environment.

Research suggests that biosolid leachate can influence decomposition rates to mineral forms and reflects the degree of organic matter stability of composts and sludge (Cabrera et al. 2005, Wang et al. 2013, El Fels et al. 2014). Leachable DOM is the carbon and nitrogen-containing soluble organic matter that can be taken up by heterotrophic bacteria during organic matter oxidation, releasing inorganic forms of CO_2, NO_3^-, and NH_4^+ (Metting 1993, Marschner and Kalbitz, 2003). Highly labile or readily-oxidized DOM has been identified by the presence of saturated functional groups (C-H, C-C, or C-OH) and specifically carbohydrates, proteins, and smaller molecular weight hydrophilic moieties. Unsaturated and aromatic functional groups (C=C, C=O), and larger molecular weight humic acids have been traditionally associated with refractory or difficult to degrade organic matter (Kalbitz et al. 2003, Wei et al. 2016).

Attempts have been made to describe the refractory or labile character of leachable DOM from solids using spectroscopic methods, including Fourier Transform Infrared (FTIR) and fluorescence spectroscopy (Zsolnay et al. 1996, Marschner and Kalbitz, 2003). FTIR spectroscopy is applied to characterize oxidizable functional groups in organic matter (Carballo et al. 2008, El Fels et al. 2014). Three-dimensional fluorescence spectroscopy is a bulk characterization tool useful for identifying classes of optically-active DOM such as aromatic protein-like, humic and fulvic acid-like, and microbial byproduct-like conjugated compounds that display an emission response when stimulated by excitation energy (Coble et al. 1990, Chen et al. 2003, Tian et al., 2012, Wang et al. 2013). In a 100-day biosolids composting experiment, fluorescence analysis indicated the decline of small molecular weight, microbial-like DOM with a corresponding increase in larger, humic acid-like molecules (Wang et al. 2013). Lastly,

size-exclusion chromatography can be applied to ascertain the molecular weight distribution of DOM pools occurring due to waste treatment or stabilization, typically transitioning to higher molecular weight fractions from stabilization (Wang et al. 2013). Studies also suggest that apparent high molecular weight DOM might be due to formation of smaller molecular weight compound aggregates, however (Sutton and Sposito, 2005).

When considering the solids or DOM generated by a new RRF configuration, limited studies systematically characterize biosolids-DOM across different RRFs for multiple collection dates. Gigliotti et al. (2002) present compositional information of DOM from singular grab-samples of waste materials including pig slurry, urban waste compost, and anaerobically digested sewage solids. While the authors found notable differences between sludge and other DOM sources, additional sampling at different RRFs was not conducted. Similarly, while Wang et al. (2013) demonstrated DOM quality shifts to more humic acid-like forms during biosolids-composting, the experiment was conducted on material from one RRF. Li et al. (2014) and Sun et al. (2016) also demonstrate the effects of anaerobic digestion and heat pretreatment on sludge DOM over time, but only on material collected during a single collection event. These results could be more universally applied with additional information on possible variation of biosolids-DOM from several RRFs with variable treatment configurations.

The first goal of this study was to characterize leachable DOM profiles in starting material obtained from different RRFs with anaerobic digestion for multiple sample dates: one facility with THP-AD, one facility with fermentation prior to AD, and one facility with only holding prior to AD. Commercially-available, waste-activated sludge

product Milorganite (Milwaukee, WI) DOM and Suwannee River Natural Organic Matter (International Humic Substances Society) were also characterized as reference materials (Kumar et al. 2014, Wang et al. 2014). We hypothesized that biosolids that had received both the THP-treatment and anaerobic digestion would contain additional refractory, larger molecular weight, and humic acid-like DOM relative to anaerobically-digested biosolids that did not have the pre-treatments, indicative of slower decomposition and mineral N releases. Our approach contributed to a better understanding of the nature of DOM and its influence of N release.

The second goal of this study was to determine the percent of mineral N released from THP-AD biosolids in 105-day (3 ½ month growing season) aerobic soil incubation experiments, and whether this differed significantly from AD biosolids without the pre-treatment. Fluorescence in leachable DOM was also tracked over time to understand which optically active DOM components may preferentially decay. The soil mesocosm-based work of Sommers et al. (1981), the bases of current U.S. management guidelines, states that 20% of organic N in AD biosolids typically mineralizes to NO_3^- and NH_4^+ during the 3-month growing period in the first-year of application ($K_{min} = 0.2$). This study examined whether differently pretreated AD biosolids collected from full-scale systems mineralized differently, potentially due to fundamental differences of the organic residues.

Due to the efficient stabilizing nature of the THP-AD technology, more installations of THP-AD are anticipated at RRFs worldwide over the next decade. This study presents a fundamental characterization of AD biosolids leachates with different

treatments and possibly different mineral N releases relevant to the agricultural land-application of biosolids.

2. Materials and Methods

2.1 Biosolids Collection

Dewatered biosolids were grab-sampled from three RRFs after anaerobic digestion, with three collection dates per RFF (SI Table 1). Sample collection occurred prior to any long-term aging or storage at the RRFs. A description of the facility anaerobic digesters is provided in Table 1 (site visits, personal correspondence with facility managers and operators). At each facility, approximately 500 mL of material was collected in acid-washed glass or HPDE containers, filled with biosolids to eliminate air prior to transport. Samples were stored on ice during transport and refrigerated at 4ºC for no more than 2 weeks prior to the nutrient mineralization experiment. Whole biosolid samples were also frozen within this 2-week period for later DOM extraction and geochemical characterization tests. Repeated extracted and measurement of DOC and fluorescence confirmed that freezing the solids was not significantly altering DOM quantity or quality over time (Figure 2, SI Figure 1).

2.2 Organic Matter and Dissolved Organic Matter (DOM) Characterization

Volatile solids (VS) content of biosolids was measured by weight loss at 550^{o}C for 2 h in a muffle furnace. DOM was extracted from biosolids with deionized water in a 1:10 w/v solid:water ratio for 24 hours following Wang et al. (2013). Suspensions were centrifuged and filtered with a 0.45 μm Whatman GF/F cellulose acetate filter. DOC and

extracts were determined with a TOC/TN-L analyzer (Shimadzu, Columbia, MD). Statistical comparisons were performed with OriginLab software (Version 2018). Statistical significance was accepted at $p < 0.05$ for one-way ANOVA followed by a *post-hoc* Tukey method test for individual mean comparisons (Kumar et al. 2014).

Approximately 15 mL of aqueous leachates were lyophilized for ~48 hours in preparation for FTIR spectroscopy on a Nicolet 9000 FTIR (Thermo Fisher Scientific, Madison, WI). The spectra of lyophilized biosolids-DOM was measured with a diamond crystal accessory in attenuated transmission reflectance (ATR) mode in the wave number range of 4000 to 525 cm^{-1} with a spectral resolution of 3 cm^{-1}. Three spectra were collected per sample collection date and the results were averaged for FTIR spectra for each RRF (Figure 3).

Fluorescence spectra for excitation-emission matrices (EEM) were collected for filtered biosolids-DOM samples adjusted to 15 mg DOC L^{-1} in 3.0 mL clear quartz cuvette cells (light path 1cm x 1 cm). Fluorescence EEMs and UV-Vis were measured by an Aqualog fluorometer (Horiba Scientific; Edison, NJ). The excitation and emission wavelength ranges were 230−600 nm with a wavelength step of 3 nm for both excitation and emission. Samples were blanked against a deionized water spectrum. Inner-filter corrections, Rayleigh-Tyndall scattering, and conversion to Raman Units (RU) using water at an excitation wavelength of 350 nm (emission range 381−441 nm) were performed on all EEMs with Aqualog software, as described in Timko et al. (2015). Additional 1st and 2nd order Rayleigh-Tyndall scattering effects were removed in MatLab with corrections developed by Zepp et al. (2004).

Three-dimensional EEMs were analyzed by two methods: i) fluorescence regional integration (FRI) established by Chen et al. 2003 and ii) local maxima identification proposed by Stedman et al. 2003, Coble et al. 2007, and others (SI Tables 2a and 3). Due to consistent measurement of fluorescence signals outside of originally defined FRI boundaries defined for fluorescence maxima of pure amino acids or aquatic material, we also adapted FRI boundaries for fluorescence maxima of biosolids leachates (SI Table 2b). Chen et al. (2003) indicates that original regional boundaries were proposed to integrate the majority of a fluorophore maxima volume, despite some overlap between fluorophore signals.

Apparent molar mass distributions in DOM samples were determined with high pressure liquid chromatography size-exclusion chromatography (HPLC-SEC) using an Agilent 1200 Series HPLC (Santa Clara, CA) with a photodiode array (PDA) detector operating at 280 nm. A guard column and two stainless steel (8 x 300 mm) SEC columns (MCXGPC 1000 and 100,000 Å, PSS Polymer Standard Service-USA, Inc Amherst, MA) were connected in series. Polystyrene sulfonate standards (PSS-Polymer Standard Service-USA) with nominal molar masses ranging from 1 to 67 kilodaltons (kDa) and a low molecular mass 4-ethylbensulfonic acid (186 Da) standard, all at ~2.5 mg/mL, were applied to develop a linear calibration of log molar mass to column retention time (Cabaniss et al 2006, Omoike et al, 2006, and Hernandez-Ruiz et al. 2012). Standards and samples were made in a circumneutral (pH 7.4) 20 mM sodium phosphate buffer solution prepared with nanopure water. Samples were prepared at 30 mg C L^{-1} in the 20 mM phosphate buffer. The 20 mM phosphate buffer was also the mobile phase for isocratic HPLC-SEC runs. Samples and standards were injected at 50 µL and a flow rate of 1

mL/min. The linear relationship between standards log molar mass (MM) and retention time was Log(MM) = -0.572 (min) + 13.4 ± 0.45, adj. R-square = 0.97. Sample peak retention times were chosen with Origin Lab software. This retention time was converted to apparent, peak molar mass (M_p) by the linear relationship of standards log (MM) to retention time.

2.3 Nitrogen Mineralization Rate Experiments

Samples from collection dates in October 2015 were amended to soil to measure nutrient mineralization. Nitrogen mineralization rates were determined by soil-biosolid mesocosm incubation experiments over a 3-month period, to replicate the growing season. A fine sandy loam soil from a historic A_p horizon was collected from the University of Maryland's Hayden Farm, Beltsville, Maryland, USA. Soil was collected April 7, 2015 from the periphery (grassy area, 15 feet from tilled soil) of a field that had not yet received inorganic or organic nitrogen that season (personal correspondence with farm manager). Soil was then kept in clean, plastic storage containers at -20°C prior to use. Soil inorganic N (NH_4-N and NO_3-N) was extracted with 2M KCl from moist samples and measured colorimetrically (Mulbry et al. 2005) and total N was determined by combustion-based analysis (LECO, Bremner and Mulvaney, 1982). These analyses confirmed low, background N levels prior to experiments, relative to biosolids amendments (Figure 1a). Both bulk soil and biosolids were sieved (2 mm) separately before mixing. Soil was then homogenized by first sieving it, then spreading it onto a large tarp, followed by folding up and recombining the soil and re-spreading it 9 to 10 times to thoroughly mix the material. Field capacity (10 kPa) of sieved, homogenized soil was determined with a pressure plate apparatus (Klute, 1986). Incubation experiments

were maintained at 80% field capacity, or 17.9% moisture on a dry weight basis, accounting for the moisture in biosolids, following Kumar et al. (2014). Soils were air-dried to 12.5% moisture prior to the experiment, and mesocosms were brought to 17.9% moisture (dry-weight basis), including the moisture from un-dried biosolids. All moisture content of soils and biosolids was determined as weight loss upon drying at 105ºC for 24 h in an oven. Eighty percent of field capacity moisture for the test soil was determined to be 17.9% water on dry soil basis, determined by pressure plate moisture release curves.

To set up mesocosms, biosolids were mixed to soils at a general first-year agronomic application rate of 25 Mg/ha, equating to 50 grams of soil, dry weight basis, to 1.12 grams biosolid, dry weight basis (Kumar et al. 2014) per replicate jar. The mixture was prepared in bulk and then split for 30 glass-jar replicates total. The experiment was set up for 30 identical incubations per treatment with the following five biosolids treatments: (i) control incubations (soil only), (ii) Milorganite, (Milorg) (iii) St. Mary's County MD facility with holding prior to AD (AD-1), (iv) Sod Run facility, MD with fermentation-AD (AD-2), and (v) DC Water Blue Plains (THP-AD). Milorganite is a kiln-dried activated sludge product (Milwaukee, WI) that was used as an amended reference material, is commercially available and was used to compare measurements with previously published results (Kumar et al. 2014).

Mesocosms were kept in a temperature and humidity-controlled chamber (80%) at 20°C, and maintained at ~17.9 % moisture, by weight, every 3-4 days. Approximately every 10 days, triplicate mesocosms of each of the five treatments were removed from the chamber for PAN measurements, for a period of 105 days. NH_4^+-N and NO_3^--N in the mesocosms was determined by extracting 10 grams of soil with 100 mL 2 M KCl on a

reciprocating shaker for 1 hour. Extracts were then centrifuged for 10 minutes and filtered through a 0.45 µm Whatman GD/X cellulose acetate filter. Nitrate and ammonia in soil extracts were analyzed colorimetrically on a Lachat QuickChem Autoanalyzer (Methods 12-107-04-1-B and 12-107-06-2-A, Lachat Instruments, Loveland, CO).

Mineral N accumulation (NH_4^+-N and NO_3^--N) of days 0 to 105 of incubation was calculated by subtracting initial mineral N levels measured in soil and biosolids mixtures on day 0 or the start of the incubation. Mineral N development and rates of N mineralization have been previously modeled by pseudo-first order kinetic model first proposed by Standord and Smith (1972) (Kumar et al. 2015, Equation 1).

$$Mineral\ N\ =\ Potential\ MN\ (1 - e^{-kt})$$

(Eqn. 1)

where MN is the accumulated mineral N (sum of NH_4^+-N and NO_3^--N mg kg^{-1} soil) during incubation, time t (days), Potential MN is the potentially mineralizable N at t_0 (mg N kg^{-1} soil), and *k* is the rate constant (d^{-1}). Data was fit to the Stanford and Smith (1972) model by the non-linear least-square technique to determine potential MN, *k*, coefficient of determination (R^2) values and generate confidence bands for the model (GraphPad Prism 6.07 software).

The fraction of potentially mineralizable N to total organic, mineralizable N at the beginning of the incubation experiment was also calculated according to Equation 2.

$$\text{Fraction N Mineralized} = \frac{(Potential\ MN,amended\ Soil - Potential\ MN,control\ soil)}{Biosolids\ Organic\ N}$$

(Eqn. 2)

2.4. Fluorescence Changes of Biosolids-DOM in during aerobic soil mineralization

DOM was extracted from biosolids-soil mesocosms on days 45 and 105 of incubations to measure fluorescence changes during mineralization. Triplicate biosolids-soil mixtures for each treatment were equally massed to extract DOM in a 1:10 ratio (weight:volume) with dionized water according to Section 2.2. DOM was also extracted from control soil incubations that did not receive biosolids addition. All DOC was adjusted to 7.5 mg C/L before fluorescence measurement and fluorescence spectra was measured for biosolids-soil and soil extracts as described in Section 2.2. The fluorescence spectra of soil-only DOM was subtracted from biosolids-soil DOM to isolate changes in biosolids-DOM only over time via Matlab (MathWorks; Natick, MA). The residual spectra of Day 45 and 105 for biosolids-DOM only and soil-only was also subtracted to evaluate changes in biosolids-DOM during aerobic soil mineralization (Figure 5).

3. Results

3.1.1. Geochemical Characteristics of Biosolids and DOM

The three types of anaerobically digested biosolid samples (3 collection dates) had different pre-treatment processes prior to anaerobic digestion (Table 1). The total % solids (TS) in dewatered biosolids was 12% greater in THP-AD than AD-1 and AD-2 and the average volatile solids in dewatered biosolids was 54.6 ± 5.6 % for all three RRFs, including multiple sample dates. The VS content for the three RRFs over 3 collection dates per plant was not significantly different by one-way ANOVA (p = 0.24). The VS% in the Milorganite amendment was 37.5%. The pH of the three dewatered biosolids also did not vary significantly across types and ranged from 7.9-8.5 The extracted biosolids

DOM pH varied less than 0.3 pH units across types, ranging from 7.47 to 7.88 ± 0.62 (Table 1).

Total organic carbon and solids total nitrogen was significantly greater in Milorganite solids than biosolids products from RRFs with anaerobically-digested biosolids (Figure 1 a.). The individual RRF biosolids TN content was not statistically different for the three AD RRFs, including multiple collection dates (Figure 1). The TN of Milorganite was significantly greater at 59.0 ± 0.1 g/kg d.w. compared to averaged biosolids N = 47.5 ± 1.9 g/kg d.w. Significantly more (2-fold) leachable organic carbon and nitrogen was extracted from the Milorganite product than the dewatered AD biosolids products (Figure 1b.). The THP-AD biosolid leached less DOC than the other two biosolids products = 17.1 ± 0.4 mg C/kg and 13.4 ± 3.1 mg N/kg d.w. The C:N ratios of biosolids-amended soil treatments and Milorganite-soil treatments averaged 13.5 ± 0.9 and was not significantly different across the treatments.

3.1.2. DOM Fluorescence characteristics

Excitation-emission matrices (EEMs) provide information on the composition and relative proportion of previously characterized DOM fluorophore components (SI Table 2 and 3, Chen et al. 2003, Coble et al. 2007, and Hudson et al. 2007, and others). We observed that the Fluorescence Regional Integration boundaries originally defined for aquatic DOM and pure amino acids did not consistently capture fluorescence signal > 400 nm excitation and emission observed in all AD-biosolids leachates. Additionally, FRI regions I and II associated with tyrosine and tryptophan-like fluorescence bisected fluorescence maxima at Ex_{max}:Em_{max} 240:340. We therefore proposed adapted FRI boundaries for biosolids-DOM leachates because FRI was originally defined to integrate

fluorescence maximas (Chen et al. 2003, Figure 3b, SI Table 2b). By classically defined FRI, the major proportion of AD biosolids-DOM fluorophores were tyrosine, microbial-by-product-like, and tryptophan-like, or T peak dominated, consistent with biomass and proteinaceous material (Baker et al, 2002, Figure 3, Table 2). By adapted FRI, AD-1 and AD-2 contained 62-65% of total fluorescence in the UV-region of 1&2, and THP-AD DOM contained 53.1%. All AD biosolids DOM also contained fulvic and humic acid-like fluorophores (Regions III and V, peaks C and A, Table 2). All anaerobically-digested DOM samples contained a low-energy absorbing fluorophore around Ex/Em: ~420/470 for multiple collection dates. This red-shifted peak fell out of previously defined FRI boundaries but has been described by D/E peak component of soil fulvic acids (Stedmon et al. 2003). Modified fluorescence boundaries integrated this signal, but the fluorescence percentage (*P%*) of Region 5 stayed within 4-9% of total fluorescence because the total integrated area for all signals increased. Milorganite-DOM lacked the distinct red-shifted fluorophore <400 nm ex:em, with major fluorescence being in protein-like (regions I, II, IV, peak T) and fulvic and humic acid associated fluorophores (region III, V, or peaks C and A, Table 2). The dominance of aromatic amino acids and microbial byproduct-like fluorescence in sludge-derived DOM samples are consistent with the combination of microbial degradation products in sludge and biomass-driven transformation processes occurring at RRFs (Luo et al. 2013, Sun et al. 2016). Presence of red-shifted humic or fulvic acid-like fluorescence have also been observed as a result of waste stabilization and release of complex conjugated aromatic material (Wang et al. 2013)

Five fluorescence maxima were consistently observed for multiple sampling dates per RRF, with less than 2% variation in classically defined FRI %*P* per region (SI Fig. 2 and 3).

3.1.3. FTIR spectral characteristics of DOM

The average absorbance FTIR spectra for each anaerobic-biosolids DOM types are overlaid in Fig. 3a for direct comparison. Reference material DOM derived from Milorganite and Suwannee River Natural Organic matter are overlaid in Fig. 3b. Both the reference materials and anaerobic biosolids-DOM contained absorption bands in the 3000- 3500 cm^{-1} range associated with broad hydroxyl stretching (Leenheer, 1981). This phenolic stretch was broader in the reference materials than anaerobically-digested biosolids-DOM, with a pronounced peak at 3288 cm^{-1} for both AD-1, AD-2, and THP-AD DOM samples overlaying the phenolic region. The peak at 3288 cm^{-1} has been associated to nitrogenous amine and amide absorption bands, consistent with the proteinaceous origins of biosolids (Fig. 3a, Huo et al. 2008, Marcato et al. 2009). The anaerobically-digested DOM samples also contained a pronounced absorption band at 2925 cm^{-1} previously described for the stretch of methyl (– CH) moieties in the 2930-2850 cm^{-1} range (Smidt and Meissl, 2007, Wang et al. 2013). The AD-1 DOM spectra contained smaller absorption bands at 1641 cm^{-1} associated with oxidized C=C and C=O vibration of aromatic ring modes, carboxylates, and amides in relation to AD-2 and THP-AD DOM samples, possibly because AD-1 DOM contained no pre-treatment to anaerobic digestion that facilitates stabilization (Table 1, El Fels et al. 2014). Additionally, AD-2 (prior fermentation) and THP-AD biosolids-DOM contained increased intensity at band 1554 cm^{-1} associated with the planar N-H vibration of amides.

Similar bands in the 1250-900 cm^{-1} range are consistent with C-O-C, C-O, and C-O-P vibrations consistent with of polysaccharides and phosphodiester-bonds found in biological breakdown products (Wang et al. 2013).

The AD DOM absorption bands in the 2000-500 cm^{-1} range contrasted that of the reference materials SROM and Milorganite DOM, suggesting more significant differences in the carbon backbones of the DOM (El Fels 2014). Major bands in SRNOM shifted and were observed at 1716 cm^{-1} (C=O vibration, associated to aldehydes, ketones, carboxylic acids, and esters), and at 1173 cm^{-1} in the 1250-900 cm^{-1} range of C-O-C, C-O, and C-O-P vibrations or polysaccharides and phosphodiesters. The Milorganite DOM contained unique bands at 1584 cm^{-1} (C=C aromatic skeleton) , 1407 cm^{-1} (COO- stretch of carboxylic acids) and 1043 cm^{-1} (polysaccharide region) (Smidt and Meissl, 2007, Huo et al. 2008, Wang et al. 2013).

3.1.4. High Performance Size Exclusion Chromatography of DOM

Anaerobically-digested biosolids DOM contained consistent peak apparent molar masses (M_p) across several collection dates. The Mp of anaerobically-digested biosolids DOM ranged between 1192 Da to less than 186 Da (SI Fig. 2a – 2c). Generally, three mass populations (M_p) were observed for anaerobically-digested biosolids-DOM across different RRFs and dates, indicating consistent heterogeneity. Although the intensity of the UV-response varied across multiple sample dates, similar molar mass peak locations were observed for biosolids-DOM. These results suggest that while relative abundance of aromatic DOM masses could vary across collection dates, similar molar mass populations remain present in anaerobically-digested biosolids DOM. Variation in the UV-response could also indicate different levels of DOC in the dilutions targeting 30 mg C L^{-1}.

The molar mass range of DOM from THP-AD biosolids was within the molar mass range of DOM extracted from biosolids with different configurations of anaerobic digestion treatment, either no pre-treatment or fermentation prior to digestion. Milorganite leachate also contained three peak molar mass populations 188 to 1182 Da (SI Fig. 2e). These peak molar mass range (M_p) of sludge and biosolids DOM are similar to previously reported wastewater sludge DOM (Hernandez-Ruiz et al. 2012). Consistent with past results, the wastewater derived DOM samples were also more heterogeneous than plant-derived, humic-acid rich Suwannee River Natural Organic Matter (SRNOM) (SI Fig. 2d., Cabaniss et al. 2000, Hernandez-Ruiz et al. 2012).

3.2. Nitrogen releases in biosolids-soil mesocosms

A pulse of NH_4^+ was released from all amended soils during the first twenty days of the incubation experiment (Figure 4 a.) The Milorganite product released a maximum of 192.2 ± 4.70 mg NH_4^+-N/kg (d.w.) by day eight, while AD-1 and THP-AD released 166.2 ±2.30 and 153.4 ± 4.23 mg NH_4^+-N/kg, respectively. A maximum of 110.9 ± 1.92 mg NH_4^+-N/kg was released from limited fermentation pretreated AD-2 on day eight. After NH_4^+ release decreased, oxidation of NH_4^+ to NO_3^- controlled mineral N levels after day twenty (Figure 4b). The 105-day net inorganic N produced by AD-1 solid (with no pretreatment) was 155.3 ± 12.07 mg N/kg, AD-2 (fermentation pretreatment) was 148.5 ± 18.19 mg N/kg, THP-AD biosolids was 139.7 ± 17.41 mg N/kg and Milorganite was 353.7 ± 15.09 mg N/kg d.w. basis.

Net Mineral N production in soil incubations followed first-order kinetics of the Standford and Smith (1972) model (Figure 5, Eqn. 1). Models had coefficient of variation (R^2) values ranging from 0.82 (THP-AD) to 0.97 (Ferm-AD-2) (SI Table 5). The

potential mineralizable N (PMN) was highest for Milorganite, followed by AD-2, AD-1, and THP-AD biosolids respectively, and lowest for the unamended soil. The 95% confidence intervals of model fits and potentially mineralizable N for the three types of anaerobically-digested biosolid treatments overlapped by the end of 3 months, while confidence intervals for Milorganite and unamended soil were independent of other treatments (SI Table 5). Overall, the Milorganite treatment could be characterized with distinctly higher mineral N releases than the three anaerobically-digested biosolids treatments, with the control soil having distinctly lower mineral N release than all other treatments, accounting for any differences in initial N content.

Similarly, the net fraction of N mineralized was not statistically different between anaerobically-digested biosolids and was greatest for Milorganite (Eqn. 2, Figure 5). The fraction of biosolids-N mineralized represents the ratio of potential mineral N released relative to the initial organic N in the amendment at Day 0, subtracting soil organic N release measured in control soil. The percent of N mineralized of the Milorganite amendment, 68 ± 14 %, was up to two times greater than the fraction of mineral N released from the three anaerobically digested biosolids experiments. The fraction of N mineralized (K_{min}) across the three AD biosolids treatment types varied as follows: AD-1 = 34 ± 14 %, AD-2 = 34 ± 13%, and THP-AD= 23 ± 8 %. While the Error propagation resulted in that no AD biosolid treatment was considered to have a statistically different mineral N release after a 3-month growing season incubation. Propagated errors carried from measuring N in triplicate experiments, model PMN confidence intervals, determining organic N by difference of TN – inorganic N, and uncertainty due to analytical methods. The uncertainty term increased significantly from averaging replicate

mesocosms TN values, and additional error propagated subtracting TN in control-soil mesocosms from TN in replicate biosolids-amended mesocosms (Eqn. 2).

3.3. Transformation of biosolids-DOM in biosolids-soil mesocosms over time

Biosolids amendments were a significant source of both carbon and nitrogen to the fine sandy loam soil mesocosms (Figure 2). DOC extracted from aged soil-only mesocosms contained red-shifted fluorescence maxima associated with peaks A and C, or fulvic acid-like and humic acid-like fluorescence that has been previously observed in soil extracts (Hassouna et al 2010, Figure 6d). This carbon may be due to cellulosic origins or lignin degradation. Biosolids-DOM, in contrast, were a source of additional carbon pools to soils with both blue-shifted and red-shifted fluorophores that have been associated to amino acids, polyphenols, protein-like degradation products (Peak B/T) as well as soil fulvic acids <400 nm (Figure 6a-c). The greatest loss in a Biosolids-DOM fluorophore maxima occurred for THP-AD-soil mesocosms at an Ex:Em of 275nm/345nm with almost complete loss of the amino acid or polyphenol associated B/T peak after 105 days of incubation time (Table 2). All biosolids-DOM treatments lost fluorescence associated with the D/E peak by day 45, suggesting that the material of this red-shifted fluorophore is easily degradable during aerobic soil mineralization of carbon. Loss of peak A and C associated material from biosolids-DOM occurred for all AD treatments (Figure 6a-c, Table 2). No measurable fluorescence was lost in the EEM of sandy soil loam soil DOM, suggesting this soil carbon pool is relatively stable and respired carbon and nitrogen predominantly came from biosolids-DOM amended to soil.

Discussion

Biosolids produce a soluble pool of organic C and N that is respired during mineralization (Cook et al. 1992, Said-Pullicino et al. 2007). Optical characterization of water-extractable DOM is a bulk, non-destructive method to examine the degree of solids stabilization or time-dependent transformations of sludges, including enzymatic-enhanced digestion or pasteurization at RRFs (Luo et al 2013, Sun et al. 2016). In this study, we utilized fluorescence and infrared spectroscopy and size-exclusion chromatography to determine the presence of refractory moieties or stabilized fluorophore content (protein versus humic acid-like) of THP-AD DOM relative to other AD biosolids, prior to soil mineralization and during aerobic degradation. Dewatered biosolids-DOM quality of the three AD RRFs tested was consistent for multiple collection dates and regardless of pretreatment or AD differences (Table 1, Figure 2, 3 and SI Fig. 2-4). Three mass populations at 165 to 1190 daltons were present in all AD DOM, reflecting the heterogeneous sources of processed sludge or wastewater organic matter (Hernandez-Ruiz et al. 2012). Aliphatic methylene bands (2920 to 2850 cm^{-1}), the C=C vibration of alkenes and aromatic components, and to the C=O vibration of amides and carboxylates (1641 cm^{-1}) detected via FTIR are associated to the refractory organics in aged soil and waste spectra (Smidt and Meissl, 2007). All three AD biosolids-DOM tested contained these refractory or sludge-related signals, and the overall absorbance pattern of the THP-AD material was not different than both AD-1 or AD-2 signals (Figure 3). The FTIR spectra of all AD-biosolids DOM was shifted and distinct from the plant-derived SRNOM DOM and WAS product Milorganite DOM.

Fluorescence spectroscopy indicated that the AD-DOM leachates were heterogeneous, containing both amino acid and microbial byproduct-like DOM pools

expected of biomass-rich material, but also humic acid-like and fulvic acid-like material that have been observed to develop during stabilization of biosolids (Wang et al. 2013, Song et al. 2015). All AD-DOM contained a low-energy absorbing fluorophore around Ex/Em: ~420/470 described as D/E Peak component of soil fulvic and humic acids, which fell outside FRI boundaries first proposed by Chen et al. 2003 (Figure 2). This Ex/Em: ~420/470 peak was not present in the waste-activated sludge product Milorganite and may be related to more extensive stabilization of the anaerobically-digested biosolids, resulting in less mineral N releases than Milorganite (Figure 4 and 5). Interestingly, the red-shifted fluorophore >400 nm ex:em was also degraded in soil mesocosms by Day 45 and was no longer detectable by day 105 (Figure 5). The second humic acid-like peak at Ex_{max}:Em_{max} 335:440 (Peak C) also degraded in the second half of the incubation experiment.

Wang et al. (2013) evaluated DOM transformations during a 100-day biosolids composting study and observed an increase in molecular weight carbon and humic-acid-like fluorescence in composted leachates materials. Development of humic acids or higher weight molecular material during stabilization has been termed "humification" and is a debated issue in soil science (Lehmann and Kleber, 2015, Olk et al. 2019). An emerging view to replace the concept of "humification", or synthesis of high molecular weight material from smaller monomers, is the concept that organic matter is a continuum of decomposing organic compounds to more soluble forms. Biosolids represent a complex, organic carbon and nitrogen rich material of proteinaceous biomass and lignin or cellulosic degradation products. The leachable biosolids DOM extracted from dewatered AD biosolids after digestion at target RRFs (Figure 2) represents a highly

heterogeneous substance characterized by five major fluorescence maxima, including humic acid-like signals previously associated to larger molecular weight, condensed aromatics. Anaerobic digestion may have liberated cellulosic or complex, condensed aromatics as Wang et al. (2013) observed during aerobic sludge composting. These "humic-acid" like signatures of AD-DOM were also observed to be the first signals to decay in the aerobic sandy loam soil that was limited in N and C prior to biosolids application (Figure 1). Our data supports the Lehmann and Kleber (2015) view that biosolids organic matter from RRFs is a complex, decomposing mixture that continued to degrade to mineral forms in soil. Zhang et al. (2017) found that C mineralization (CO_2 production) of municipal composts was a function of compost type over 50 days of incubation. In this study, only soil N mineralization rates were followed to determine K_{min} values that can be used in biosolids management. Future work connecting C quality measurement (spectroscopy), CO_2 production, and N mineralization on biosolids with additional stabilizations of limed treatment or aerobic digestion may provide insights into design parameters and complex relationships between carbon quality and agronomic N releases of treated wastes.

Our results suggest that while different configurations of pre-treatments to anaerobic digestion may benefit on-site methane production or pathogen destruction, the overall starting quality and mineralization rates of the dewatered AD biosolids tested herein were similar. The starting OC, TN, DON, VS content, C:N ratios, and DOM quality of the AD biosolids were not significantly different for multiple collection dates from the target RRFs. Only leachable DOC of THP-AD solids was 10 mg C/kg less than other AD leachates. Similarly, the fraction of biosolids-N mineralized in the 105-day

incubation experiment was also not statistically different (Figure 4 and 5). In contrast, the waste-activated sludge Milorganite product exhibited contrasting DOM quality (by FTIR and optics) and greater fraction of N mineralized than the AD-biosolids products. Kumar et al. (2014) observed a similarly greater mineral N release of 44% for soil amended-Milorganite compared with a 31-35% N release for anaerobically-digested solids on silty clay loam. In this experiment, 68 ± 14 % of initial Milorganite organic N mineralized while 23-34 % ± 21% of organic N in AD-biosolids mineralized to PAN forms in a fine sandy loam soil. Differences between our study to other studies can also be attributed to soil type. Soils with higher clay and organic matter content are cited for increasing N-mineralization rates by supporting biotic activity, while higher sand content may reduce mineralization rates (Kumar and Goh, 2000, Kumar et al. 2014). Although Part 503 of USEPA (1994) guidelines for agronomic biosolids application outlines that anaerobically-digested biosolids should be applied assuming a K_{min} = 20% mineral N release, both this study and past reports indicate that anaerobically-digested biosolids may still mineralize in a range of 11 – 45% depending on soil type, biosolids, and experimental set up (Rigby et al. 2016).

Several methods exist for determining first-year mineral N releases of biosolids. Rigby et al. (2016) provides a comprehensive review and analysis of biosolids mineralization literature, including a summary of more than twenty-five studies on anaerobically-digested solids alone. In our experiment, mesocosms were set up in accordance with the destructively-sampled replicate incubation design of Sommers et al. (1981) referenced in Part 503 of USEPA (1994) biosolids application guidelines. In this design, errors propagated when averaging TN values in replicate mesocosms and from

errors carrying during computation of K_{min} for this experiment (Eq. 2, Fig. 5). Kumar et al. (2014), Zarabi and Jalali (2013), and others have altered the Sommers et al. (1981) design to measure mineralization rates in larger-scale bulk incubations with non-destructive sampling, taking repeated measurements from one bulk soil-amendment mixture. Although bulk incubation may reduce variability, our replicate incubation design reflects analytical and experimental uncertainty inherent to multiple experiments that is not consistently reported. Wang et al. (2003a) conducted AD-biosolids mineralization tests in a column-based, leaching design and determined a PAN fraction development of 29% on brown forest soil and 17% on volcanic soils. This leaching-based method may better represent removal of mineral N akin to *in situ* processes, but the column method has been cited in both over and underestimating N mineralization due to increased soluble organic N and C releases (Wang et al. 2003b, Rigby et al 2016). Given the design-dependent range of mineral N releases for anaerobically-digested biosolids, this study's determinations are reasonably in the range of past results (Figure 5, Rigby et al. 2016). Our results suggest however, that for the purpose of relative comparison, THP-AD biosolids can be applied at similar application rates as other AD biosolids or until additional studies are completed for consensus. Further mesocosm experimentation with different design, soil types, or site-specific *in situ* field measurements (Gilmour et al. 2003, Hanselman et al. 2003) where differently pretreated AD biosolids are applied could support targeted biosolids use.

4. Conclusions

Leachable DOM profiles of anaerobically-digested biosolids were similar for three RRFs over multiple collection dates and contained a notable fluorescence signals

for low-energy stimulated ex:em >400 nm, suggestive of condensed aromatic structures released from digestion of solids. We proposed modifications to previously published FRI boundaries to better integrate biosolids-DOM fluorescence signals. Dewatered AD-DOM leachate quality and quantity significantly contrasted the Milorganite product. The overall fraction of mineral N released after the 3-month incubation of the AD biosolids was also significantly less than that of Milorganite, but not statistically different among the AD solids with different pre-treatments. Leachate humic acid-like signals degraded in aerobic biosolids-soil amended mesocosms, consistent with organic carbon decomposition and not polymerization over time. This study provides novel information on DOM leachate quality and soil mineralization rates of anaerobically-digested biosolids with different pre-treatments in support of biosolids management programs.

5. Figures – Chapter 2

Table 1: Details of three RRFs with anaerobic digestion (AD) and dewatered biosolids collected for experiments. Reported RRF information was obtained through personal correspondence with RRF supervisors. Total solids, volatile solids, and pH of solids and DOM represent the average of three collection dates for each RRF.

	THP-AD (DC Water)	**AD-1 (St. Mary's Co)**	**AD-2 (Sod Run)**	**Milorganite**
Configuration of Anaerobic Digesters	THP (160 ° C,	Holding tank prior to digestion	Fermentation of Primary Solids	Kiln-dried Waste Activated Sludge
Digester Flow Rate	0.19 MGD	0.03 MGD	0.11 MGD	N/A
Average Percent Methane in digester biogas (reported)	60-65%	~ 35 %	55-58 %	N/A
Typical retention time in any pre-treatment prior to AD (reported)	~30 minute RT	N/A	N/A	N/A
Typical hydraulic and/or solids retention time of AD systems	15-25 days (general RT)	~17.6 days (general RT)	25.3 $\pm$ 1.0 days (2017)	N/A
Total Solids (%) of final biosolids	30.3 ± 1.3 %	18.3 ± 0.7 %	18.0 ± 1.0 %	93.4 %
Volatile Solids (%) in dewatered biosolids	57.6 ± 2.4 %	50.7 ± 6.1 %	56.1 ± 4.6 %	37.5%
pH of final solids (1:2 solids: DI H_2O)	8.49	7.93	8.33	6.34
Average pH of DOM, multiple collection dates	7.88 ± 0.61	7.47 ± 0.62	7.66 ± 0.52	6.34

Figure 1: a) Organic carbon and total nitrogen (TN) of dewatered biosolids and soil before mesocosm experiments. b) Leachable dissolved organic N in itinial biosolids extracts for RRFs on a dry weight basis. Error bars represent standard deviation of three averaged collection dates. * Indicates significant difference ($p < 0.05$) in average relative other samples in set (n=3 sample dates) by a one-way ANOVA with *post-hoc* Tukey HSD test.

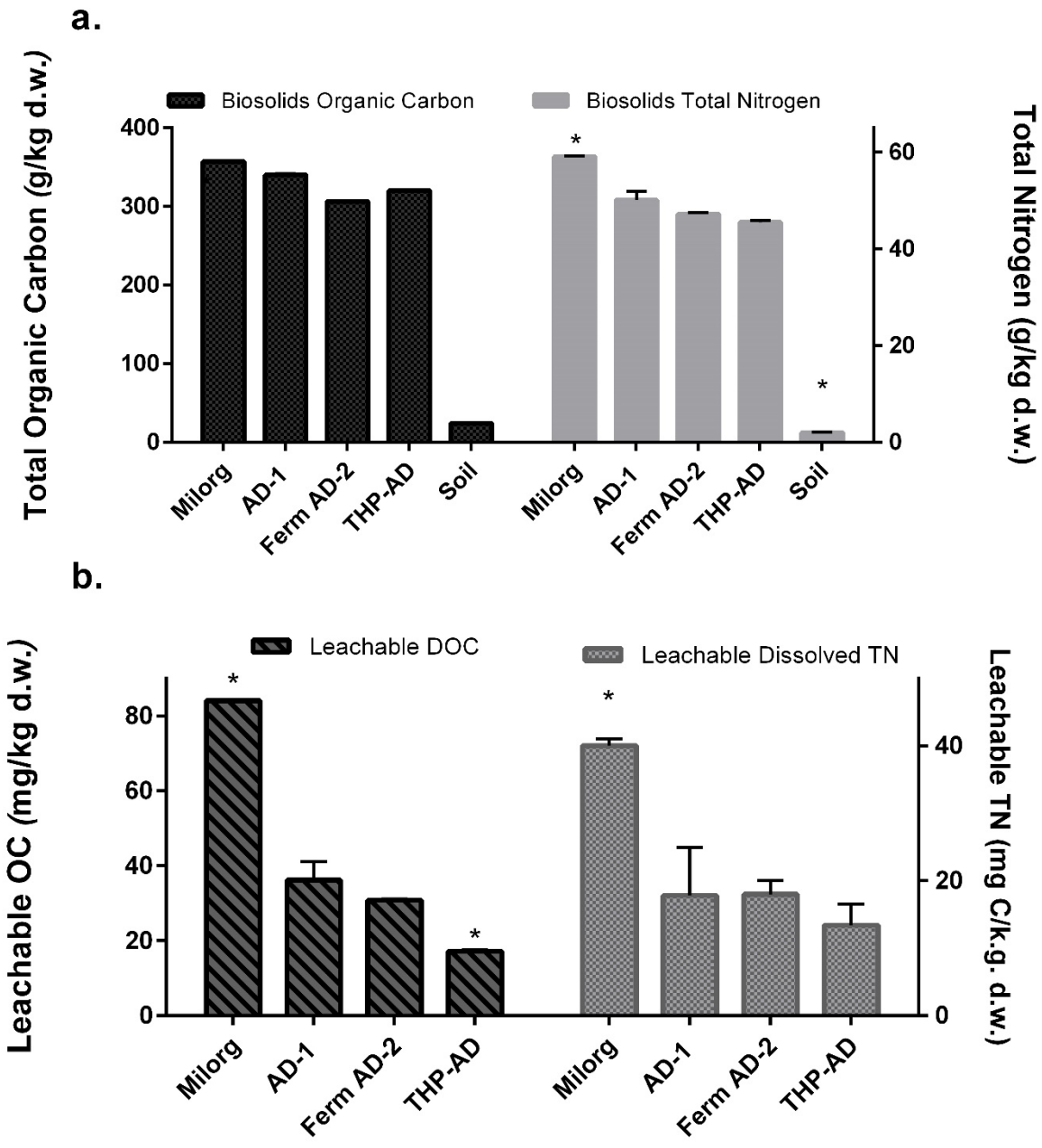

Figure 2: Fluorescence characterization of biosolids-DOM extracts at dewatering facilities. Each excitation-emission matrix represents the average of n=3 sampling dates. A) Fluorescence Regional Integration boundaries on EEMs and %*P* results according to classically defined regions published in Chen et al. (2003). B) Adapted FRI boundaries for biosolids-DOM that encapsulates fluorescence beyond ex: 400 nm and combines bisected fluorescence maxima of region I and II.

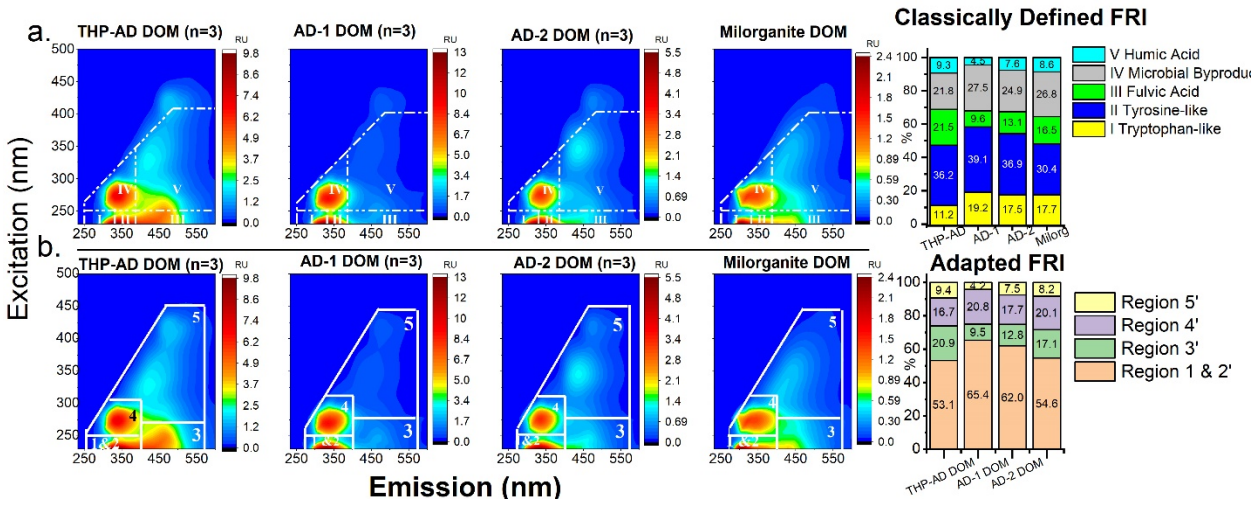

Figure 3: FTIR spectra of extracted biosolids-DOM (top panel) and DOM reference materials (lower panel). Distinct peaks (cm-1) are noted above peaks.

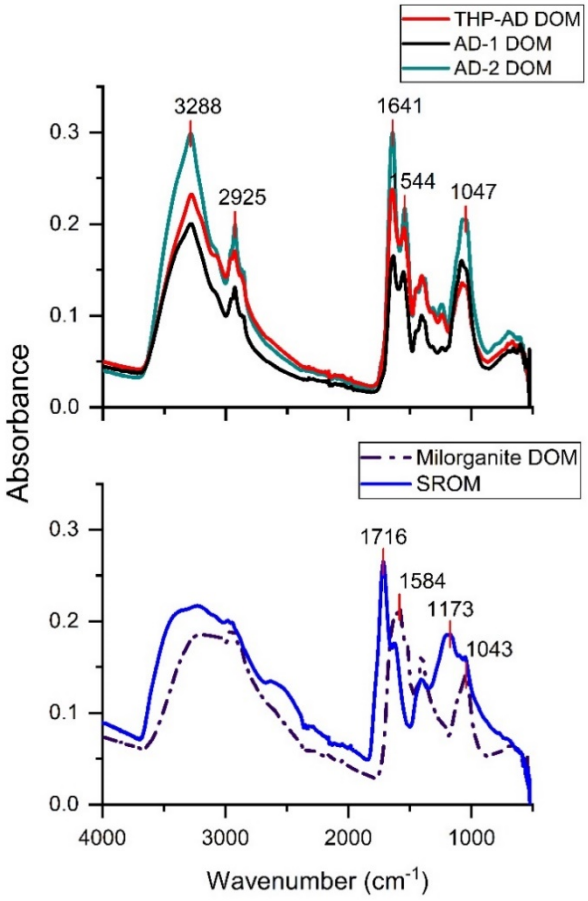

Figure 4: Mineral NH_4^+ (a.) and NO_3^- (b.) development in biosolids-soil incubations.

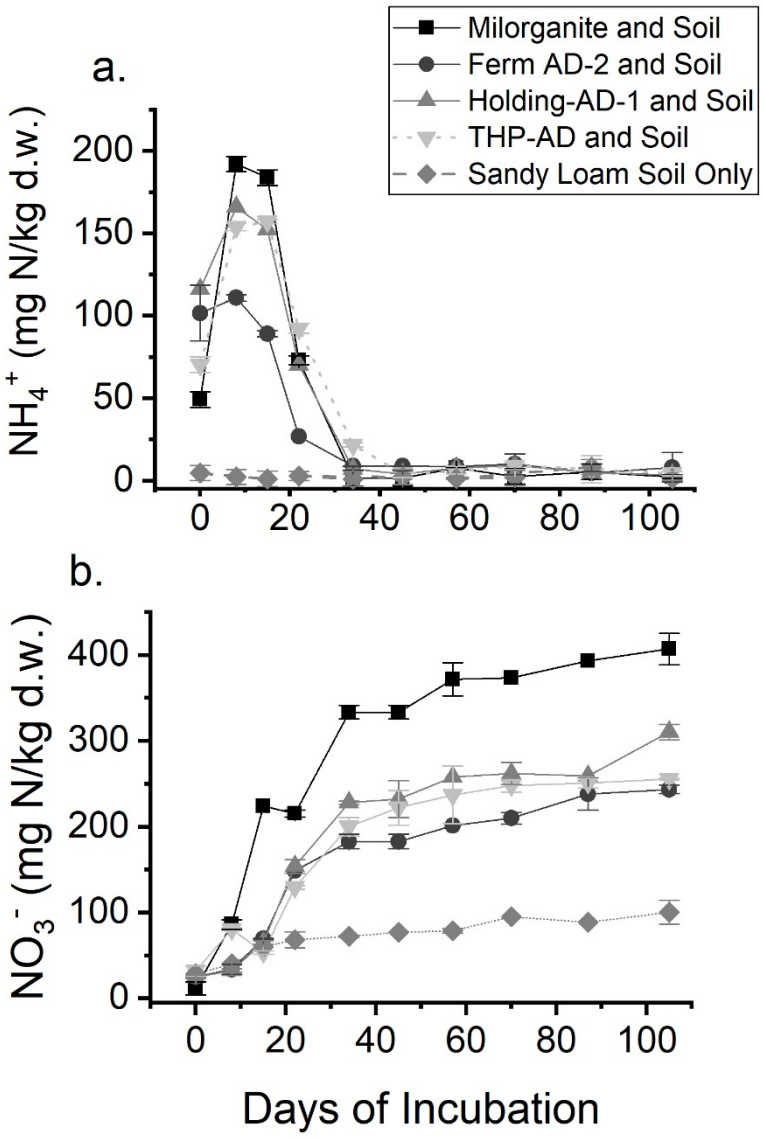

Figure 5: First-order kinetic fit of net mineral N (NO_3^- and NH_4^+) produced from aerobic incubation of biosolids treatments with confidence band shaded in grey. The fractions of nitrogen mineralized (K_{min}) per treatment are indicated below model fits and are based on the first order kinetic model (Eqn. 1, Figure 5) and initial biosolids organic N supplied to soil mesocosms (eqn. 2).

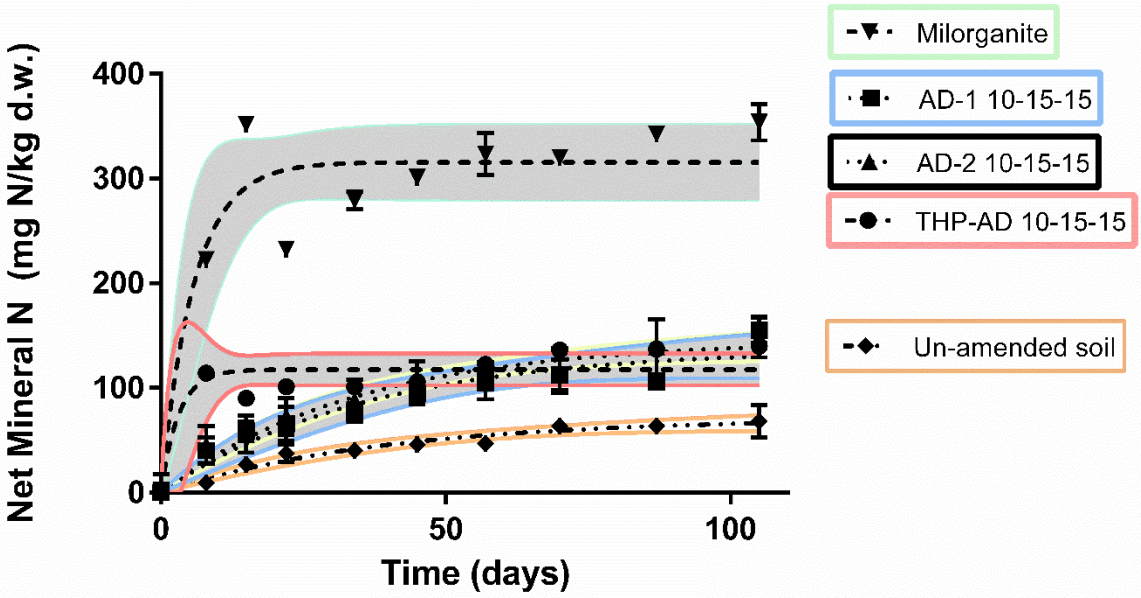

Computation of Fraction of Mineral N Released % (Eqn. 2)	Milorganite	Holding AD-1 Biosolids	Ferm. AD-2 Biosolids	THP-AD Biosolids
	68 ± 14 %	34 ± 14 %	34 ± 13%	23 ± 8%

Figure 6: Fluorescence changes in Biosolids DOM transformations over time in aerobic soil incubations mesocosms (a,c,and e). The fluorescence spectra of soil incubations (g.) were subtracted from biosolids-soil mixtures to isolate biosolids DOM decomposition. Differences in biosolids DOM from day 45 to 105 are indicated (b.,d., f.).

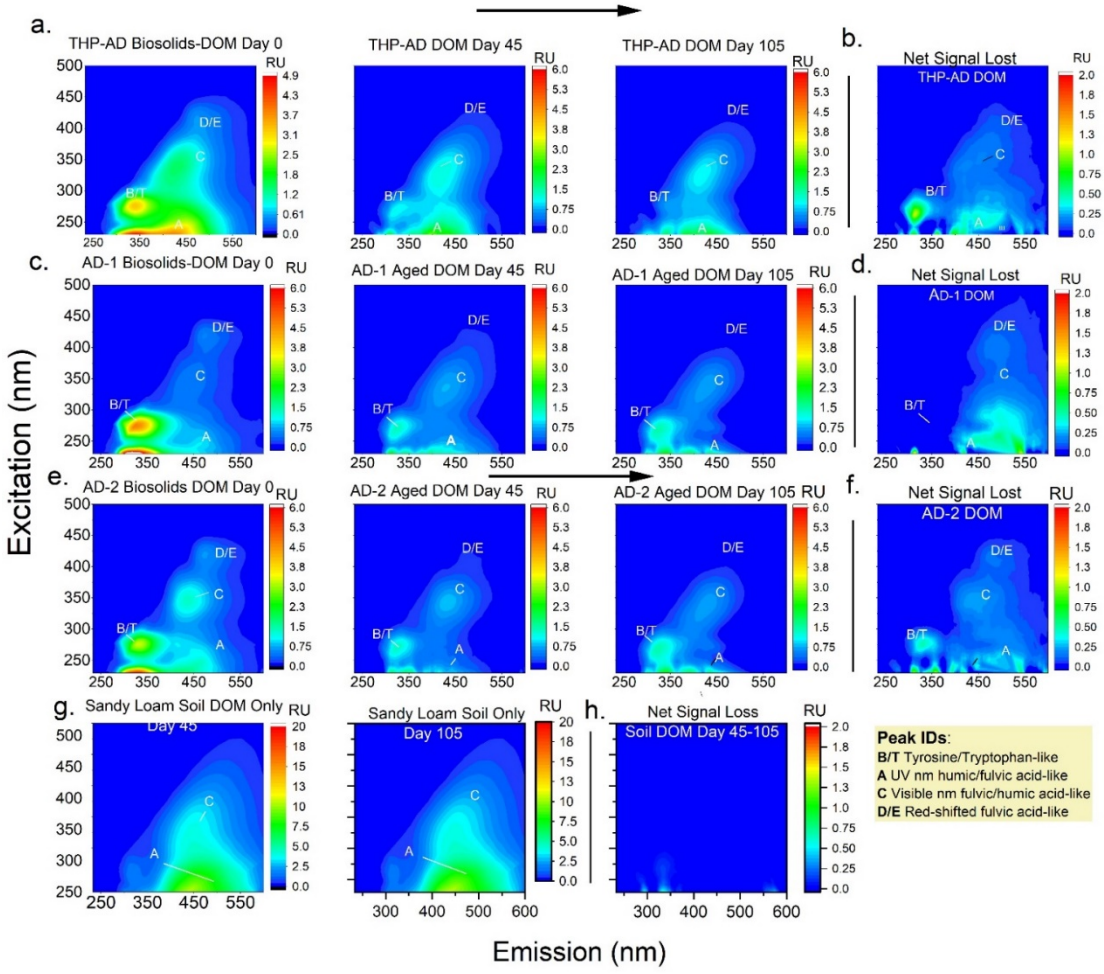

Table 2: Biosolids-DOM Fluorophore Maxima in soil incubations over time.

Literature Associated Peak:	**Peak B/T**	**Peak A**	**Peak C**	**Peak D/E**
	Raman Units/Abs@ 254	**Intensity (RU)**	**Intensity (RU)**	**Intensity (RU)**
Exact Ex:Em Location: THP-AD • Day 0 • Day 45 • Day 105 • Signal Lost Day 45 -105	275nm/345nm: 3.23 1.20 0.14 1.06	233nm /435 nm: 3.60 2.3 2 0.36	321nm/441nm: 1.45 1.20 1.08 0.17	407nm /481 nm: 0.54 0.24 0.14 0.10
AD-1 • Day 0 • Day 45 • Day 105 • Difference Day 45 - 105	275nm/339nm: 4.41 1.32 1.33 0	233nm/428nm: 1.10 1.3 0.45 0.45 (shifted)	353nm/441nm: 0.48 0.75 0.71 0.12	416nm/477nm: 0.69 0.20 0.07 0.13
AD-2 • Day 0 • Day 45 • Day 105 Difference Day 45 -105	275nm/339nm: 3.30 1.31 1.41 0.42	236nm/448nm: 1.48 0.56 0.77 0.30	347nm/441nm: 1.29 0.82 0.69 0.23	419nm/478nm: 0.64 0.14 0.05 0.13
Control Soil • Day 45 • Day 105 Difference Day 45 -105	269nm/322nm: 1.4 1.4 --	236nm/455nm: 9.8 9.9 --	320 nm/455 nm: 3.9 4.0	--

6. Supporting Information

SI Figure 1: Field work and mesocosm set-up photos. Photos a.) and b) are soil collection at 5 – 15 cm depth of fine sandy loam soil from a historic A_p horizon at University of Maryland's Hayden Farm, 10 feet away from crop. Initial inorganic N in soil was determined and accounted for (subtracted) in N mineralization rate determinations. Photo c.) shows the destructively sampled mesocosms of soil and biosolids mixtures in temperature (20◦C) and humidity-controlled dark growing chamber. Photo d.) shows the water extraction of dissolved organic matter from biosolids samples before amendent to soil mesocosms and DOM characterization.

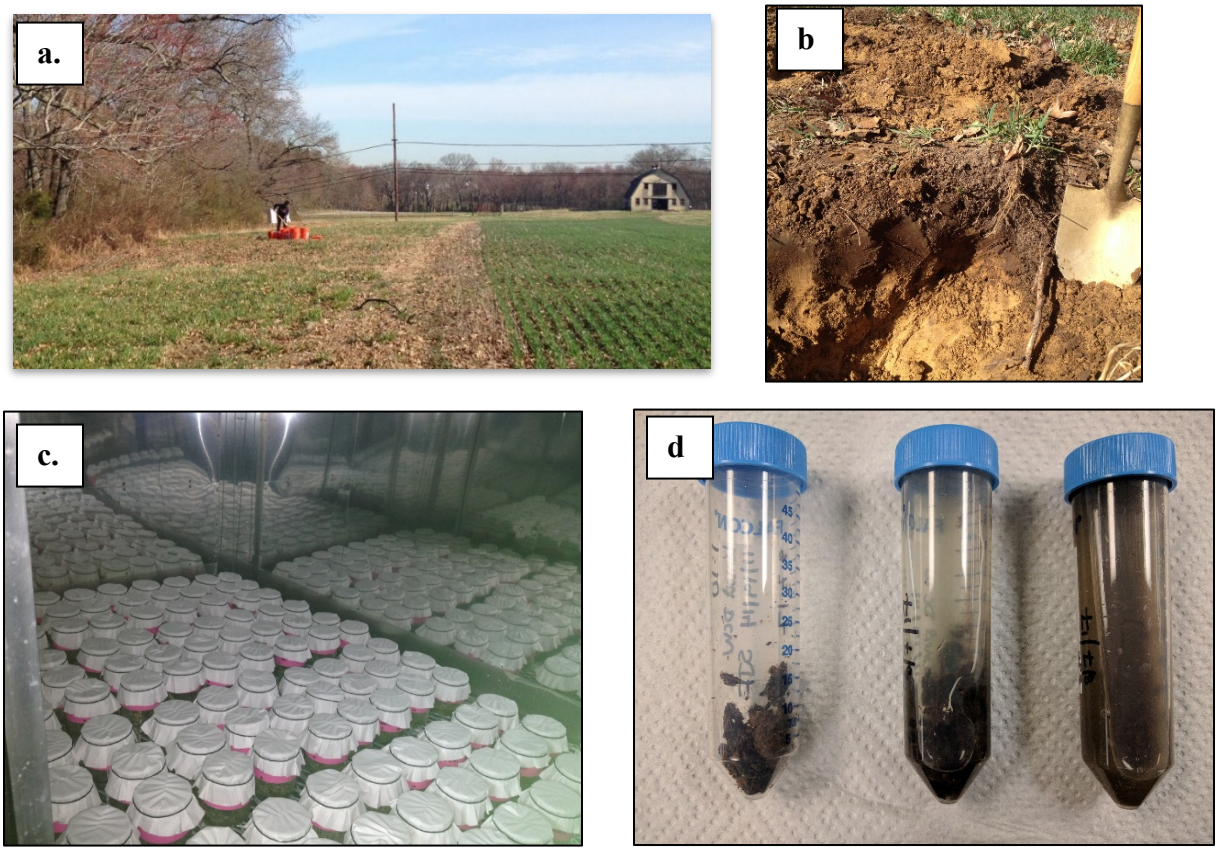

SI Table 1: Biosolids and soil collection dates. Asterisk (*) indicates biosolid sample date used for N mineralization experiments.

	AD Biosolids and Soil Collection Sample (MM-DD-YYYY)		
THP-AD	4-22-2015	10-14-2015*	1-10-2017
AD-1	4-21-2015	10-6-2015*	1-10-2017
AD-2	10-1-15*	1-10-2017	10-15-2017
A_p Horizon Sandy Loam Soil, Beltsville, Maryland, USA	4-7-15		

Additional Fluorescence Regional Integration (FRI) Analysis Applied to EEMs, Based on Chen et al. (2003):

Total fluorescence of DOM was integrated for five previously described regions; (I) "tyrosine-like", (II) "tryptophan-like", (III) "fulvic acid-like", (IV) "microbial by-product-like, and (V) "humic acid-like" (Chen et al., 2003, SI Table 1). Following Hernandez-Ruiz et al. (2012) the total volume (ϕ_i) of each region of the EEM boundaries is summated by:

$$\phi_i = \Sigma_{Ex}\Sigma_{Em} I(\lambda_{Ex}\lambda_{Em}) \Delta\lambda_{Ex}\Delta\lambda_{Em}$$

where $\Delta\lambda_{Ex}$ is the excitation wavelength interval, ΔEm is the emission wavelength interval and I (Δ_{Ex}, Δ_{Em}) is fluorescence intensity at each excitation-emission wavelength pair. The total number of data points for each region are counted to produce the fractional projected excitation-emission factor (F_i). The normalized fluorescence intensity volume (ϕ_{in}) beneath region of the DOM sources is then computed:

$$\phi_{in} = F_i \, \phi_i$$

The fluorescence percentage of each region is calculated by

$$P = \phi_{in} / \phi_{T,n} * 100\%$$

Where (ϕ_{Tn}) is sum of all normalized fluorescence of all regions. The final fluorescence percentage of each region (organic matter type) of each sample date (SI Figure 2) were also averaged by sample collection date (Figure 2). FRI was also conducted over modified boundaries adjusted to encapsulate fluorescence maxima in biosolids DOM, as well as signal beyond an excitation of 400 nm (SI Table 2). Volume of each regions were summated with equations 1-3.

Statistical comparisons of normalized fluorescence regions over multiple dates were performed with OriginLab software (Version 2018). Statistical significance was accepted

at $p < 0.05$ for one-way ANOVA followed by a *post-hoc* Tukey method test for mean region comparisons (SI Figure 2).

FRI was also conducted over modified boundaries adjusted to encapsulate fluorescence maxima in biosolids DOM, as well as signal beyond an excitation of 400 nm (SI Table 2). Volume of each regions were summated with equations 1-3.

SI Table 2a: Excitation and emission (Ex/Em) wavelength boundaries applied for classically defined fluorescence regional integration (FRI) analysis of biosolids-dissolved organic matter extracts. Based on Chen et al. (2003).

Region	**Description**	**Ex/Em wavelength boundaries (nm)**
I	Tyrosine-like protein	230–250/233–330
II	Tryptophan-like protein	230–250/330–380
III	Fulvic acid-like organics	230–250/380–600
IV	Soluble microbial by-product	250–340 diagonal/260–380
V	Humic acid-like organics	250–340, 340-400 diagonal /380–600

SI Table 2b. Modified FRI Regions for Biosolids-DOM Leachates:

Region	**Potential Fluorophore Composition**	**Ex/Em wavelength boundaries (nm)**
1 & 2	Tyrosine-like, Tryptophan-like, or polyphenol	230–250/250–400
3	UV ʎ fulvic or humic acid-like	230–275/400–550
4	Soluble microbial by-product or polyphenol-like	250–325 diagonal/270-400
5	Visible ʎ excited humic or fulvic acid-like	275–340 diagonal/260–575

SI Table 3: Fluorescent (FDOM) Component Peaks proposed by Stedman et al. 2003 and Coble et al. 2007:

Peak	Potential Fluorophore Type, considering source as well	Ex_{max}	Em_{max}(nm)
B	Tyrosine-like protein	275	305
T	T_1, Tyrosine-like, protein-like (T_2 for phenolic sources, Maie et al. 2007)	275	340
N	Associated with phytoplankton productivity	280	370
A	Humic-like and fulvic acid-like	260	380-460
M	• Anthropogenic from wastewater and agriculture • Marine humic-like	290-310	370-410
C	Visible Humic-like	320-360	420-480
D	Soil fulvic acid	390	509
E	Soil fulvic acid	455	521
P	Pigment-like	398	660
	Other, UVA Humic-like Fulvic acid, terrestrial, autochthonous	250 (385)	504

SI Table 4: Peak Intensities and assignments of Biosolids-DOM presented in Figure 3, with FRI.

Peak Assignment	**Peak T/B**		**Peak A**		**Peak C**		**Peak D/E**	
Sample (n=3 dates)	**Intensity (RU)**	**Ex/Em (nm)**	**Intensity (RU)**	**Ex/Em (nm)**	**Intensity (RU)**	**Ex/Em (nm)**	**Intensity (RU)**	**Ex/Em (nm)**
THP-AD	6.69	272/349	4.94	242/458	2.17	329 /424	1.55	410/480
AD-1	8.79	272/343	1.78	245/471	0.77	335/448	0.69	416/488
AD-2	3.30	275/342	1.19	245/461	1.18	347/441	0.52	419/478
Milorganite	1.35	345/272	0.89	233/431	0.40	335/431	--	--
Suwannee River Natural Organic Matter (SRNOM)	--	--					--	--

SI Figure 1: EEMs of multiple collection dates per RRF indicate five consistent fluorescence maxima per sample. Classically defined FRI boundaries (Chen et al. 2003) are indicated. Fluorescence signal was consistently observed outside FRI boundaries and motivated adaptation of boundaries descripted in SI Table 1b and Figure 3.

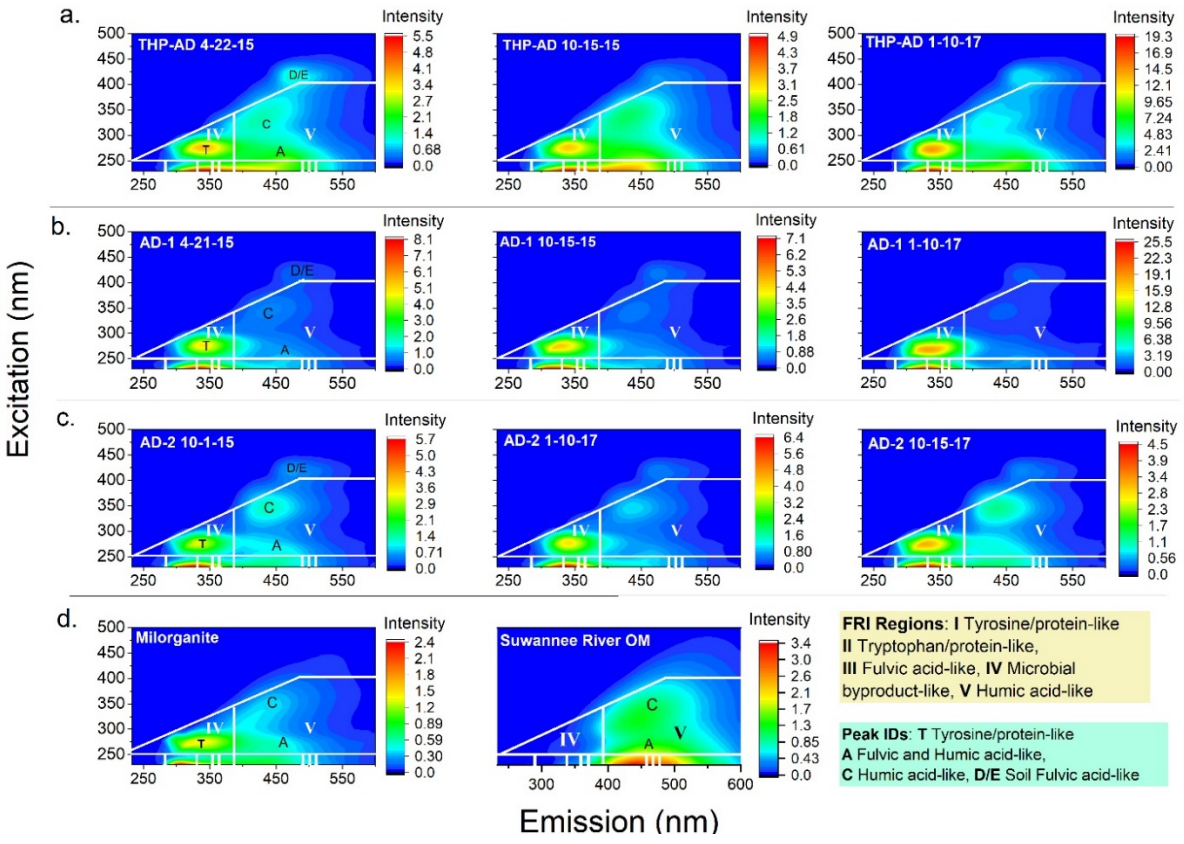

SI Figure 2: Normalized relative proportion of classically defined FRI boundaries for RRF DOMs for all collection dates. %*P* varied 2-3% per region, per RRF, for across multiple collection dates.

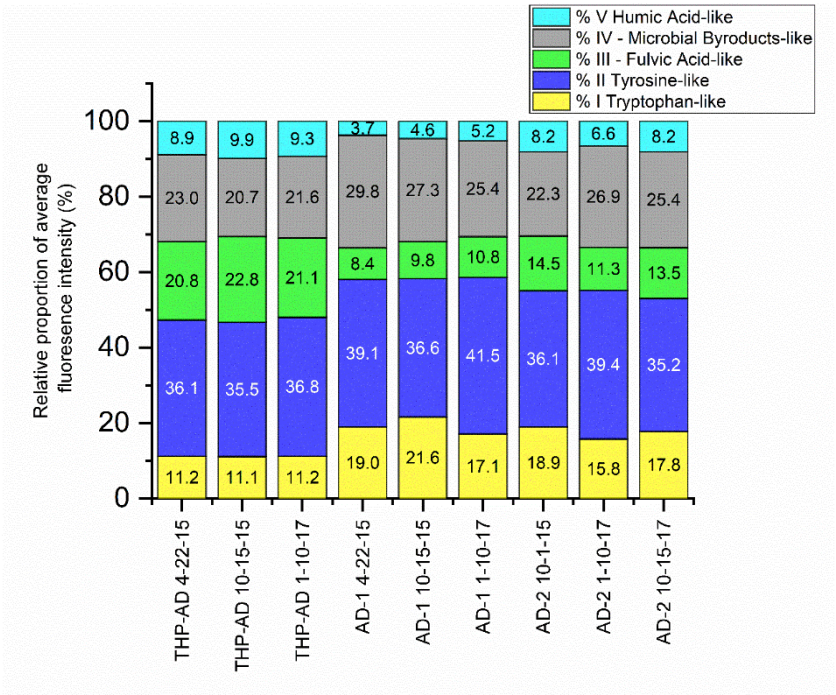

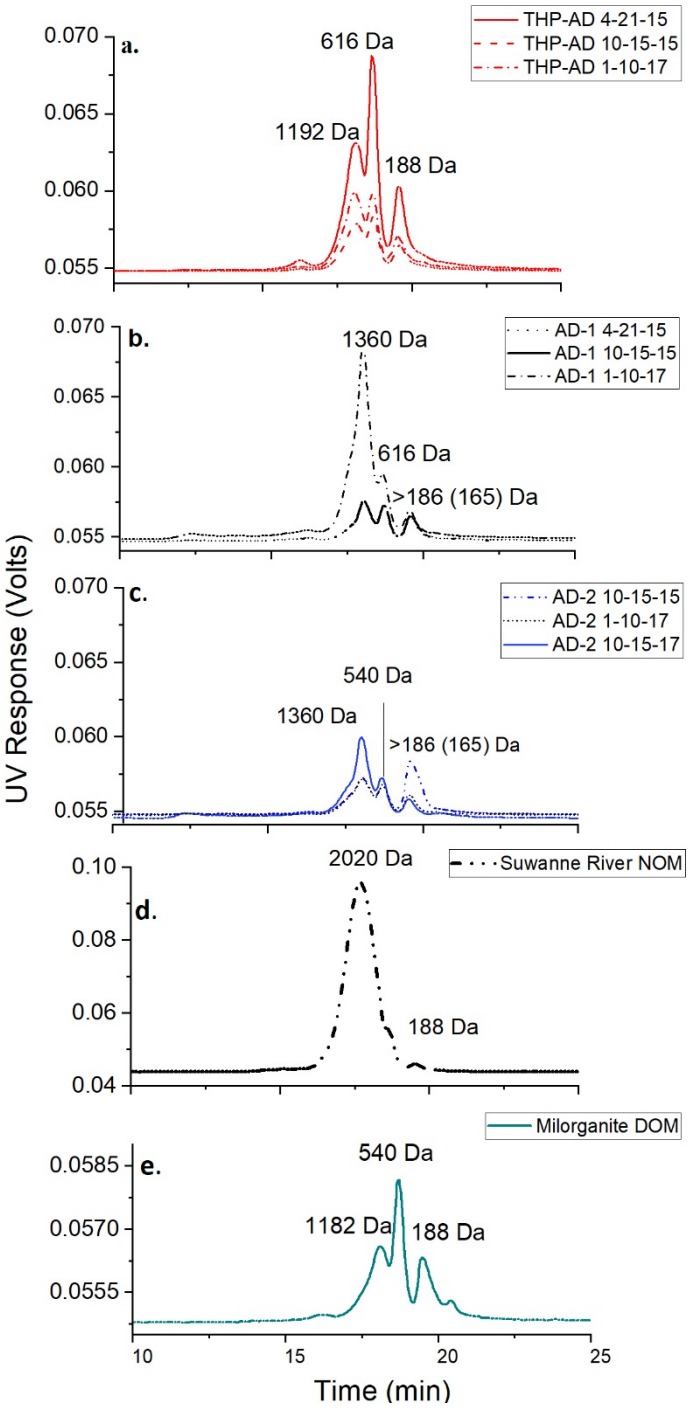

SI Figure 3: HPLC-SEC chromatographs for anaerobically-digested (AD) biosolids DOM for three sample dates per WWTP. Date of biosolids collection DD-MM-YY format. a) DOM from WWTP with THP-AD system. B) Biosolids-DOM from RRF without pretreatment and c) fermentation prior to anaerobic digestion (AD) exhibited similar molar mass distributions and polydispersity as THP-AD biosolids-DOM. Reference material D.) SRNOM contrasted the sludge-DOM chromatographs while the waste-actived sludge product e) Milorganite DOM exhibit similar molar mass distributions to AD Materials. The apparent molar mass of peak locations (M_p) based on PSS polymer standards are indicated.

SI Table 5: Standard and Smith model results for Potential N Mineralization (PMN) and rate k determined by (1972) for biosolids-amended soil.

Treatment	Potential MN (mg kg^{-1}) With 95% Confidence Interval	*k* (day^{-1}) *k* Confidence Intervals	R^2 of Model Fit
Unamended Soil (Control)	71.02 58.21 to 83.84	0.3200 0.016 to 0.038	0.96
THP-AD Biosolids	117.6 102.4 to 132.8	0.078 0.046 to 0.111	0.82
Holding AD-1 Biosolids	138.0 104.0 to 171.9	0.005 0.012 to 0.034	0.92
Ferm. AD-2	147.5 124.8 to 166.8	0.0272 0.016 to 0.038	0.97
Milorganite	315.5 278.9 to 352.2	0.06141 0.030 to 0.310	0.87

Chapter 3: Biosolids stabilization processes produce substantially different leachable DOM and complicates traditional fluorescence analysis for characterization

Abstract

Leachable dissolved organic matter (DOM) from biosolids and sludge can be characterized to assess biological or chemical transformations during batch and pilot-scale composting or treatment studies. Wastewater-derived biosolids are often land applied after stabilization processes such as lime treatment (LT), anaerobic digestion (AnD), and aerobic digestion (AeD). Limited work has systematically characterized water-extractable biosolids-DOM from multiple full-scale resource recovery facilities (RRF) according to treatment. In this study, we collected samples from different stabilization processes and found that LT, AnD, and AeD biosolids have contrasting DOM profiles. Leachable DOM was characterized by dissolved organic carbon (DOC), high-performance size exclusion chromatography (HP-SEC), and excitation emission matrix (EEM) fluorescence spectroscopy. Digested biosolids-DOM developed higher molecular weight DOM of 1360 Da and red-shifted fulvic and humic-acid like fluorophores (em: >400 nm) attributable to physical and biological transformation of sludge during stabilization. Fluorescence spectroscopy of DOM across full-scale solid sludge treatment trains also reflected development of several red-shifted fluorophore maxima. Semi-quantitative analysis of EEMs by fluorescence regional integration (FRI), peaks A, C, T, and B assignment, or fluorescence indices did not consistently capture biosolids-DOM fluorophore maxima of biosolids and sludge-DOM as literature metrics were previously defined on the relative maxima of aquatic and soil DOM. We propose two alternate definitions of FRI boundaries and peak area analysis targeting biosolids-

DOM fluorescence maxima specifically that results in 5-20% difference in fractional fluorescence area (P%) computations, and A:C and B:T ratios. This suggests that anthropogenic DOM requires ground-proving EEM metrics to specific local maxima and complimentary chemical analysis to interpret and develop rapid fluorescence analysis for biosolids stabilization or process control. Parallel factor analysis (PARAFAC) was also successfully applied on the biosolid-DOM EEM dataset to propose three unique models for LT, AnD, and AeD-stabilized biosolids-DOM that reflect fundamental differences due to treatment. The models were compared to the OpenFluor spectral database and revealed both ubiquitous amino acid-like components as well as unique red-shifted components with limited database matches, indicative of unique leachable material from anthropogenic organic matter.

1. Introduction

Treated wastewater residuals or biosolids are utilized as a soil amendment because they enhance nutrient and organic carbon content of agricultural soils while reducing costlier inorganic fertilizer use (Singh et al. 2008, Lu et al. 2012). Biosolids are applied globally with an estimated 8 million tons of dry solids per year (t DS yr 1) applied to agricultural lands in Europe and the US alone (Gendebien et al. 2008, NEBRA et al. 2007, Lagae et al. 2009, Rigby et al. 2016, SDNAL 2009, ANZBP, 2013). Due to extensive application, biosolids can be a significant source of dissolved organic matter (DOM) and carbon introduced to the environment (Lapen et al. 2008, Fischer et al. 2019). DOM is a heterogenous mixture of hydrophilic and hydrophobic organic constituents with varying molecular size-distributions. Previous work indicates that soil-derived DOM plays a clear role in the movement and bioavailability of nutrients, metals, nanoparticles,

and organic chemicals such as pesticides (Kalbitz et al. 1998, Chefetz et al. 2008, Delgado-Moreno et al. 2010, Chen et al. 2015). DOM contains oxidizable carbon and nitrogen that can readily diffuse into microbial membranes and therefore influences biogeochemical cycling in soils as well (Chefetz et al. 2008).

Given the complex role of DOM in terrestrial systems, numerous reports have characterized the water-extractable DOM from organic soil amendments deriving from green composts, swine, dairy, poultry litter (Baker et al. 2002, Hunt and Ohno, 2007, Mangalgiri et al. 2017), and municipal treatment facilities (Gigliotti et al 2002, El Fels et al. 2014). Sludge and biosolid-DOM has been assessed for transformations in sludge batch reactor studies (Luo et al. 2013, Li et al. 2014, Sun et al. 2014) and during aerobic composting (Chefetz et al. 1998, Wang et al. 2013). While these studies indicate time-dependent transformations of proteinaceous material at resource recovery facilities (RRFs) or in agricultural settings, many experiments are conducted on singular grab-samples from an individual RRFs. Limited work has systematically tested whether differences in full-scale municipal stabilization significantly alters finished biosolids-DOM characteristics before land application.

The rate of biosolids application is a function, in part, on various upstream stabilization methods to target the anticipated plant-available nitrogen (N) release during the first-year growing season (US EPA, 1994, Rigby et al. 2016). Major on-site RRF stabilization methods include (i) lime treatment (LT), (ii) anaerobic digestion (AnD), and (iii) aerobic digestion (AeD) of solids. These treatments are designed to ‘stabilize’ solids by reducing pathogenicity, vector attraction, and odors before the material is distributed as a soil amendment. It is well documented that these stabilization methods also alter organic

matter composition of the solid material. Differently processed biosolids can result in a 50% difference in the inorganic N released from organically-bound N in a growing season (Rigby et al. 2016). AeD biosolids are applied under the assumption that they decompose to release greatest mineralizable N (25-30%) in the first growing season of application, followed by AnD solids (15-20%), then LT solids (10%) (US EPA, 1995, NSW EPA 1997, Rigby et al. 2016). Although biosolids deriving from different RRF stabilizations are known to decompose at significantly different rates, no known work has systematically characterized leachable DOM from various full-scale stabilization schemes, applying recent advances in DOM spectroscopy.

Three-dimensional fluorescence or excitation-emission matrix (EEM) spectroscopy is a widely-used bulk characterization tool for DOM that exhibit an emission response when stimulated by excitation energy due to the presence of optically-active electron configurations (i.e. fluorescent DOM or FDOM, Del Vecchio et al. 2004, Cory et al. 2005). Due to the rapid analysis time and ease of use, fluorescence measurement of DOM is applied in wastewater monitoring to replace intensive fractionation or mass spectrometer-based characterization. Previous work has attributed FDOM signals to descriptive, operationally-defined categories of amino acid-like, microbial byproduct-like, and fulvic acid-like and humic acid-like (Coble et al. 1990, Chen et al. 2003). Several strategies focus on quantifying EEMs by fluorescence regional integration (FRI, Chen et al. 2003, Zhou et al. 2013), parallel factor analysis (PARAFAC) (Stedmon et al. 2003, Murphy et al. 2007), and peak-picking (Coble et al. 1996, 2003). While EEM analysis provides a multitude of information on FDOM, each qualitative to semi-quantitative strategy applied post-hoc includes different assumptions and limitations,

coupled with the fundamental limit of only measuring information on the smaller pool of DOM itself (Korak et al. 2014, Rosario-Ortiz and Korak, 2016). For instance, peak-picking definitions and also modeled PARAFAC components do not represent any specific fluorophores due to quenching and charge-transfer processes that are present in complex mixtures like DOM (Sharpless and Blough, 2014).

The first goal of this study was to propose categorical descriptions of water-extractable DOM from final dewatered material of common and contrasting sludge stabilizations of LT, AeD, and AnD for multiple RRFs per treatment. A second goal was to sample across full-scale solids treatment trains to appraise sludge-derived DOM transformations due to treatment processes. Significant effort has been dedicated to characterizing DOM quality across the water treatment side of wastewater treatment or water recycling facilities (Henderson et al. 2009). Murphy et al. (2011) found that a fluorescence dataset on the wastewater treatment side (n=1479 EEMs) converged to a universal 5-component PARAFAC model. To our knowledge, limited work has similarly characterized fluorescence markers of DOC quality during solids-treatment at full-scale RRFs. FDOM measurement in solids-treatment represent the opportunity to develop as a process and design tool for waste stabilization (Sun et al. 2016).

The final goal of this study was to critically apply EEM analysis tools of i) FRI, ii) peak-picking assignment, iii) fluorescence index computation, and iv) PARAFAC to the biosolids-DOM dataset. These analytical EEM methods are utilized across agricultural, engineering, freshwater, and marine science research, but often independently (Kowalczuk et al. 2009, Hernandez-Ruiz et al. 2012, Tian et al. 2012, Wang et al. 2013). The multivariate technique of PARAFAC is best applied on datasets that contain enough

spectral variation to produce stable and verifiable models. This is typically achieved with larger sample sets, however (Murphy et al. 2014). A complementary tool to PARAFAC is the OpenFluor database that began in 2014 (Murphy et al. 2014). This database allows for systematic deposition and comparison of PARAFAC-modelled spectra. By the end of 2018, the database contained an estimated 875 entries from mostly aqueous DOM sources including oceanic, groundwater, lake, stream samples, wastewater, and recycled greywater. Only four entries included EEMs from soil, leaf, or agricultural extracts, and no known entries currently exist for sludge or biosolids extracts. To this end, we aimed to submit PARAFAC results for biosolids-DOM EEMs to the OpenFluor database.

Due to the complexities of quantifying fluorescence data, additional DOM characterization complements FDOM measurement (Henderson et al. 2009, Minor et al. 2014). Therefore, size exclusion chromatography (SEC) was conducted on biosolids-DOM extracts to ascertain the molecular weight distribution of DOM pools. Biosolids represent a significant source of DOM to terrestrial systems that decompose at different rates depending RRF stabilization method (Rawley et al 2016). This study examines whether water-leachable DOM from biosolids reflects similar variation due to treatment. Furthermore, we present a novel and critical characterization of biosolids-DOM fluorescence data on the widely-used organic soil amendment.

2. Materials and Methods

2.1 Biosolids and Sludge Collection

Final dewatered biosolids were grab-sampled from nine RRFs with different waste stabilization processes including (i) anaerobic digestion (AnD), (ii) aerobic

digestion (AeD), and (iii) lime treatment (LT). All RRFs where located in the Washington, DC and Maryland, USA region and sampled in 2016-2017. Biosolids were collected directly at dewatering equipment prior to long-term storage or aging. Three different RRFs were sampled per stabilization category and facility information is summarized in Table 1. DC Water and Sewer Authority (DC WASA) archived (frozen) limed biosolids from 2014-2015 were also included in the study. At each facility, grab samples were collected in 500 mL acid-washed glass containers and completely filled with biosolids to remove air prior to transport. Additional samples were taken across the unit processes of anaerobic and aerobic digestion treatment trains when possible. Samples were stored on ice during transport until being frozen at -20ºC the same day as collection. Before DOM extractions and characterizations, residuals were defrosted overnight 4 ºC. Repeated, consistent results for DOC quantification and fluorescence characterization confirmed that freezing the solid was not affecting the extracted DOM quantity or quality over time.

2.1 Total and Volatile Solids, Dissolved Organic Matter (DOM) Extraction, DOC, and pH measurement

The total solids (%TS) of biosolid grab samples was determined by precisely measuring wet solids and drying samples at 105ºC for a minimum of 12 hours, cooling, and reweighing of dry matter following EPA Method 1684. Volatile solids (%VS) of dried residues were then determined by ignition at 550ºC for 2 hours, then cooling and reweighing. Water-exactable DOM was extracted from biosolids with deionized water in a 1:10 w/v solid:water ratio on an orbital shaker at room temperature for 24 hours (Zmora-Nahum et al. 2005, Said-Pullicino et al. 2007, and Wang et al. 2013).

Suspensions were centrifuged at 10,000 rpm and the supernatant was filtered with a 0.45 μm cellulose acetate membrane filter. Treatment train sludge samples with high water (95%) were centrifuged directly and then filtered. DOC of extracts was determined as non-purgeable organic carbon via a platinum oxidation catalyst and non-dispersive infrared gas analyzer (Shimadzu TOC/TN-L, Columbia, MD). The instrument was calibrated with a glycine standard curve and with repeat testing of standards as unknown to assess drift and reproducibility. DOC of each sample was analyzed with repeated injections to meet the criteria that coefficient of variation for peak areas was less than 2% per sample.

The pH of biosolids-DOM extracts was measured with an Orion Star A211 meter and Mettler Toledo LE409 pH probe, calibrated with low ionic strength buffer, as the ionic strength of DOM extracts was well-below low ionic strength calibrants.

2.2 High Performance Size-Exclusion Chromatography of Biosolids Extracts

Apparent molar mass distributions in biosolids-DOM samples were determined with high pressure liquid chromatography size-exclusion chromatography (HPLC-SEC) using an Agilent 1200 Series HPLC (Santa Clara, CA) with a photodiode array (PDA) detector operating at 280 nm at the Arizona Lab for Emerging Contaminants (Tuscon, AZ). Two stainless steel (8 x 300 mm) SEC columns (MCXGPC 1000 and 100,000 Å, PSS Polymer Standard Service-USA, Inc Amherst, MA) were connected in series, equipped with a guard column. Standards of polystyrene sulfonate (PSS-Polymer Standard Service-USA) with nominal molar masses ranging from 1 to 67 kilodaltons (kDa) and a low molecular mass 4-ethylbensulfonic acid (186 Da) standard, all at ~2.5 mg/mL, were utilized for a linear calibration of log (molar mass) to column retention

time (Cabaniss et al 2006, Omoike et al, 2006, and Hernandez-Ruiz et al. 2012). Aquatic DOM reference material Suwannee River Natural Organic Matter (SRNOM, Lot 2R101N) was obtained from the International Humic Substances Society and characterized as a reference material (IHSS). All standards, samples, and reference materials were brought to a concentration of 30 mg C L-1 and adjusted to a pH ~7.4 in a 20 mM sodium phosphate buffer solution prepared with nanopure water. The 20 mM phosphate buffer was also the mobile phase for isocratic HPLC-SEC runs. Samples and standards were injected at 50 µL and a flow rate of 1 mL/min. The linear relationship between standards log molar mass (MM) and retention time was Log(MM) = -0.572 (min) + 13.4 ± 0.45, adj. R-square = 0.97. Peak retention times were identified with Origin Lab software. This retention time was converted to apparent, peak molar mass (Mp) by the linear relationship of standards log(MM) to retention time.

2.3 Fluorescence Measurements

Biosolids DOM was extracted at least three times per solid sample and each extraction was measured for fluorescence independently. After DOC determination, filtered biosolids-DOM extracts were diluted to a final carbon concentration of 7.5 to 15 mg DOC L-1. SRNOM was also reconstituted and adjusted for fluorescence measurement. Potential impacts of inner-filter effects were reduced by confirming that the maximum absorbance of samples ≤ 15 mg DOC L-1 was less than 0.1 absorbance units (AU) at 254 nm before applying additional corrections (Hudson et al. 2007). The pH of diluted DOM samples was within or adjusted with NaOH or HCl to a final pH of 7.0 ± 1.0 before all spectroscopic analyses. Ultraviolet-visible (UV-Vis) absorbance spectra and fluorescence spectra of dilutions were collected in 3.5 mL clear quartz

cuvette cells (light path 1cm x 1 cm). Absorbance spectra and fluorescence EEMs were both measured using an Aqualog fluorometer (Horiba Scientific; Edison, NJ). The excitation and emission wavelength ranges were 230−600 nm with a wavelength step of 3 nm for excitation and emission scans. All samples were blanked against a high purity water spectrum. Inner-filter corrections, Rayleigh-Tyndall scattering, and conversion to Raman Units (RU) using water at an excitation wavelength of 350 nm (emission range 381−441 nm) were performed using the Aqualog software on all EEMs following procedures described in Timko et al. (2015). The 1st and 2nd order Rayleigh-Tyndall scattering effects were removed, and the surrounding data was interpolated post hoc in MatLab® (Zepp et al. 2004) to a point that also satisfied preprocessing requirements for PARAFAC modeling (Murphy et al. 2013).

2.4 Excitation Emission Matrix Quantitation and Analysis

Three-dimensional EEMs of biosolid extracts were analyzed by four methods: i) fluorescence regional integration (FRI), (ii) peak area analysis iii) fluorescence indices, and iv) PARAFAC modeling.

2.5 Fluorescence Regional Integration (FRI)

The fluorescence EEMs of DOM extracts (n=3 extractions per RRF) were individually integrated for five classically described regions; (I) “tyrosine-like”, (II) “tryptophan-like”, (III) “fulvic acid-like”, (IV) “microbial by-product-like, and (V) “humic acid-like” (Chen et al., 2003, SI Table 1). The volume of each region of the EEM boundaries was summated and normalized by the total FRI boundary volume to achieve a fluorescence percentage (P %) for each region (Chen et al. 2003, Hernandez-Ruiz et al.

2012). FRI boundaries were also adapted to biosolids-DOM fluorescence maxima and the volume in adapted regions were then summated following Chen et al. (2003) (SI Table 2). Additional details of FRI computation are provided in the Supplementary Information.

2.6 Local Maxima Analysis and Previously Described Peak Regions

EEMs from various RRFs and repeat extractions were averaged by three treatments of LT, AeD, and AnD stabilization and local fluorophore maxima were identified with Matlab® (MathWorks, MA) software. Coble et al. (1996), Coble et al. (2007) and Gabor et al. (2014) have defined characteristic peak region boundaries A: UV region humic-like, B: tyrosine-like, C: visible region humic-like, and T: tryptophan-like (SI Table 2a). Peak A, B, C, and T boundaries were applied to average EEMS and compared against local maxima location. The ratio of maxima in previously defined regions of Peaks A:C and T:C, as well as the ratio of maxima proximal to classically-defined boundaries, were determined in Matlab® (Mathworks, MA, SI T).

2.7 Optical Properties Calculations and Visualization

Indices of E2/E3 (an absorbance ratio), ¬ humification indices (z, o: zHIX, oHIX), biological index (BIX), and fluorescence index (FI) were computed on individual EEMS of DOM extracts for each RRF and results were then averaged for a standard deviation. Computations were completed in Matlab according to index definitions, descriptions, and literature references summarized in SI Table 4. EEM locations of classically defined HIX, BIX, and FI are visualized on Figure 4.

2.8 Parallel Factor Analysis (PARAFAC)

PARAFAC models were developed with the drEEM 1.0 toolbox following the procedures described in detail by Murphy et al. (2013) for Matlab® (MathWorks; Natick, MA). EEMs were modeled by treatment type, with at least three RRFs and 3-4 extractions and fluorescence measurements per RRF solid, i.e. limed solids (n = 12 EEMS), AeD solids (n = 11 EEMs) and AnD (n = 12 EEMs). PARAFAC models were deliberately built for each treatment type individually because treatment types yielded fundamentally different fluorophore compositions and locations in qualitative assessment, which would be not be appropriate to use PARAFAFC modeling. Input data was preprocessed according to best practices recommended by Murphy et al. (2013) and normalized before preliminary analyses. EEMs spanned Ex:Em ranges of 240–597 nm and 233-600 nm. Exploratory analyses of excitation and emission loadings confirmed that a four-component model was best suited for LT and AeD-biosolids DOM models and a five-component model was appropriate for AnD-biosolids DOM (Figure S2 of supporting information). A convergence criterion of 10-8 was used for the three models and model convergence was confirmed with 60 to 120 random iterations. All data was reverse-normalized at the end of the analysis following Murphy et al. (2013). Split-half analysis validated the three models through data split comparison with alternating sample distribution (SI Figure 3).

3. Results

3.1 Total Solids, Volatile Solids, Water-Extractable Dissolved Organic Carbon Content, and pH of Extracts

Volatile solid content reflects easily oxidizable organic matter in wastewater residuals. The average %VS of limed biosolids was 52.1 ± 13.8%, although raw solids prior to 20% lime addition, by weight, may contain 75-81% VS (Table 1, DCWASA personal correspondence). The VS% was therefore reduced in AeD and AnD solids to 61.2 ± 4.8% and 65.4 ± 1.5 respectively. Water extractable DOC content has been previously proposed as an indicator of maturity and stability from manures and municipal waste, with extractable DOC exponentially decreasing during aerobic composing of solids (Wu et al. 2000, Zmora-Nahum et al. 2005). In this study, limed biosolids contained the greatest leachable DOC of 36.5 ± 17.7 mg DOC/kg d.w. Extractible DOC was reduced in AnD solids to 28.1 ± 9.8 DOC/kg d.w. and reduced 5-fold for AeD solids to 6.2 ±1.3 DOC/kg d.w. (Figure 1). Also accounting for ~20 to 30% weight added by lime addition, bulk organic matter from LT biosolids therefore released the greatest amount of DOC, which is consistent with limited biological stabilization (Zmora-Nahum et al. 2005) during lime addition. Additionally, the high pH 11 of limed biosolids extracts may have resulted in additional carbon solubilization due to the additional deprotonation of (poly) phenols. Reduction of extractable DOC from the digested solids indicates that neutral to acidic pH and additional biological stabilization significantly decreases the quantity of leachable DOM from dewatered biosolids.

3.2 High Performance Size Exclusion Chromatography of Biosolids-DOM

The apparent mass populations of biosolids-DOM extracts were more heterogenous and contained smaller molecular weight material of Mp = 165-1360 Da (Figure 2a-c) than aquatic SRNOM reference material primarily with a Mp = 2020 Da (SI Figure 2). Polydispersed and heterogeneous primary sludge-DOM was also observed in Hernandez-Ruiz et al. (2012). LT-biosolids DOM contained two apparent molar mass peaks (Mp) at 540 Da and 188 Da for all three RRFs tested (Figure 2a). AnD DOM extracts contained an additional, higher molecular weight population at 1360 Da, as well as smaller molecular mass fractions at 617 Da and 165 Da (Figure 2c). The apparent molar mass distributions of AeD DOM materials also contained three distinct mass populations ranging from 165 Da to 1360 Da. Interestingly, AeD-biosolids extracts also contained significantly broader, low retention peaks of Mp = 54,000 or > 67,000 Da (SI Figure 1d). These high molecular weight fractions suggest influence from dewatering polymers, small particulates, or potentially supramolecular associations in AeD-DOM (Sutton et al. 2005). Because aquatic DOM molar masses have not exceeded ~2000 Da by mass spectroscopic determinations (Peuravuori et al. 2007), further physical filtering (0.2 μm) or mass-spectrometry would be necessary to understand the role of supramolecular assembly or dewatering polymers in biosolids-DOM. Mass populations in the range of 165-1360 Da we observed are characteristic of monomer classes of amino acid to isolated fulvic and humic acids (McAdams et al. 2017). The Mp present at 1360 Da in both AeD and AnD-biosolids DOM suggests that higher molecular weight DOM may develop during biological digestion and is extractable from the neutral to acidic pH

solids. Relative Mp intensity varied across RRFs of a given treatment type, suggesting that biosolids-DOM mass fractions are variable in absolute abundance.

3.3 Biosolids-DOM Fluorescence Spectroscopy

Digested biosolids-DOMs that contained a molecular weight fraction at 1360 Da also contained several 'red-shifted' fluorophores in the visible wavelength EEM region compared to LT-biosolids DOM (Figure 3). LT-biosolids extracts contained the greatest concentration of FDOM in UV ex:em regions with the highest intensity fluorescence maxima observed at 276nm:348 nm, previously associated in the region of amino acids, microbial byproducts, and agricultural manures (Figure 3a.,b., Chen et al. 2003, Baker et al. 2002). LT-biosolids FDOM also contained two local maxima at ex:em of 231nm:378 nm and 318:384 nm (Figure 3b.). The three clustered fluorophore maxima were reproduced in multiple extractions of LT biosolids across three RRFs sampled with this stabilization (Figure 3b.)

AnD-biosolids DOM was also characterized by an overall fluorophore maximum at ex:em 231:336 nm, previously associated to protein and microbial-byproduct associated fluorescence, but also contained two local maxima that were present in longer wavelength regions at ex:em: 342:430 nm and 411:487 nm. (Figure 3c, d). These red-shifted maxima were detected in all DOM extracts from the three AnD-RRFs sampled, albeit to different intensities (Figure 3c). AeD-biosolids DOM also contained both UV and visible energy fluorophores at ex:em 231:335 nm and 231:417 nm, as well as a red-shifted fluorophore at ex:em of 342:430 nm in the EEM regions broadly associated with humic and fulvic acids (Figure 3 e.,f. SI Tables 1 & 2, Chen et al. 2003 and others).

Molecular weight and fluorescence characterization suggest that LT-biosolids DOM is more homogeneous than other DOM tested. Extracts from biologically digested AeD and AnD DOM contained both UV and visible wavelength fluorophores as well as a higher molecular weight fraction of 1360 Da. Broad emission bands of individual fluorophores can span 100-200 nm and complex mixture effects complicate inferring that the red-shifted fluorophores from digested extracts is the same molecular size fraction measured at 1360 Da without coupling of SEC to fluorescence measurement, however (Lacowitz, 2006, Maie et al. 2007, Wünsch et al. 2017). Red-shifted fluorophores (ex:em > 350 nm) have been previously characterized for condensed, conjugated and likely polyaromatic π systems of DOM described for cellulosic humic acids or melanoidins (Coble et al. 1996, Chen et al. 2003, McAdams et al. 2017). A proprietary sludge dewatering polymer added at 0.25% (weight basis) post-digestion obtained from DCWASA did not contain measurable fluorescence alone, but could influence the fluorescence response of biosolids-DOM mixtures (Shapless and Blough, 2014, SI Figure 2). Overall differences between fluorophore content and SEC mass fractions of biosolids-DOM reflect that the two analytical techniques do not necessarily describe the same features of DOM, but both analyses indicate variations in heterogeneity between DOM extracted from biosolids of contrasting stabilizations.

3.4 Quantitative Analysis: Classic and Adapted Fluorescence Regional Integration (FRI)

EEMs contain thousands of data points on the optical properties of a DOM and researchers have developed several strategies for quantifying this information. We applied four methods: i) fluorescence regional integration (FRI), (ii) peak area analysis

iii) fluorescence indices, and iv) PARAFAC modeling to the fluorescence data and critically evaluated each approach.

Fluorescence regional integration (FRI) ascribes defined boundaries for integration of fluorescence intensity volumes (SI Table 1, Chen et al. 2003). These boundaries were first described on relative fluorescence maxima of individual compounds of tryptophan and XAD-fractionated aquatic and wastewater effluent samples. Classically defined FRI of LT-biosolids extracts indicated that most of the fluorescence was tyrosine-like, 34.9%, microbial byproduct-like, 34%, and tryptophan-like,15% (Figure 4d.). Fluorescence was also present in fulvic acid and humic acid-like regions III and V. Visualization of classically-defined FRI Regions on LT-biosolids EEMS indicated that fluorescence within regions III and V contain the partial maxima and shoulders of fluorophores maxima contained in region IV. Regions I and II also shared one fluorescence local maxima. To avoid this, adapted FRI for biosolids-DOM (Figure 5) includes the fluorescence maxima at 230 nm:360 nm in one combined region 1 & 2 as 34% of total fluorescence. The red-shifted fluorescence maxima at 276 nm:351 nm was encapsulated with an adapted FRI, shifting the total fluorescence of this region from 5% to 10% of total signal.

AeD and AnD biosolids DOM EEMs also contained the greatest proportion of fluorescence intensity in classically defined FRI regions I and II of tyrosine-like (~35%) and tryptophan-like (14-17%). Microbial-byproduct fluorescence (region IV) decreased 7-12% in AnD and AeD-DOM relative to LT-DOM (Figure 4d). Fulvic and humic acid-like fluorescence P% increased 5-10% for both AeD and AnD-biosolids DOM relative to LT-biosolids extracts. Notably, both AeD and AnD biosolids DOM contained

fluorescence intensities outside classically defined FRI region V boundary beyond ex: 400 nm (Figure 4b and c, Chen et al. 2003). Humic acid-like fluorescence is therefore either underestimated or biosolids-DOM fluorescence beyond FRI region V, or chemically contrasts DOM that original FRI boundaries were defined with. We propose adapted FRI boundaries that extend to an excitation of 450 nm to integrate all red-shifted signal in AnD and AeD-biosolids DOM (Figure 5). Doing so increased modified Region 5 signal by 5% of total signal. Region 3 integration also increased by 10% for all DOM (Figure 4d. and 5). While the adapted FRI proposed improves quantification of total fluorescence signal and centers summation around biosolids-DOM specific EEM maxima, complimentary characterizations are needed to fractionate and confirm chemical meaning of biosolids-DOM fluorescence signals. Currently, only associations to previously detected fluorescence signals from contrasting environments can be made.

3.5 Peak Area Assessment

Another quantitative EEM strategy is to analyze relative maxima within previously described peak regions or ex:em pairs (Figure 4e.-h. Gabor et al. 2014). Coble et al. (1996) ascribed local maxima in freshwater, coastal, and marine water samples as peaks as A, C, B, and T (SI Table 2). Peak assignment supports in describing fluorophores or standardizing computation of peak ratio changes across biogeochemical gradients (i.e. A:C, M:T, and T:C intensity ratio, Coble et al. 1996, Baker 2001, Korak et al. 2014). Fluorophore maxima of LT-biosolids DOM were not contained in previously defined peak B, T, C, or A regions but fluorescence occurred across all boundaries (Figure 4e). AnD and AeD biosolids contained relative fluorescence maximum within boundaries previously ascribed to Peak T/tyrosine-like fluorophores and on the Peak C

boundary associated to humic-acid like material. Local fluorophore maxima were not contained within the boundaries of Peaks B or A, but these regions also contained fluorescence signals.

The ratio A:C peaks or UV:Visible humic-like material was computed on averaged EEMs per stabilization category (Table 2). The ratio of classically defined A:C ratio was LT-DOM=1.2, AeD=1.8, and AnD=2.3 but these values varied 5-6% for AeD and AnD-DOM, and 20% for LT-DOM when computed on the nearby, actual maxima of fluorophores nearest to peak boundaries (Table 2). While classically defined A:C ratio were greater for digestion biosolids DOM but visual representation of classically defined peak boundaries indicate that the A:C ratio was computed on differently positioned and potentially unrelated fluorophore maxima, giving a potentially misleading result. The A:C ratio for LT-biosolids DOM was computed for blue-shifted maxima also associated to the amino acid-like fluorescence (Chen et al. 2003) while the C peak of AeD and AnD DOMs was red-shifted (Figure 4e). Coble et al. (1996) defined A:C ratios to confirm that two humic acid-like fluorescence peaks in aquatic matter do not co-occur equally and the ratio can vary across samples. Verifying that this ratio is computed on red-shifted fluorescence maxima of biosolids-EEMs improves accuracy and connects the result to the original definition of the metric. Resin fractionation would be necessary to confirm the red-shifted biosolids DOM fluorophores in fact exhibit operationally-defined humic acid-like properties, i.e. no solubility at pH < 2 (Olk et al. 2019).

The classically-defined Peak T:C ratio of protein:humic-like material has also been previously examined for the influence of agricultural wastes (Peak T) into un-impacted watersheds (Baker et al. 2002, Hudson et al. 2007, 2008). AeD and AnD had greater T:C

ratios, suggesting more protein-associated than humic-like material, but were computed on spatially different fluorophore maxima compared to LT-DOM (Table 2). The classically-based T:C ratio of LT-DOM of 1.7 changed 12% to a modified T:C = 1.5 when adjusted to local maxima. Peak ratios calculations based on boundaries developed for fluorescence maxima of natural surface waters are improved by adjusting definitions to proximal maxima of biosolids-DOM.

3.6 Optical Properties-derived Indices

Numerical results of absorbance and fluorescence indices are summarized in SI Table 3 and visually represented on fluorescence EEMs in Figure 4i-l. The E_2/E_3 ratio (UV absorbance at 250 nm/365 nm) of LT-DOM, AeD-DOM, and AnD-DOM were 16.2 ± 10.0, 9.9 ± 8.19, and 7.24 ± 2.47, respectively, suggesting that digested material had higher molecular weight distributions (Helms et al. 2008) but significant variation across RRFs or extraction dates is indicated by large standard deviations. Without further experimentation, it remains unclear at this point if the interpretation about molecular weight holds in for very different sludge-DOM when compared to the interpretation of Helms et al. (2008) for aquatic and marine DOM. Humification indices zHIX and oHIX were greatest in AnD-DOM, followed by AeD and LT-DOM, consistent with lower H/C and greatest humification in AnD solid extracts (Ohnom 2002), but again interpretation of this ratio in sludge-derived DOM may not warranted due to the presence of fundamentally different fluorophores when compared to aquatic DOM. Visualization of HIX indicated that the metric was computed over fluorophore shoulders adjacent to relative maxima but captured the red-shifted local maxima of digested biosolids DOM at ex/em: 254nm/450 nm. Conversely, BIX was greatest in LT-DOM, 1.70 ± 0.62, followed

by AeD-DOM, 0.67 ± 0.11, and AnD-DOM, 0.81 ± 0.19, consistent with microbial additions to humic material (Parlanti et al. 2000, Huguet et al. 2009). This metric was developed on EEM maxima of marine and estuarine systems and has similar shortcomings for sludge-DOM as described above. Visualization of the BIX applied to biosolids-DOM EEMs indicate that the metric was computed between local maxima (Figure 4i-k). The FI computation did not include local maxima of this dataset. While these overall trends in absorbance and fluorescence indices point to an increase in microbially-driven humic material in digested biosolid-DOM, absolute values of fluorescence indices would be more precise by re-defining metrics local maxima of this dataset (He et al. 2013). Adopting interpretation of absorbance and fluorescence-derived indices from freshwater, brackish or coastal regions and transformations do not appear to be appropriate for sludge-derived DOM. Future work should re-define indices in concerted experiments targeting transformations common to the specific constituents of sludge-DOM.

3.7 PARAFAC Models and Comparisons to the OpenFluor Database

Parallel factor (PARAFAC) analysis decomposes multi-way EEMs spectra into model fluorescence components. However, overfitting of varied EEMs into one PARAFAC models can result in artifact components or oversimplify the complexity across EEMs (Mostofa et al. 2019). Therefore, PARAFAC models were developed for different biosolids-DOM treatments in this study. LT and AeD biosolids DOM was modeled using four unique components while AnD-biosolids DOM was modeled with five components (Figure 5, SI Table 5), which better reflected the fluorescence regions observed in the dataset. The three EEM-PARAFAC models explained 99.6%, 99.4%, and

98.9% of variability for limed, AeD, and AnD-biosolids DOM models, respectively. The greatest average Fmax for all three models was present for the C1 components modeled with an Exmax: 275 nm to Emmax: 326-348 nm (Figure 6). The C1 Exmax:Emmax has been previously associated near B & T peaks of amino-acid like material, polyphenols, or soluble microbial by-products (SI Table 1 & 2, Maie et al. 2007, Gabor et al. 2014,). The C1 components from biosolids-DOM also had the greatest number of match models in the OpenFluor database. This suggests that this component is ubiquitous in nature across environments including aquaculture wastes (Nimptsch et al. 2015, Hambly et al. 2015), singular small organic compounds (Wünsch et al. 2015), estuarine and marine systems (Cawley et al. 2012), and leaf litter leachate (Garcia et al. 2018) (SI Figure 5). The C4 component of AnD-biosolids DOM contained several database matches modeled for treatment trains of Australian water recycling plants (Murphy et al. 2011). Interestingly, LT and AeD biosolids-DOM PARAFAC models did not contain these database matches at a 0.97 similarity score, suggesting more similarity of leachate from anaerobically digested solids to the wastewater side of treatment facilities. AeD EEM-PARAFAC component C2 matched wastewater models at a 0.95 similarity threshold, however. LT EEM-PARAFAC models did not contain database matches to previously modeled wastewater components at a 0.90 threshold, suggesting significant differences in leachable organic matter wastes with caustic LT versus other wastewaters and biosolids-DOM.

LT-DOM contained one modeled component C4 that was red-shifted with Emmax -emissions in visible light (>400 nm), while AeD and AnD-DOM models contained two components each with an Emmax >400 nm, (Figure 4d). Red-shifted

fluorescence signals has been previously associated to humic acid-like and fulvic acid-like material. Biosolids-DOM EEM-PARAFAC components had limited spectral matches in OpenFluor depending the similarity threshold, however (SI Figure 5). XAD resin fractionation could confirm if these signals behave as fulvic and humic acids with various pH solubilities.

Overall, LT EEM-PARAFAC components contrasted AnD and AeD models, further confirming a similar influence of biologically stabilizations on leachate. The three biosolids PARAFAC models were deposited in the OpenFluor database (www.openfluor.org) will be made publicly available after publication. The PARAFAC models will also be available for direct downloads via the Dryad platform (https://datadryad.org/) and additional sludge-DOM EEMs could be amended to PARAFAC models to assess differences and similarities from the three models proposed. There is an opportunity for solids extracts research to utilize the open source platforms for quantitative comparisons and development of PARAFAC components.

3.8 Additional Fluorescence Spectroscopy on DOM across Solid Stabilization trains

Samples were collected across sludge treatment trains at four RRFs with anaerobic digestion and aerobic digestion of solids (Figure 5, a). Because treatment trains were sampled on singular sampling events, PARAFAC could not be reliably performed on these EEMS. Due to limitations of quantifying fluorescence data by classically-defined FRI, aquatic indices, boundary-based peak picking on sludge DOM, we tracked development of fluorophore maxima across sludge treatment trains (Figure 6, Table 2). At DC Water and Sewer Authority (Washington, DC), sludge-DOM after early physical treatment steps of gravity settling and centrifugation was dominated two UV-region

relative maxima in the regions of by microbial byproduct-like and amino acid-like fluorescence (Figure 5a). Material then enters the 30-minute conditioning step of thermal hydrolysis pretreatment (THP) at 165ºF under 55 - 138 PSI to enhance downstream anaerobic digestion (Wilson and Novak, 2009). Three additional red-shifted fluorophores developed in FDOM after THP treatment consistent with significant transformation solids and leachable dissolved material after heat and pressure. The red-shifted peak ex/em: 411 nm/487 nm was present after THP pronounced in final biosolids post anaerobic digestion.

Red-shifted fluorophore maxima similarly developed in DOM sampled across the solids anaerobic digestion treatment train of the Sod Run, MD facility (Figure 5b). Primary sludge influent to digesters was dominated by two blue-shifted fluorophores (1 & 2) and digested DOM and final biosolids extracts contained additional red-shifted fluorophores in humic and fulvic-acid associated regions. Final Sod Run biosolids extracts contained a red-shifted local maximum (5) beyond 400 nm present not accounted for by the conventional boundaries of FRI.

FDOM transformations across additional treatment trains of the St. Mary's facility (AnD) and Tochester, MD facility (AeD) were less pronounced (SI Figure 4). Fluorophore composition shifted or changed intensity, but heterogenous red-shifted fulvic acid-like to humic acid like maxima were present before digestion. Fluorophore maxima > 400 nm appeared to develop after digestion. Less pronounced transformations in some treatment trains may be due to the influence of previously solubilized and dissolved carbon. Overall, full-scale observations across the biological stabilization of sludge indicates development of several red-shifted fluorescence maxima in FDOM due to treatment.

4. Discussion

4.1 Implications for Biosolids Residuals Management

DOM leachates from LT, AnD, and AeD biosolids were characterized by distinct fluorescence signals and molar mass populations for each treatment type. AnD and AeD-DOM were characterized with additional molecular mass population of 1360 Da and red-shifted fluorophores that has been previously associated to humic and fulvic-acid like material. AeD and AnD-biosolids DOM had a red-shifted local maximum at Exmax:Emmax: 414 nm:470 nm that could be modeled as a distinct PARAFAC component and was outside the boundaries of classically-defined FRI. The increase in complexity of sludge-DOM EEMs across DCW and SR digestion processes suggests in situ production or release of conjugated and poly-aromatic DOM. This type of DOM may be produced by the breakdown cellulose or lignin, biological material, or produced during chemical or microbial polymerization of organic carbon. Microbial polymerization is a disputed process (Kleber and Lehmann, 2019) that is the most feasible in anaerobic reducing environments (Hebting et al. 2003). Sludge in the THP-AnD treatment train of DCW also undergoes heat and pressure treatment, which may trigger a degree of maillard reaction. The shift in small molecular weight, amino acid-like extracts in LT material to increased humic acid-like and fulvic acid-associated signatures in DOM in digested sludge suggests complex transformations occur to the solid matrix that may release condensed, polyaromatic material containing increased water-soluble functional groups (Kleber et al. 2019). LT, AnD, and AeD biosolids are land applied assuming different mineralization rates over a given growing season. Our data reflects that major sludge

stabilizations also categorically alter the quantity and quality of dissolved organic matter released from solid residuals.

4.2 Recommendations for Quantitative Analysis of Anthropogenic DOM Pools

This study critically applied and compared multiple EEM analysis tools of i) FRI, ii) peak-picking, iii) PARAFAC modeling to the biosolids-DOM dataset. FRI is a means to quantify EEM matrix of data of >10,000 data and can be independently computed in Excel or MATLAB® environments (Hernandez-Ruiz et al. 2012, Zhang et al. 2015, and others). Classically-defined FRI has the disadvantage of pre-described linear boundaries that bisected broad fluorophore volume into two distinct but neighboring regions (microbial-like and humic acid-like), which reduces chemical meaning and quantification of the fluorescence signal (Figure 4a). LT-biosolids DOM have additional CaOH2 added during treatment. This may have contributed to a unique chemical environment that altered blue-shifted protein-like fluorophores between boundaries originally centered on fluorescence maxima pure solutions of amino-acids or fractionated aquatic samples (Chen et al. 2003). Chen et al. (2003) did not describe fluorescence beyond an ex: 400 nm and instrumentation was not set up to do so. In this study, we propose adapted FRI boundaries encapsulating signal detected to an Ex: 450 nm and Em: 550 nm. We also eliminated the boundary between regions I and II, and shifted the boundary of region III to better encapsulate fluorescence maxima. Zhou et al. (2013) demonstrated that the precision of FRI is improved by integrating over the smallest wavelength increment possible (1 nm) and employing the composite Simpson's rule for numerical integration. If FRI is employed, we suggest targeting FRI boundaries on data-specific local maxima and

shoulders for highly anthropogenic DOM that is dissimilar to aquatic samples. Complimentary analyses of XAD-based fractionation or mass spectroscopy would confirm that fluorescence in adapted FRI regions exhibit operationally defined properties of humic acids and fulvic acids (Olk et al. 2019). Ultimately, PARAFAC modeling is more sophisticated in the ability to mathematically deconvolve overlapping fluorescence maxima instead of bisecting signals (Stedmon et al. 2003).

Quantifying peak intensity within A, C, T, and B boundaries also aids with description and quantification of peak ratio changes. These peak boundaries were described for local maxima of freshwater, estuarine, and marine systems with a mixture of anthropogenic influence (Coble et al. 1996, Baker et al. 2002, Gabor et al. 2014). Biosolids-DOM local fluorophore maxima were not consistently represented by previously published boundaries of A, C, T, and B boundaries. Computation of A:C or B:T of shoulders or parts of different fluorophores in biosolids-DOM varied 5 to 20% when calculating ratios of peaks on actual peaks. Similarly, although fluorescence indices could be computed on the dataset, visual representation of indices confirm that HIX, BIX, or FI are not necessarily across computed on local fluorophore maxima or shoulders of related fluorophores. HIX was first defined on instrumentation where excitation was fixed for a given emission scan. While all metrics had biogeochemical meaningful and basis when originally defined, this meaning is obscured when applied to EEMs of contrasting chemical compositions and fluorophore positions. Therefore, we have proposed two analytical adjustments to quantify maximum fluorescence signal for sludge and biosolids leachate. Future work and experimentation will improve underlying

chemical and environmental interpretation of metrics as well (Rosario-Ortiz and Korak, 2016).

Biosolid-DOM EEMs were modeled by stabilization category to reduce artifact components and these models were compared to the OpenFluor database. There are currently significantly less entries for anthropogenic organic matter leachates into OpenFluor spectral database and Dryad databases compared to aquatic and terrestrial systems. Open source and comparative platforms are therefore powerful tools for developing understanding of complex leachate DOM. Our results indicate that the biosolids leachate contain both ubiquitous blue-shifted and unique red-shifted fluorescence components compared with previous spectral PARAFAC entries, consistent with our findings using FRI and peak picking. Gabor et al. (2015) compared leachate solution chemistry on forest catchment soils – a debated and variable procedural step in leachate research. Salt solutions and H2O-based extractions generated different soil-derived DOM fluorescence signals that could be modeled by PARAFAC. While water-based leaching of biosolids based this and several recent composting studies (Wang et al. 2015, Zhang et al. 2015, Sun et al. 2015) no known work has explored the effect of different leachate chemistry on biosolids-FDOM. Concerted testing of leachate chemistry on municipal solids is an example of future work that could correlate leachate FDOM signals to other biosolids stabilization measurements, such as CO2 respiration rates, inorganic nutrient releases, or BOD5/COD (Wang et al. 2013). We propose that biosolids-DOM specific models in OpenFluor and Dryad databases has the potential to advance the utility of leachate research across experimental designs and scales of

biosolids experimentations. Targeted EEM metrics and PARAFAC models developed herein also aid in rapid analysis of biosolids-DOM transformations.

5. Figures – Chapter 3

Table 1: Description of waste stabilizations and resource recovery facilities (RRF) sampled for this study. Total and volatile solids are also reported.

	Treatment Description:	**Sampled Facilities with Treatment:**	**Average Total Solids %**	**Average Volatile Solids %**
Lime Addition:	Caustic $CaOH_2$ addition to raise solids pH > 11. Lime added to ~20% of final solid, weight basis (personal correspondence)	1. Archived (frozen) samples from DC Water and Sewer Authority (DC WASA), Washington, DC 2. Little Patuxent, MD 3. Laurel, MD	35.0 ± 4.7	52.1 ± 13.8 (%VS of raw solids without lime added is 75-81%, personal correspondence)
Aerobic Digestion:	Retention of solids in aerobic, aerated basins for a minimum of 15 days	4. Worton, MD 5. Tochelster, MD 6. Wicomico Shores, MD	21.1 ± 6.5	61.2 ± 4.8
Anaerobic Digestion:	Retention of solids in anaerobic reactors for a minimum of 15 days. Methane biogas produced and often coupled to combined heat and power generators	7. DC Water and Sewer Authority (DC WASA): Thermal Hydrolysis Pre-treatment to Anaerobic digestion 8. Sod Run, MD 9. St. Mary's, MD	22.7 ± 6.5	65.4 ± 1.5

Figure 1: Extractable DOC (mg) per kilogram biosolid on a dry weight basis. The average pH of water-soluble organic matter extracts is listed above each type. Limed biosolids DOC was not corrected for weight due to lime addition to solids. Denotation (**) represent a significant difference in extractable DOC/kg d.w. solid observed for aerobically digested material compared to the two other treatments, by a one-way ANOVA and unpaired *t* test between types.

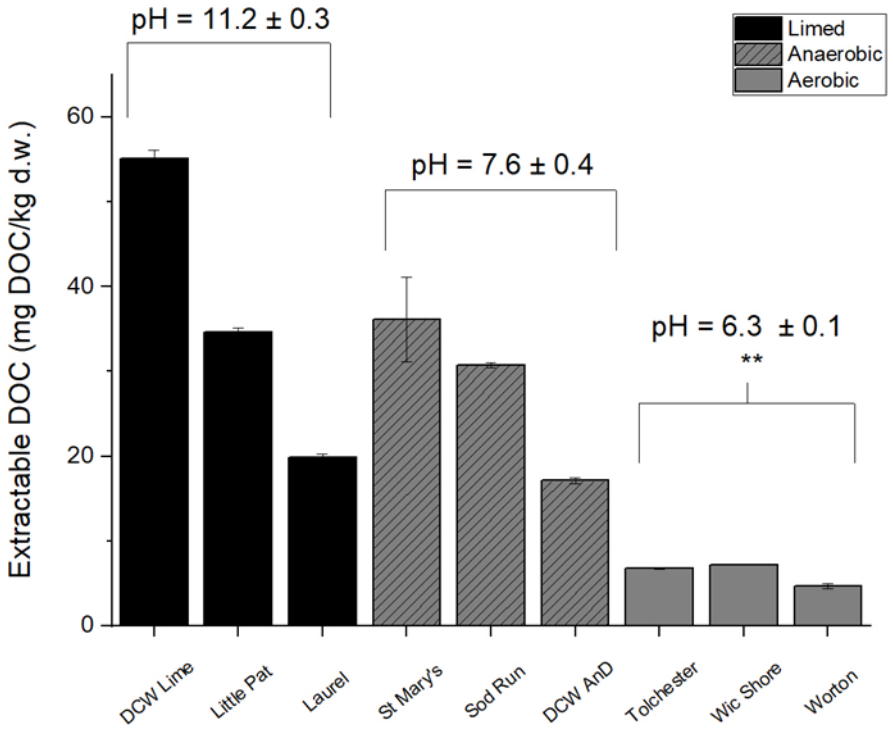

Figure 2: HP-SEC Chromatographs of biosolids-DOM. a) limed, b) anaerobically-digested, and c) aerobically digested waste stabilization classes pH ~7.4 for multiple resource recovery facilities. The apparent molar mass (Mp) of eluted DOM peaks are indicated on chromatographs.

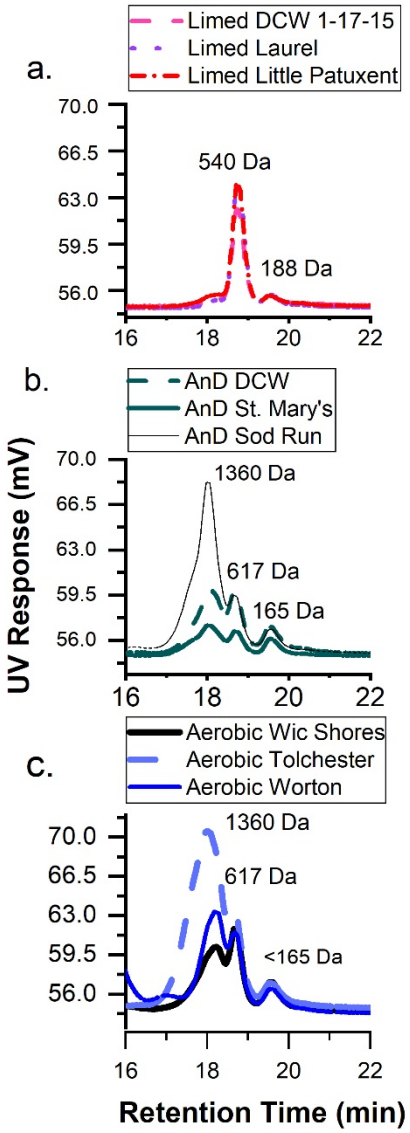

Figure 3: Excitation emission matrices (EEMs) of biosolids-DOM from multiple RRFs and stabilizations. A., c., and e.) Averaged EEMs of all biosolids-DOM by LT, AnD, and AeD stabilizations with fluorescence maxima indicated. B.,d., and f.) EEMs of DOMs extracted (n=3) from final biosolids collected at individual RRFs with LT, AnD, and AeD. Local maxima are indicated with numbers .

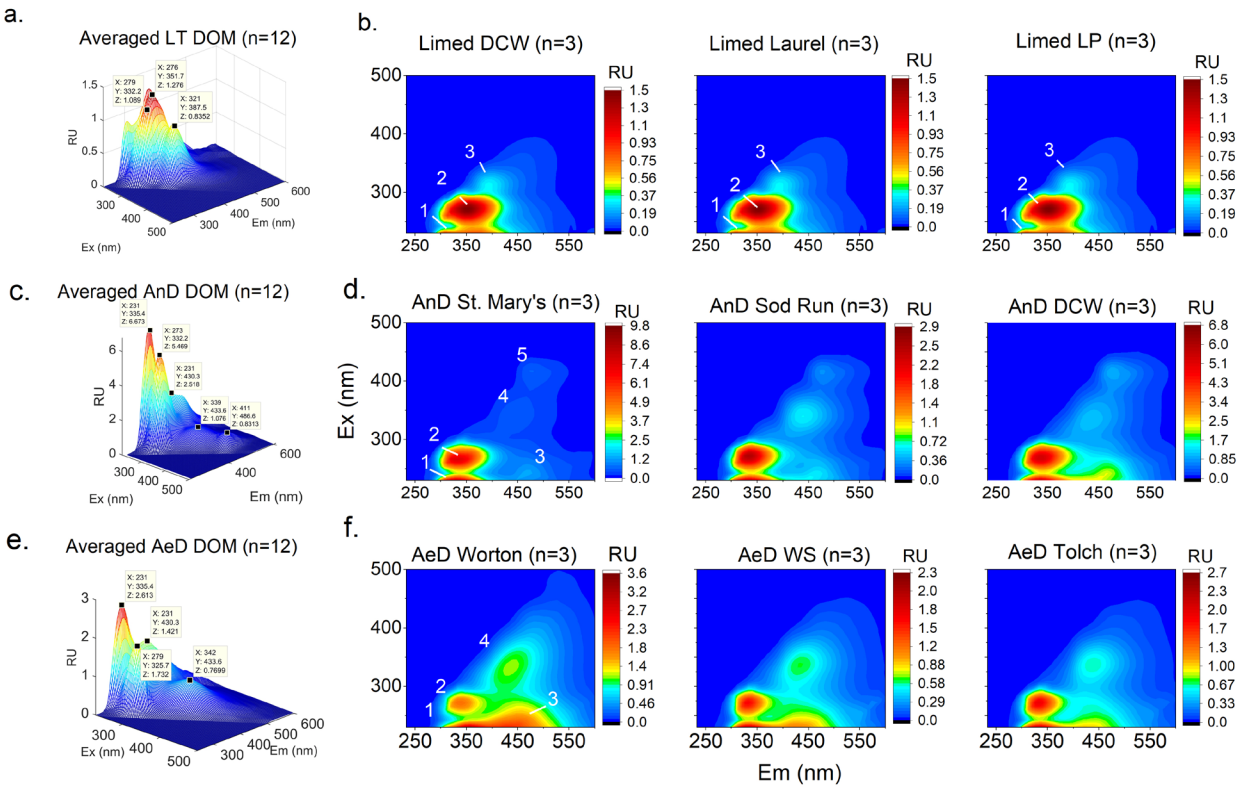

Figure 4: Visualization of three classically defined quantitative methods for averaged EEMs applied to biosolids-DOM averaged by treatment types of LT (n=12), AnD (n=12), and AeD (n=11) biosolids DOM. A-c) FRI regions, d.) results of FRI. error bars represent standard deviation of P% for multiple EEMs per RRF solid, e-h) previously defined peak A, C, B, and T boundaries and local maxima (white circle) of underlying EEM, i-l) Fluorescence indices HIX, BIX, and FI denoted on biosolids-DOM and SRNOM EEMs. Additional description and results of FRI, Peak A:C boundaries and index computation are summarized in SI Tables 1-3.

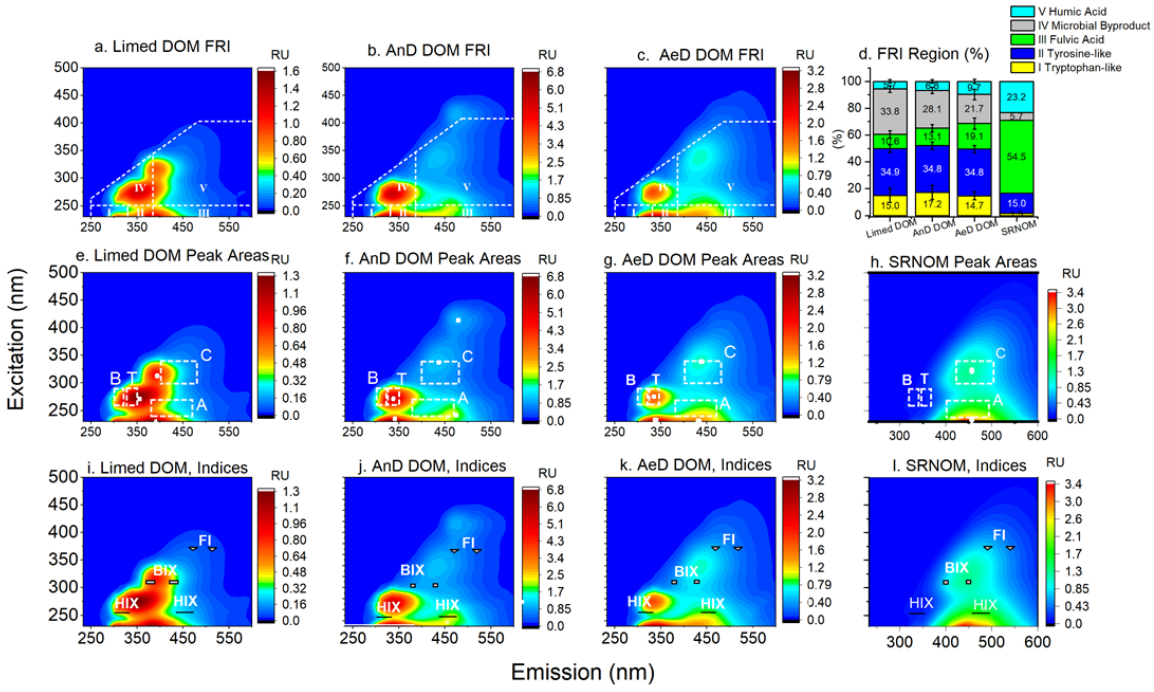

Figure 5: Boundaries and results of fluorescence regional integration (FRI) adapted for biosolids-DOM fluorescence maxima.

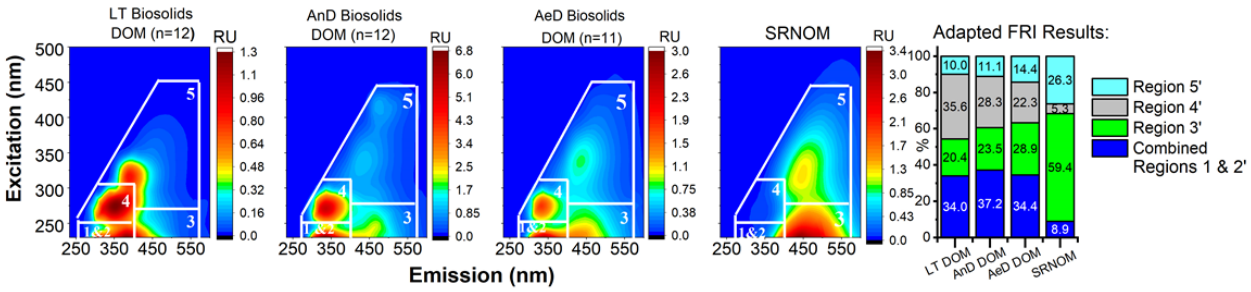

Table 2: Determination A:C and T:C Peak ratios by classically defined boundaries and adapted for proximal maxima of biosolids DOM, peak T:C ratio and was also computed.

	Ratio of Peak A:C Maxima, Classically Defined	**A:C Ratio adapted for proximal maxima to A:C**	**Ratio of Peak T:C Maxima, Classically Defined**	**Adapted Ratio of Biosolids-DOM Proximal Maxima to T:C**
Reference and Goal of Ratio	Coble et al. 1996 UV:Visible Humics	Value and % Difference to Classic Ratio	Baker et al. 2002: Protein-like:Fulvic-like	Value and % Difference to Classic Ratio Indicated
LT Biosolids DOM (n= 12)	1.2	1.5, 20%	1.7	1.5, 12%
AeD Biosolids DOM: (n = 11)	1.8	1.9, 6%	2.3	2.3
AnD Biosolids DOM: (n = 12)	2.3	2.4, 5%	5.1	5.1
Suwannee River Natural Organic Matter		Classic boundaries capsulated Maxima	Not Applicable to SRNOM Low fluorescence in T region	Not Applicable to SRNOM

Figure 6: Biosolids-DOM EEM-PARAFAC model fingerprints of a) LT-biosolids-DOM, b) AeD biosolids, and c) AnD biosolids-DOM. D. Table of maximum excitation and emission Ex_{max}, Em_{max} (nm) and average F_{max} of each component. Further details of models are presented

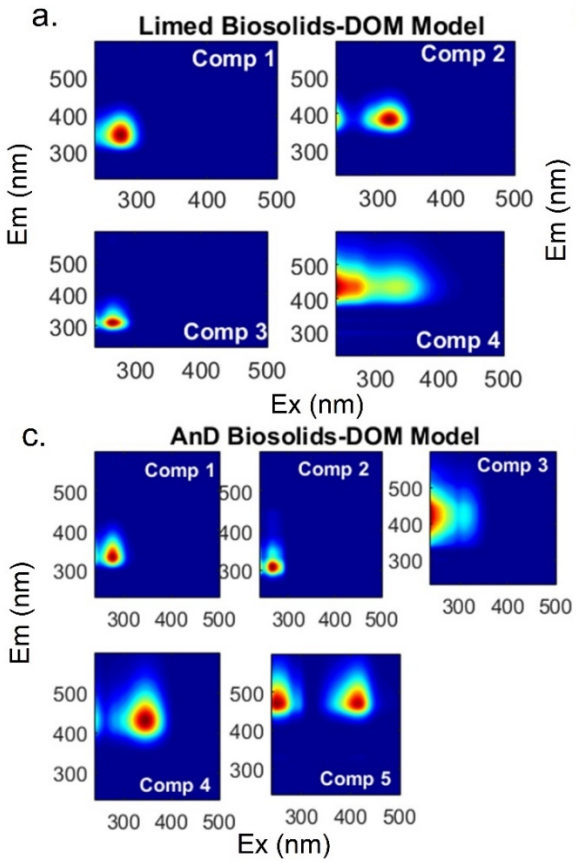

d.

Component:	C1	C2	C3	C4	C5
Limed Ex_{max}, Em_{max} (nm)	276, 348	318, 384	267, 310	270 (333), 437	
AeD Ex_{max}, Em_{max} (nm)	273, 326	342, 430	252 (402), 480	282 (306), 384	
AnD Ex_{max}, Em_{max}(nm)	276, 332	264, 310	240 (312), 420	345, 430	249 (414), 470
Limed F_{max} (n=12)	1.09	0.80	0.57	0.24	
AeD F_{max} (n=11)	1.69	0.70	0.42	0.43	
AnD F_{max} (n=11)	4.63	2.33	1.46	0.90	1.02

Figure 7: Excitation-emission matrices (EEMs) and evolution of multiple Ex/Em maxima on sludge-DOM across full-scale anaerobic digestion treatment trains. EEMs of additional treatment trains are presented in SI Figure 5.

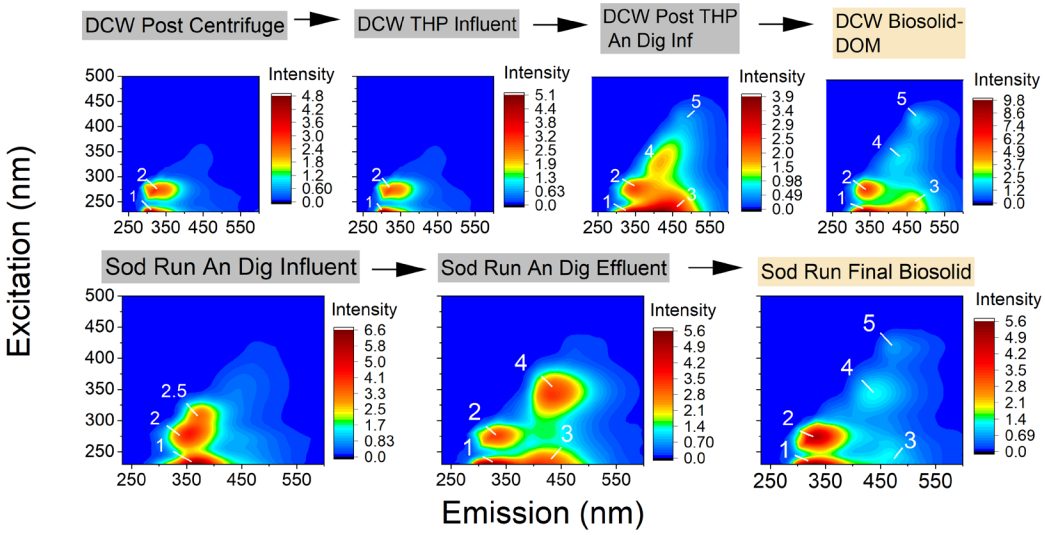

6. Supporting Information

SI Figure 1: a. SEC chromatograph for 67K-182 Da standards, retention times (min) labeled above peaks. Standards were injected in triplicate. b. Resulting calibration curve of PSS Standards Retention times versus Log(Molar Mass). The linear relationship between standards log molar mass (MM) and retention time was Log(MM) = -0.57264(min) + 13.44113 ± 0.45004, with an adj. R-square = 0.972. Error bars represent average RT of triplicate injections per molar mass standard; error bar magnitude was smaller than the point size displayed.

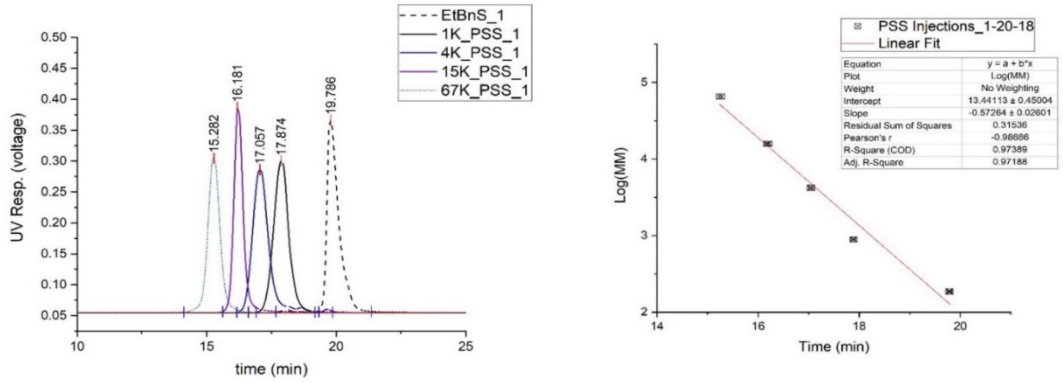

SI Figure 1c: Chromatograph of SROM. Apparent molar mass of peak (M_p) locations are indicated in daltons (Da) . Majority of SROM corresponded to an M_p of 2020 Da with small signal corresponding to 188 daltons. d. Full chromatograph of AeD-biosolids DOM and evidence of particulates, polymer, and/or supramolecular assembly.

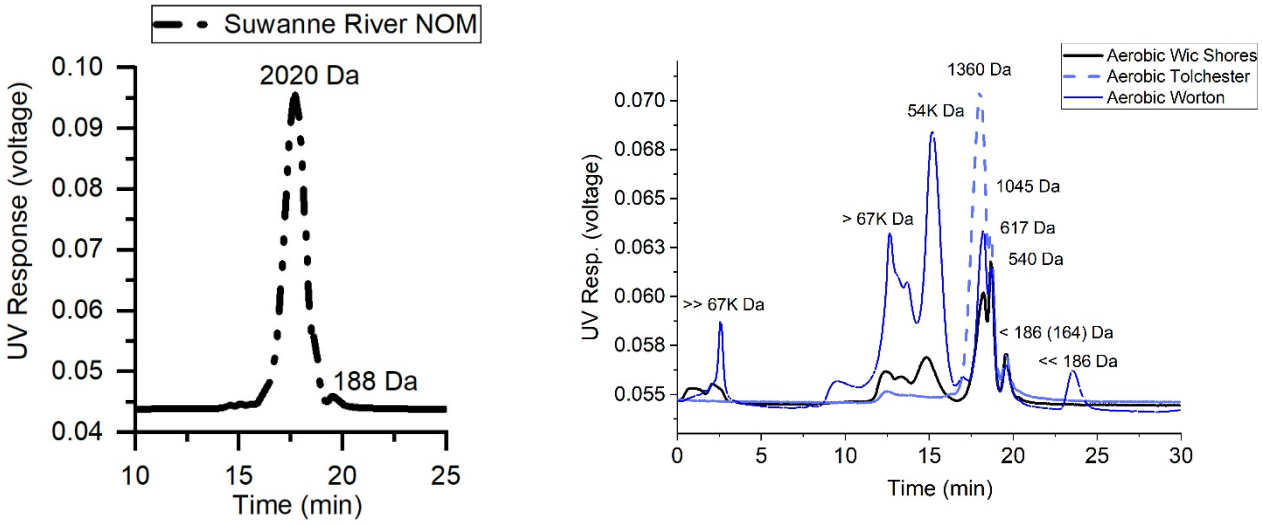

SI Figure 2: Xenochemical influence on biosolids-DOM. **(**a) Biosolids-DOM Extracts. Extracts from the Worton, MD facility were blue in color, (b) EEM of proprietary dewatering polymer added to sludge before final dewatering. Fluorescence was assessed at 7.5 mg C/L and contained minimal fluorescence contribution (>0.08 RU) to biosolids-FDOM.

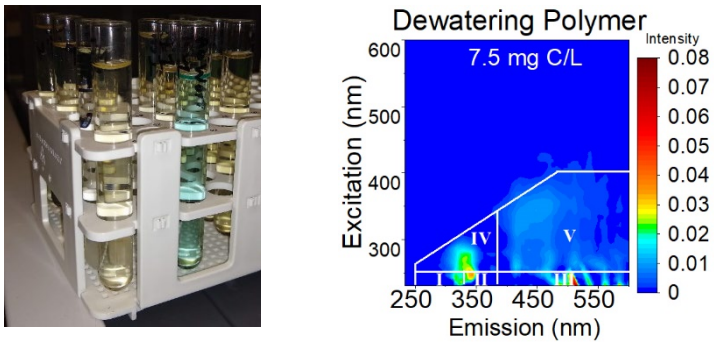

SI: Computation for Fluorescence Regional Integration (FRI)

The fluorescence EEMs of replicate DOM extracts (n=3 per 9 RRFs) was individually integrated for five previously described regions; (I) "tyrosine-like", (II) "tryptophan-like", (III) "fulvic acid-like", (IV) "microbial by-product-like, and (V) "humic acid-like" (Chen et al., 2003, SI Table 1). Following Chen et al. (2003) and others, the total volume (Φ_i) of each region of the EEM boundaries is summated by:

$$\Phi_i = \Sigma_{Ex}\Sigma_{Em} I(\lambda_{Ex}\lambda_{Em}) \Delta\lambda_{Ex}\Delta\lambda_{Em} \quad \text{(Eqn. 1)}$$

where $\Delta\lambda_{Ex}$ is the excitation wavelength interval, ΔEm is the emission wavelength interval and I (Δ_{Ex}, Δ_{Em}) is fluorescence intensity at each excitation-emission wavelength pair. The total number of data points for each region were computed to produce the fractional projected excitation-emission factor (F_i). The normalized fluorescence intensity volume (Φ_{in}) beneath region of the DOM sources was then computed:

$$\Phi_{in} = F_i \, \Phi_i \quad \text{(Eqn. 2)}$$

The fluorescence percentage of each region is calculated by the ratio of normalized regional volume to total FRI volume:

$$P = \Phi_{in} / \Phi_{T,n} * 100\% \quad \text{(Eqn. 3)}$$

Where (Φ_{Tn}) is sum of all normalized fluorescence of all regions. The final fluorescent region percentages (*P)* for each EEM was averaged by solid stabilization type. Standard deviation of *P* regions were computed based on multiple EEM FRI analysis per stabilization.

FRI was also conducted over modified boundaries adjusted to encapsulate fluorescence maxima in biosolids DOM, as well as signal beyond an excitation of 400 nm (SI Table 2). Volume of each regions were summated with equations 1-3.

SI Table 1: Excitation and emission (Ex/Em) wavelength boundaries applied for fluorescence regional integration (FRI) analysis of biosolids-dissolved organic matter extracts. Based on Chen et al. (2003).

Region	**Description**	**Ex/Em wavelength boundaries (nm)**
I	Tyrosine-like protein	230–250/233–330
II	Tryptophan-like protein	230–250/330–380
III	Fulvic acid-like organics	230–250/380–600
IV	Soluble microbial by-product	250–340 diagonal/260–380
V	Humic acid-like organics	250–340, 340-400 diagonal /380–600

SI Table 2: Adapted Ex/Em wavelength boundaries applied for fluorescence regional integration (FRI) analysis of biosolids-dissolved organic matter extracts.

Region	**Potential Composition**	**Ex/Em wavelength boundaries (nm)**
1 & 2	Tyrosine-like, Tryptophan-like, or polyphenol	230–250/250–400
3	UV ʎ fulvic or humic acid-like	230–275/400–550
4	Soluble microbial by-product or polyphenol-like	250–325 diagonal/270-400
5	Visible ʎ excited humic or fulvic acid-like	275–340 diagonal/260–575

SI Table 3: Fluorescent (FDOM) Component Peaks areas summarized in Stedman et al. 2003, Coble et al. (2007), and Gabor et al. (2014)

Peak	**Potential Fluorophore Type, considering source as well**	**Ex (nm) Range**	**Em (nm) Range**
B	Tyrosine-like protein	260-290	300-320
T	T_1, Tyrosine-like, protein-like (T_2 for phenolic sources, Maie et al. 2007)	260-290	326-350
A	UV Region Humic-like and fulvic acid-like	240-270	380-470
C	Visible Humic-like	300-340	400-480

SI Table 4: Results of Fluorescence Index Computation. Indices were computed on individual EEMs and averaged by treatment type. Standard deviation of averages of treatment type are also reported.

	E_2/E_3	Humification Indices (z, o): zHIX oHIX	Modified Biological Index BIX	Fluorescence Index: FI
Description	Ratio of UV absorbance at 250 nm to that at 365 nm	At fixed Ex: 254 nm z: ratio of area under (Em: 435–480 nm)/ Area under (Em 300–345 nm) o: ratio of area under (Em: 435–480 nm)/ Sum (Area under +(Em: 435–480 nm) and (Em 300–345 nm)	Ratio of signal at Em: 380 n.m. /430 n.m., at Ex: 310 nm Ratio of β/α emission at fixed wavelength. Modified as β = 380 n.m. α = 430 n.m	Ratio of signal at Em: 470 nm/em 520 nm at Ex 370 nm.
Interpretation	Decreasing E_2/E_3 values reflect that the DOM matrix has a higher average molecular weight	Higher numbers previously indicated lower H/C ratios shifting the emission to longer wavelengths and a greater degree of humification. Developed with soil extracts.	Increase in BIX suggests autochthonous production or microbial input to humic substances of aquatics and marine systems	Precursor material for DOM is of a more microbial (FI ~1.8) in nature or more terrestrially derived (FI ~1.2).
Reference	Helms et al. 2008	o = Ohno (2002) z = Zsolnay et al. (1999)	Parlanti et al. (2000) Huguet et al. (2009)	McKnight et al. (2001)
Limed Biosolids DOM (n= 12)	16.2 ± 10.0	z: 0.41 ± 0.18 o: 0.28 ± 0.09	1.70 ± 0.62	2.15 ± 0.14
Aerobic Digestion: (n = 11)	9.9 ± 8.19	z: 1.08 ± 0.46 o: 0.50 ± 0.10	0.67 ± 0.1	2.01 ± 0.08
Anaerobic Digestion: (n = 12)	7.24 ± 2.47	z: 0.75 ± 0.52 o: 0.37 ± 0.16	0.81 ± 0.19	2.24 ± 0.24

SI Figure 3: Excitation and emission loadings of 4 and 5 component EEM-PARAFAC models generated during preliminary analysis. Loadings were appraised for the following features (Murphy et al. 2013): (i) minimal overlap between the excitation and emission spectra, (ii) excitation spectra that may have multiple peaks, but emission spectra exhibit a single distinct peak, (iii) excitation spectrum has two or more peaks indicating consecutive excited state absorption bands, some absorption (excitation) occurs between these peaks, and (iv) excitation and emission spectra do not exhibit abrupt changes over very short wavelength distances.

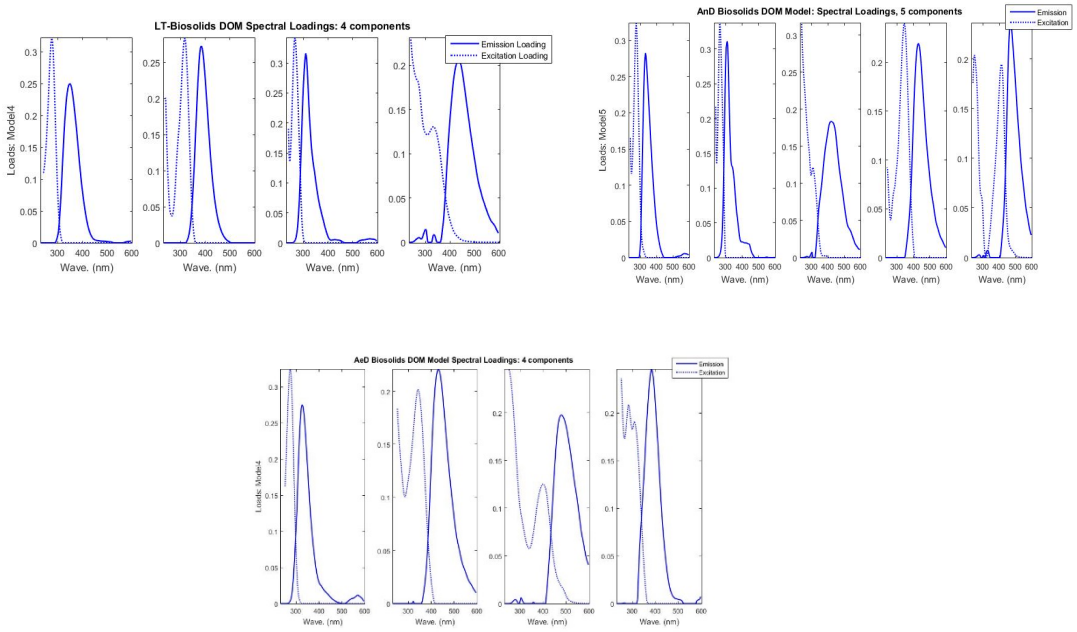

SI Figure 4: Split Half Validations of PARAFAC Models

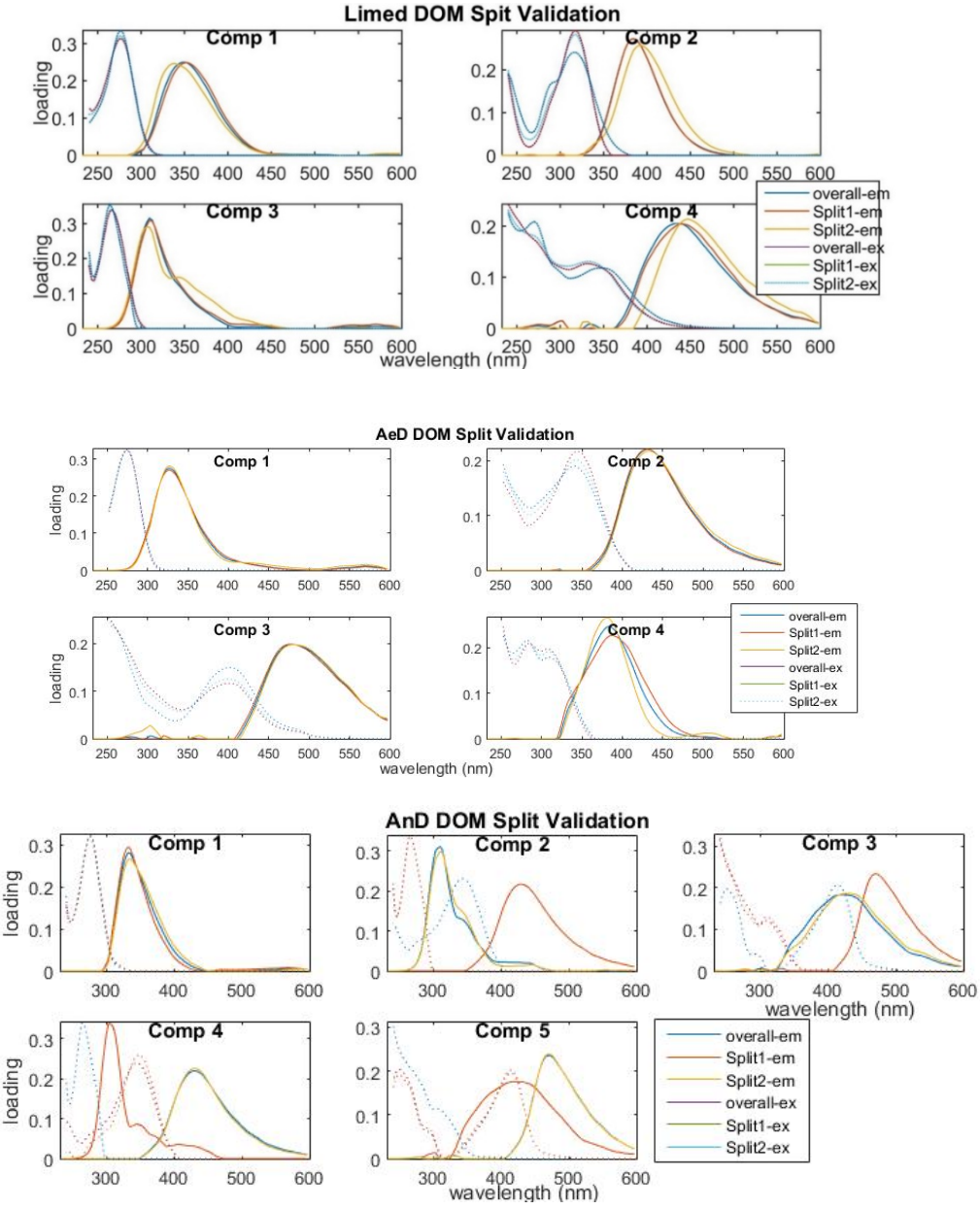

SI Figure 5: Component comparisons at a 0.97 threshold for three biosolids-DOM PARAFAC models deposited to the OpenFluor plugin for OpenChrom.
Model Name: **Limed Digestion**

C1

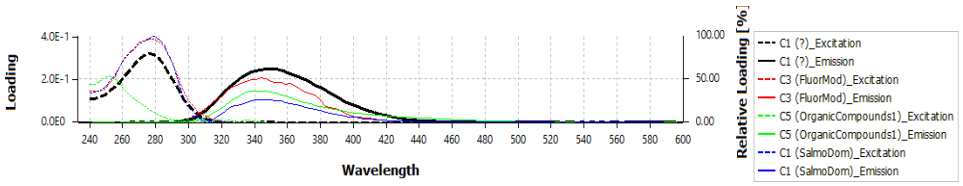

C2

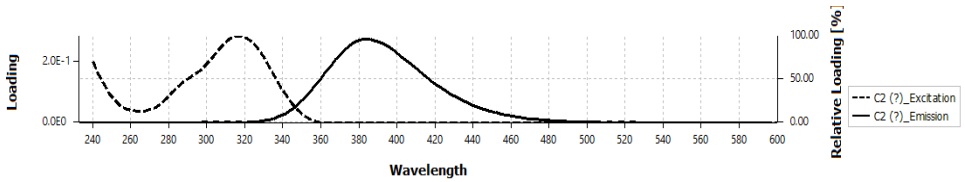

C3

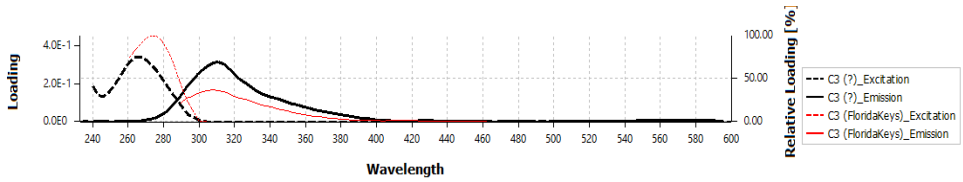

C4

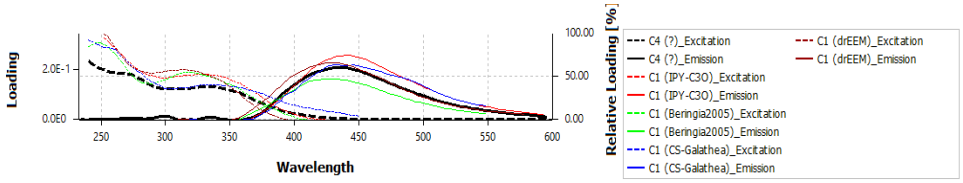

Matched Models: 8 / 70, Min, Min Similarity Score: 0.97, Software: OpenFluor plugin for OpenChrom Version: 1.3.0.2017101902, Matched Components (Excitation/Emission)

Model Name: **Aerobic digestion:**

C1

C2

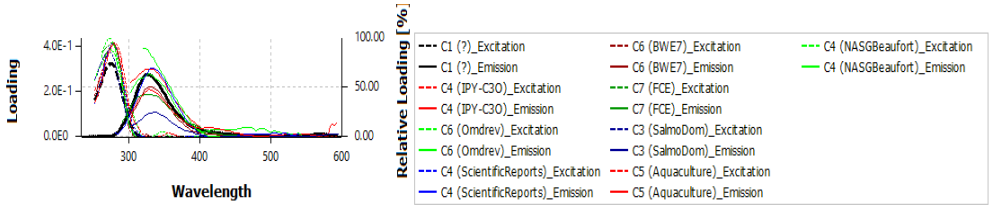

C3

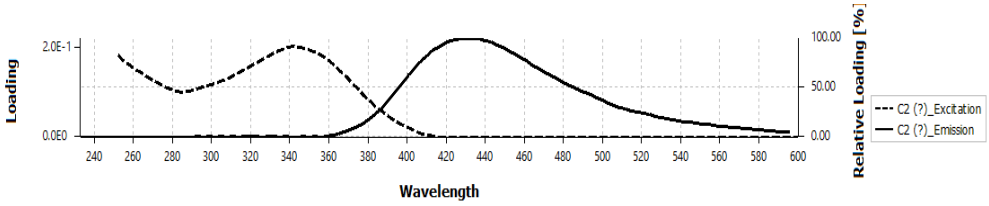

C4

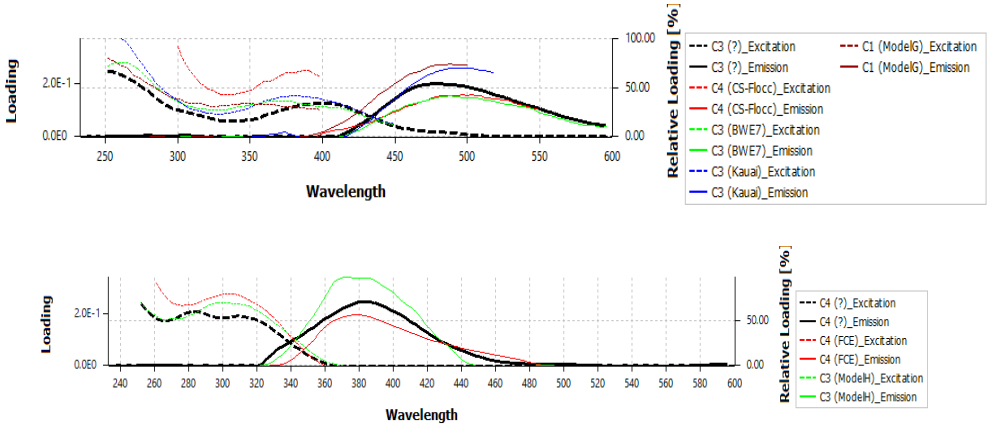

Matched Models: 12 / 70, Min Similarity Score: 0.97, Software: OpenFluor plugin for OpenChrom Version: 1.3.0.2017101902, Matched Components (Excitation/Emission)

Model Name: **Anaerobic digestion**

C1

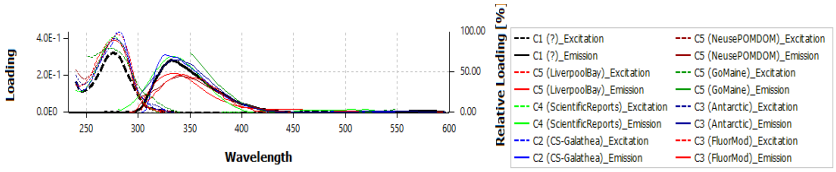

C2

C3

C4

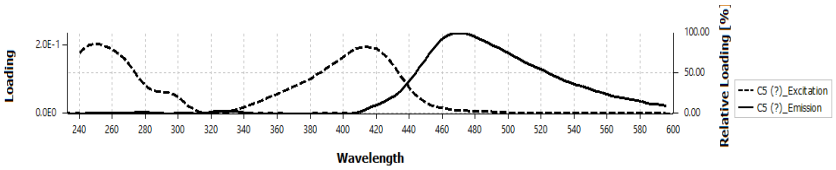

C5

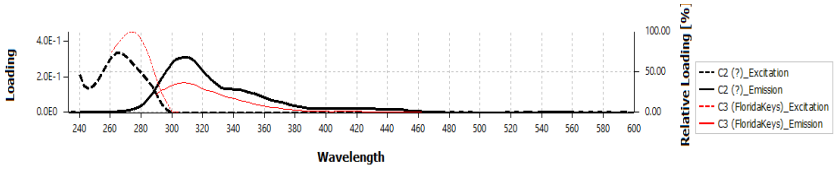

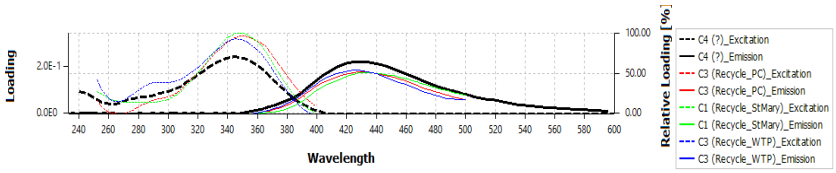

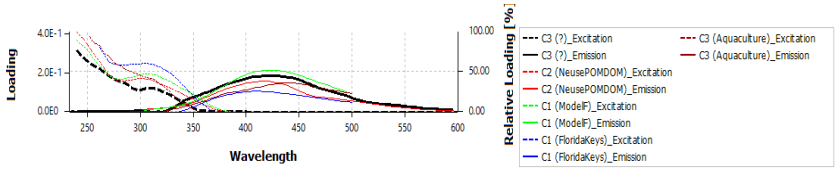

Matched Models: 13 / 70
Min Similarity Score: 0.97

SI Figure 5: Fluorescence spectroscopy of two additional AnD and AeD treatment trains: St. Mary's (St M.) and Tolchester, MD (Tolch) facilities.

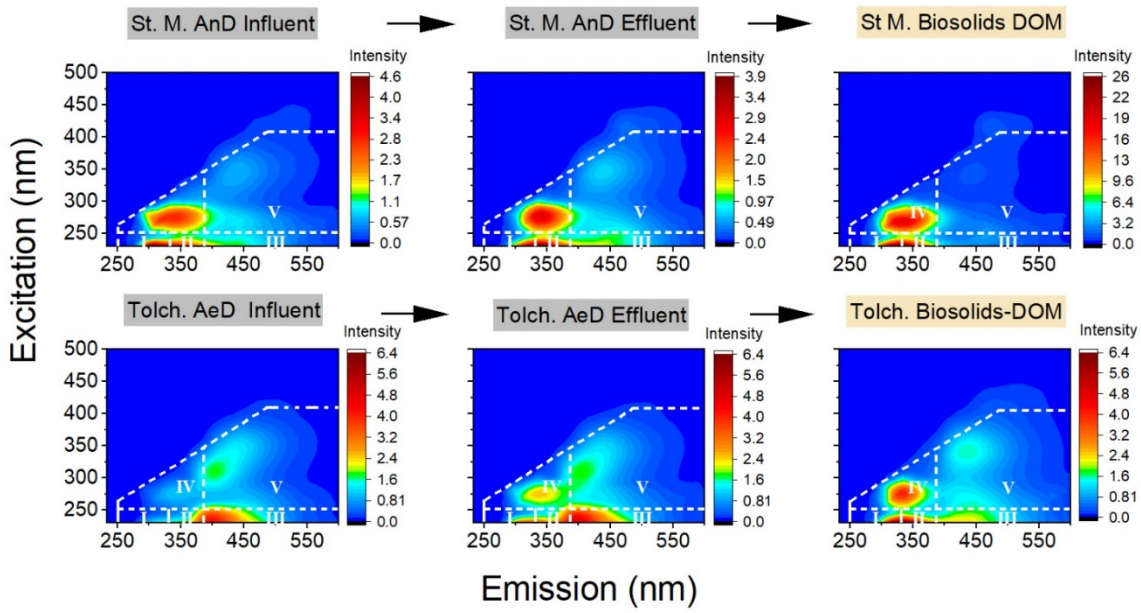

Chapter 4: Fluorescence Suppression Experiments to understand interactions of halogenated antimicrobials with contrasting biosolids-DOM pools

Abstract

The fluorescence suppression (quenching) of biosolids-DOM by contaminants triclocarban (TCC) and 2-4 dichlorophenol (2-4 DCP) was measured with three-dimensional fluorescence spectroscopy. We constructed theoretical excitation emission matrices (EEMs) of contaminants and biosolids-DOM according to a simple superposition model. We then compared constructed spectra to experimental mixtures to parse quenching of both DOM and additional contaminant. Despite biosolids leachates from different stabilizations of lime treatment, aerobic digestion, and anaerobic digestion having contrasting red-shifted (low energy stimulated) fluorescence of humic or fulvic acid-like qualities (Chapter 3), similar blue-shifted (high energy) fluorophores in all biosolids-DOM was quenched by the contaminants. Chemical differences between 2-4 dichlorophenol and triclocarban did not appear to result in different DOM fluorophores being suppressed. Both 2-4 DCP and TCC were also quenched by biosolids-DOM. The suppressed high-energy biosolids fluorophores of Ex_{max}: 238-271 nm and Em_{max}: 307-354 nm have been previously associated to small aromatic compound fluorescence such as tryptophan, tyrosine, or phenols. By use of the superposition model, we show that signals for both the added "quencher" and DOM can be suppressed. Fluorescence quenching represents complex electrochemical interactions and charge-transfer dynamics. Future work is needed to directly connect these experiments to other assays (microbial bioavailability, K_{DOM} measurements) to confirm that fluorescent interaction

measurements translate to scalable implications for the environmental fate of emerging contaminants in biosolids.

1. Introduction

Treated wastewater residuals or biosolids are land-applied as a soil amendment to recycle residuals that enhance nutrient and organic carbon content of agricultural soils (Lu et al. 2012, Cogger et al. 2012). Although there are significant societal and agronomic benefits to recycling biosolids, treated residuals are a well-documented source of CECs (McClellan et al. 2010). While CECs can be consistently measured in biosolid matrices, the US EPA (2018) identified that a lack of data exists for risk assessment, bioavailability, and mobility assessment of 352 pollutants deriving from biosolids. DOM in soil and aquatic systems has a broadly demonstrated role in the movement and bioavailability of metals, nanoparticles, and organic contaminants (Kalbitz et al. 1998, Chefetz et al. 2008, Delgado-Moreno et al. 2010, Chen et al. 2015). In Chapter 3, I described biosolids that have categorically distinct water extractable DOM dependent on resource recovery facility (RRF) stabilizations of lime treatment (LT), anaerobic digestion (AnD), and aerobic digestion (AeD). The effect of stabilization specific biosolids-DOM on the mobility and bioavailability of contaminants is currently unknown.

DOM is a biogenic and heterogeneous mixture of aliphatic and aromatic carbon structures with various polar functional groups of carbonyls, quinones, polyphenols, or carboxylic acids (Cory et al. 2005). DOM therefore can have complex interactions with CECs of varying physicochemical characteristics. DOM has been shown to modify the bioavailability of dissolved antibiotics (Chen et al. 2015). Fluorescence quenching

experiments has been previously used to study interactions between organic contaminants and fluorescent DOM (Hernandez-Ruiz et al. 2012, 2013, Pan et al. 2012). Three-dimensional fluorescence spectroscopy is widely applied across aquatic, marine, and engineering sciences to describe heterogeneous components in DOM that exhibit an emission response when stimulated by excitation energy (i.e. fluorescent DOM or FDOM, Del Vecchio et al. 2004). Quenching is the process by which two compounds interact, in several possible ways, to decrease fluorescence response of energy-stimulated matter. These interactions can be dynamic or collisional, or static, where ground-state complexes are formed and suppress fluorescence emission of the "quenched" molecule (Lakowicz, 2006). Pan et al. (2012) demonstrated that fluorescence spectroscopy is a method to measure the combined quenching interactions between sediment-derived humic acids and the antibiotic ofloxacin.

Absorbance and fluorescence spectroscopy stimulates a bulk, complex mixture of chromophoric (light absorbing) and subsequently any fluorescent (light emitting) DOM (Minor et al. 2014). A simple superposition model is implied in certain application of absorbance and fluorescence spectroscopy, such as Parallel Factor Analysis (PARAFAC), where it's assumed that chromophores and fluorophores absorb and emit light as independent, non-interacting compounds. With the superposition model assumption, an excitation emission matrix (EEM) can then be idealized as a sum of individual absorbance or fluorophore spectra that are electronically isolated. A simplistic superposition model cannot be assumed because the constituents of DOM interact via complex charge-transfer dynamics between electron donating and accepting chromophores (Sharpless and Blough, 2014). Considering charge-transfer relationships,

we offer a modification to previous DOM-PPCP quenching experiments with aromatic contaminants (Holbrook et al. 2005, Wang et al. 2017, and others). Herein, we present EEM spectra based by purely additive mathematical construction of biosolids-DOM spectra added to the spectra of the aromatic contaminant, assuming the superposition model. We then measured the EEM of the experimental mixture of biosolids-DOM and additional contaminant. Differences between theoretical EEM constructions, spectra of contaminants in high purity water, and EEMs of experimental mixtures offer a means to clarify complex interactions of not only different pools of DOM being quenched, but also the contaminant itself, contrary to the simple superposition model.

Several research studies have conducted quenching experiments with Suwannee River Natural Organic Matter (SRNOM), riverine DOM, and wastewater effluents with various organic contaminants (Holbrook et al. 2005, Wang et al. 2017). No known work has probed interactions of antimicrobial triclocarban and 2-4-dichlorophenol with biosolids derived DOM. Our goal was to examine whether distinct DOM pools derived from (i) LT, (ii) AnD, and AeD stabilized biosolids have distinct interactions with two common CECs of variable solubilities and chemical structures: triclocarban (TCC) and 2-4 dichlorophenol (2-4 DCP) that have been previously detected in biosolids (Halden et al. 2010, Bright and Healey 2003). These experiments can then be used to indicate fundamental differences in functional group interactions and charge-transfer behaviors.

Biosolids are applied to target, and not exceed, seasonal nitrogen demand of various cropping systems to protect waterways from eutrophication (US EPA, 1994, Rule 50, Rigby et al. 2016). Application guidelines varies for biosolids produced from different stabilization methods, and these stabilizations can generate different pools of organic

carbon of various polar and non-polar chemical moieties, solubilities, and size distributions. Our goal was to assess whether contrasting pools of biosolids-DOM from different stabilization processes lead to distinct chemical interactions with CECs towards a more complete risk assessment of CECs deriving from variable biosolids matrices.

2. Material and Methods

2.1 Biosolids Collection, Extraction, and DOC Analysis

Dewatered biosolids were grab-sampled from nine RRFs total with different waste stabilizations of (i) anaerobic digestion (AnD), (ii) aerobic digestion (AeD), and (iii) lime treatment (LT) at RRFs in the Washington, DC and Maryland, USA area as detailed in Chapter 2 of this dissertation. All biosolids remained frozen at -20ºC before DOM extractions and characterizations. Residuals were defrosted overnight at 4 ºC. Repeated, consistent results for DOC quantification and fluorescence characterization confirmed that freezing the solid did not affect the extracted DOM quantity or quality over time. Water-exactable DOM was extracted from biosolids as previously described with 1:10 w/v solid:water ratios on an orbital shaker at room temperature for 24 hours, centrifuged at 10,000 rpm, and filtered with a 0.45 µm Whatman GF/F cellulose acetate membrane filter. DOC of extracts was determined as non-purgeable organic carbon via a platinum oxidation catalyst and non-dispersive infrared gas analyzer (Shimadzu TOC/TN-L, Columbia, MD). The instrument was calibrated with a glycine standard curve and with repeat testing of standards as unknown to assess drift and reproducibility. DOC of each sample was analyzed with repeated injections to meet the criteria that coefficient of variation for peak areas was less than 2% per sample.

2.2 Quenching Mesocosm Set-Up

Stock solutions of high purity 2-4 DCP (Sigma Aldrich) and TCC (Sigma Aldrich, 99.9% Grade) were prepared at an equal molar concentration of 1.58 mM in in high purity acetone (Sigma Aldrich, 99.9% Grade). The stock concentration was chosen to target equal molar dosing of 1.58 uM 2-4 DCP and TCC. The final molar concentration of 1.58 uM is under the aqueous solubility of TCC and 2-4 DCP. Chemical properties of TCC and 2-4 DCP are summarized in Table 1.

All DOM extracts were adjusted to 7.5 mg C/L prior to fluorescence spectroscopy. Dilutions were also adjusted to a final pH of 7 ± 1.0. Four mL of diluted DOM from specific RRFs were added to amber glass vials and spiked with 4 uL of acetone, or, acetone and TCC or 2-4 DCP to bring the final concentration of acetone to 0.1% in all samples (including unspiked DOM), and spiked samples to a final concentration of 1.58 uM of contaminant (500 ug/L TCC, 258 mg/L 2-4 DCP). Spiked DOM microcosms were set up in duplicate per RRF and chemical type. Vials were covered in foil and oscillated for 24 hours at room temperature. Suwannee River Natural Organic Matter (SRNOM) obtained from the International Humic Substances Society (IHSS) was reconstituted, adjusted to a neutral pH and DOC of 7.5 mg C/L, spiked with additional chemical, and incubated in a similar fashion to biosolids-DOM.

2.3 Fluorescence Analysis, Construction of Theoretical EEMs, and Residual Analysis

Ultraviolet-visible (UV-Vis) absorbance spectra and fluorescence spectra of dilutions were collected in 3.5 mL clear quartz cuvette cells (light path 1 cm x 1 cm). Absorbance spectra and fluorescence EEMs were both measured using an Aqualog fluorometer (Horiba Scientific; Edison, NJ). The excitation and emission wavelength ranges were 230−600 nm with a wavelength step of 3 nm for excitation and emission

scans. Due to possible fluorescence response of added aromatic contaminates or acetone, Biosolids-DOM spiked with 0.1% acetone were blanked with 0.1% acetone in high purity. biosolids-DOM spiked with additional contaminants 2-4-DCP or TCC were blanked against the spectra of 0.1% acetone with TCC or 2-4 DCP against high purity water spectrum. Inner-filter corrections, Rayleigh-Tyndall scattering, and conversion to Raman Units (RU) using water at an excitation wavelength of 350 nm (emission range 381−441 nm) were performed using the Aqualog software on all EEMs following procedures described in Timko et al. (2015). The 1st and 2nd order Rayleigh-Tyndall scattering effects were removed, and the surrounding data was interpolated post hoc (Zepp et al. 2004) in MatLab® (MathWorks, MA)

Theoretical DOMs and contaminant only EEMs were summed in MatLab (MathWorks, MA) assuming the superposition model. The difference of theoretical EEMs and experimental EEMs were computed with in MatLab to result in residuals of quenched DOM *and* EC (Difference 2), or first residual). The fluorescence spectra of the contaminant in high purity water was then subtracted from the first residual or difference plot to produce a second residual (Difference 2), or quenched DOM and without quenched effects of the EC.

3. Results and Discussion

Application of the superposition model allowed for theoretical constructions of DOM with additional contaminants to parse out complex charge-transfer effects that may quench the fluorescence response of both the quencher (added 2-4 DCP or TCC) and the DOM. Absorbance spectra of biosolids-DOM and biosolids-DOM spiked with contaminant (blanked by the absorbance of 2-4 DCP or TCC) indicated that the

superposition assumption held for absorbance (Figure 1). Residual differences between theoretical and experimental mixture EEMs for all biosolids-DOM types and SRNOM indicated that the superposition model did not hold for fluorescence measurements, however (Figures 2-8). Altered fluorescence response consistent with the electronic interaction model where quenching of DOM and the quencher can occur.

Limed biosolids FDOM from Little Patuxent (LP) and Laurel facilities were characterized by three blue-shifted (UV range) fluorophores previously associate with amino acid-like or polyphenol fluorescence as well as a slightly red-shifted fluorophore not captured by conventional fluorescence indices (Fischer, Chapter 3, Jaffee and Maie, 2006, Baker et al. 2002). The 1st quenching residual computed for the difference between theoretical and experiment DOM and TCC mixtures indicated a broad fluorescence suppression from Em: 300 nm-450 nm and a more limited one at Ex: of 250 – 300 nm. LT Biosolids-DOM local fluorescence maxima at ex: 350 nm was not involved in quenching (Figure 4). The fluorescence spectra of TCC in high purity water contained an Ex_{max}:Em_{max} of 265 nm:403nm and 2-4 DCP in high purity water contained an Ex_{max}:Em_{max} of 274 nm:403nm (Figure 3). Computation of the 2nd residual, subtracting the spectrum of the contaminant from the 1st residual, confirmed that in the experimental mixture of LT biosolids-DOM and TCC, TCC was also quenched. The 2nd residual for LT Little Patuxent and Laurel RRF biosolids-DOM resulted in a quenched region of DOM at Ex_{max}: 270 nm and Em_{max}:307 nm, as well as Ex_{max}: 230 m and Em_{max}:307 nm. This quenched region corresponded to the most blue-shifted fluorophores present in LT biosolids-DOM, previously described for microbial byproduct-like and tyrosine and tryptophan-like fluorescence.

Despite containing additional red-shifted fluorescence maxima previously associated to humic acid-like and fulvic acid-like fluorescence (Fischer - Chapter 3), AnD biosolids-DOM from DC Water (THP-AD) and Sod Run, MD exhibited quenching largely of UV "blue-shifted" or higher energy fluorescence, similar to LT biosolids-DOM (Figure 6 and Figure 7). Computation of the 1st residual indicates that both 2-4-DCP and TCC were quenched by AnD-biosolids DOM. Computation of the 2nd residual indicated that "blue-shifted" local maxima at an Ex_{max}:Em_{max} 270 nm:330 nm of AnD-biosolids-DOM was quenched for two leachates tested from AnD Sod Run material and DC Water Biosolids. Similar Ex_{max}:Em_{max} and intensities of DOM quenching was observed for either TCC and 2-4 DCP, despite these compounds having different solubility and functional groups (Table 2). Greater quenching was observed for DC Water derived DOM than Sod Run derived material, but this could be due to variations in dissolved carbon concentrations. Both AnD-biosolids DOM tested had comparable levels of quenching for either 2-4 DCP or TCC.

Major quenching of AeD-Biosolids DOM occurred in the "blue-shifted" high energy fluorophore previously associated to small aromatic compounds, such as amino-acids tryptophan and tyrosine (Chen et al. 2003, Baker et al. 2002, Figures 7, 8, and Table 2). Quenching of AeD-biosolids DOM leached from the Tolchester, MD facility similar for both 2-4 DCP (RU = 0.2) and TCC (RU = 0.23). Quenching of AeD-DOM, Wicomico Shore was also similar for both 2-4 DCP (RU= 0.12) and TCC (RU = 0.12). While less signal from AeD-DOM, Wicomico Shores was quenched, differences in dissolved organic carbon due to dilution may have caused variations in quenching effects

between DOM pools. This variable could be explored by normalizing data to the absorbance at 254 nm to adjust for differences in DOC data.

Quenching of SRNOM contrasted the biosolid-DOM quenching trend with minimal detectable quenching of SRNOM observed from TCC (Figure 10). Detectable red-shifted quenching of SRNOM from 2-4 dichlorophenol occurred at an Ex_{max}:Em_{max} of 258 nm:434 nm at an RU=0.37. SRNOM does not contain blue-shifted, Peak B or T, or amino acid or polyphenol associated material and is characterized by with red-shifted humic acid-like and fulvic acid-like fluorescence (Chapter 3).

Although biosolids-DOM contained both red-shifted and blue-shifted fluorescence, the majority of DOM quenching and interaction occurred for blue-shifted amino acid-like or poly phenol-like regions in contrast to SRNOM. Biosolids-DOM quenching was consistent for multiple replicates of the same DOM and contaminant. Previous work has found that the amino acid-associated fluorescence is quenched by the humic acids-like components, but humic acid-like fluorescence is not readily quenched after titrations of amino acids into a given sample (Wang et al. 2015). These authors postulate that efficient intermolecular energy transfer from quenched amino acids to humic-acid like DOM occurred. Wang and Zhang (2014) have indicated that smaller molecular weight aromatics, such as polyaromatic hydrocarbons (PAHs) may efficiently charge-transfer to DOM compartments (conjugated, humic acid-like material) because the emission spectra of PAHs overlap with the absorbance spectra of DOM. In this study, we observed quenching of smaller molecular weight contaminants TCC (315.6 Da) and 2-4 dichlorophenol (163 Da) containing 2 to 1 aromatic features respectively, as well as blue-shifted DOM. This suggests complex charge transfer dynamics between both the

contaminant added and blue-shifted amino acid associated components, potentially to red-shifted components. Specific functional groups are cited to support intermolecular energy transfer between electron donor groups, such as indoles and polyhydroxylated aromatics, to acceptor groups such as oxidized aromatics and quinones (Boyle et al., 2009; Del Vecchio and Blough, 2004). The contaminants 2-4 DCP contains a hydroxylated aromatic that could serve as an electron donor. Limited work discusses or presents measurement of the emerging contaminant quencher being suppressed by DOM.

Electronic quenching interactions can occur in ground states during static associations or from charge-transfer of excited states in collisional interactions dynamically (Lakowicz, 2006). Temperature-based experiments or fluorescence lifetime measurements can discern between different quenching mechanisms according to the Stern-Vohlmer relationships. Higher temperatures may trigger faster diffusional and collisional quenching. If greater fluorescence of a signal is quenched at cooler temperatures, however, the quenching mechanism is considered static. Static molecular interactions may be considered more environmental significant because they are based on ground state chemical associations, rather than random collisional interactions. Pan et al. (2012) modeled the antibiotic ofloxacin (OFL) to generate 30-90% dynamic quenching with a combination of static quenching interactions with humic acid isolated from sediments. Pan et al. (2010) found that herbicide dicamba had both static or collisional quenching interactions with different fluorescence maxima, i.e. different pools of soluble extracellular polymeric substances (EPS) from activated sludge aeration tanks. EPS fluorescence of peaks B and C, or amino acid-like and humic acid-like material, were quenched via static processes, while fulvic acid-associated peak A was dynamically

quenched. Future work research with anthropogenic biosolids-DOM described herein could employ temperature-based experiments to clarify whether the blue-shifted quenching we observed was statically or dynamically driven.

The DOM partition coefficient of a contaminant (K_{DOM}) is DOM specific and quantifies specific partitioning of chemicals to DOM rather than ultra-pure water (Pan et al. 2008, Chen et al. 2015). Experimental designs for determining K_{DOM} include contaminant-plated glass desorption experiments (Wei-Hass et al. 2014) or dialysis-based measurements (Gu et al. 2007). While K_{DOM} was not determined in these experiments, future work could measure K_{DOM} in connection to fluorescence quenching experiments to extend electronic interaction measurement other experiments measuring physical partitioning.

It is well demonstrated that DOM interact with organic contaminants have been shown to reduce bioavailability of the contaminant. DOM in solution with the antibiotic tetracycline was recently shown to reduce the expression of antibiotic resistance genes. Chen et al. (2015) found that adsorption of DOM on bacterial cell surfaces inhibited tetracycline diffusion into cells and diminished free tetracycline in solution, reducing the effective dose. This affect was measured by cultivating *E. coli* with both an antibiotic resistance gene *tet(M)* and flow cytometry-optimized *gfp* gene encoding for a green fluorescence protein. Bacterial luminesce tests (BLT) such as Microtox® have been utilized to measure the inhibitory effects of triclosan (Villa et al. 2014) or suppression of the effect by DOM on toxic metals lowest observable effect concentrations (Hiesh et al. 2004). Quenching experiments offer a mechanistic

measurement that can explain the influence of DOM on the toxicity of contaminants in bioassays.

4. Conclusions

We applied a simple superposition model to construct theoretical excitation emission matrices (EEMs) of contaminants and biosolids-DOM interactions at a pH of 7. We then compared constructed spectra to experimental mixtures to parse quenching of both DOM and additional contaminant. Despite biosolids leachates from different stabilizations of lime treatment, aerobic digestion, and anaerobic digestion containing contrasting red-shifted (low energy stimulated) fluorescence of humic or fulvic acid-like qualities (Chapter 3), only similar blue-shifted, high energy stimulated fluorophores in all biosolids-DOM was quenched by the contaminants. Chemical differences between 2-4 dichlorophenol and triclocarban did not appear to result in different DOM fluorophores being suppressed. Both 2-4 DCP and TCC were also quenched by biosolids-DOM. The suppressed high-energy biosolids fluorophores of Ex_{max}: 238-271 nm and Em_{max}: 307-354 nm have been previously associated to small aromatic compound fluorescence such as tryptophan, tyrosine, or phenols. By use of the superposition model, we show that signals for both the added "quencher" and DOM can be suppressed. Fluorescence quenching represents complex electrochemical interactions and charge-transfer dynamics. Future work is necessary to connect fluorescence experiments to other assays measuring environmental fate of emerging contaminants in biosolids

Chemical and Use	Structure	Aqueous Solubility	pKa
2-4-Dichlorophenol Breakdown product of triclosan, chemical precursor in manufacturing	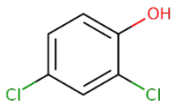	4.5 x 10^3 mg/L at 20 °C[1]	7.44[2]
Triclocarban antimicrobial agent, antiseptic	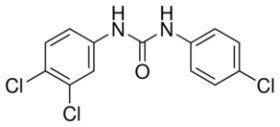	0.6479 mg/L at 25°C[3]	12.7[4]

5. Figures: Chapter 4

Table 1: Chemical properties of EC quenchers used in this study.

References to Table 1:

[1] Yalkowsky SH, Dannenfelser RM; Aquasol Database of Aqueous Solubility. Version 5. College of Pharmacy, Univ of Ariz - Tucson, AZ. PC Version (1992)

[2] Serjeant, E.P., Dempsey B.; Ionisation Constants of Organic Acids in Aqueous Solution. International Union of Pure and Applied Chemistry (IUPAC). IUPAC Chemical Data Series No. 23, 1979. New York, New York: Pergamon Press, Inc.

[3]US EPA EPI Suite™ WSKOW v1.41

[4] Wu, C., Spongberg, A.L. and Witter, J.D., 2009. Adsorption and degradation of triclosan and triclocarban in soils and biosolids-amended soils. Journal of agricultural and food chemistry, 57(11), pp.4900-4905.

Figure 1: Absorbance plots of AnD Sod Run Biosolids-DOM blue) with and without TCC, with blanked with the absorbance of TCC (orange). TCC in 0.1% acetone and high purity water only (grey) had high absorbance at 259 nm. The overlay of AnD-DOM only and AnD-DOM with TCC confirm that the TCC spectra is effectively blanked and has a simple additive effect on the absorbance spectra.

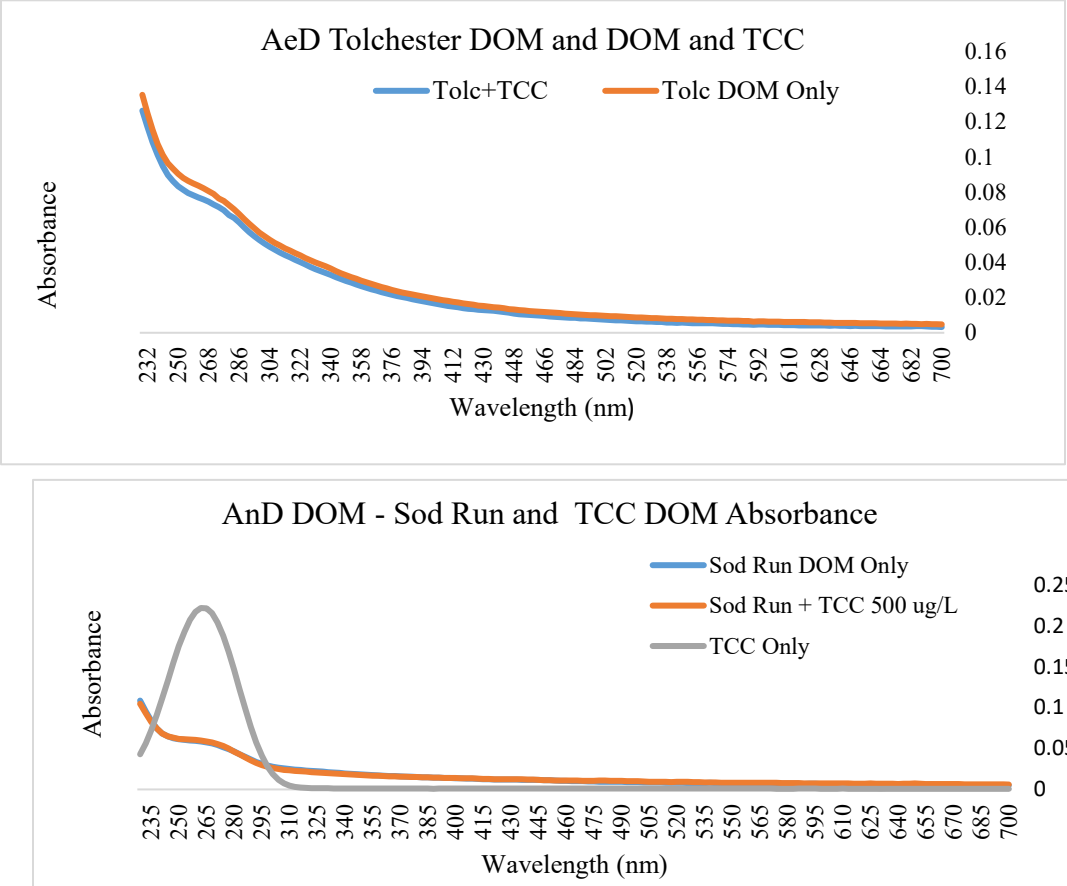

Figure 2: Absorbance plots of AeD Tolchester (Tolc) Biosolids-DOM with and without TCC (blue) and with TCC blanked (orange). The lack of significant variance in absorbance confirm the superposition model held and that added TCC was effectively blanked from AeD biosolids DOM

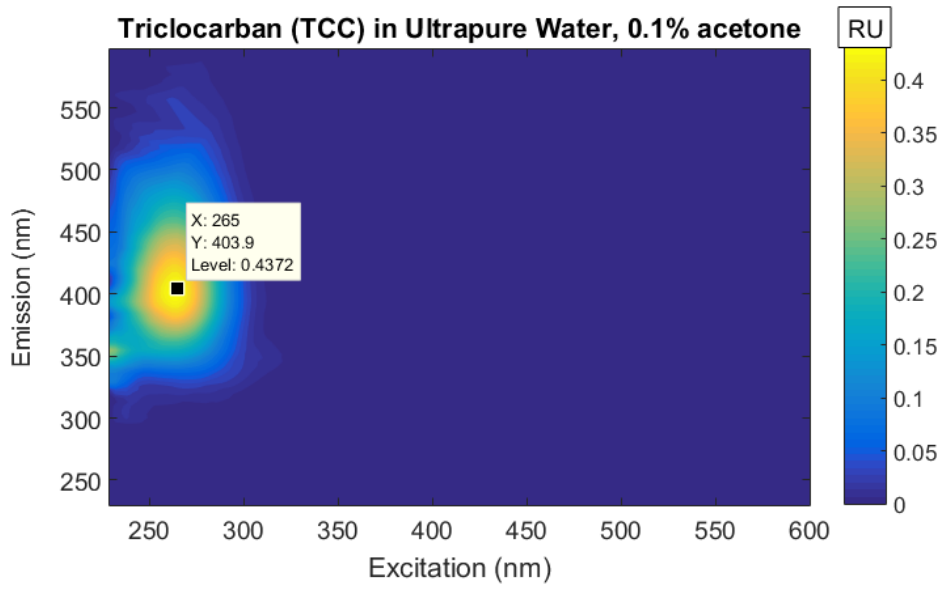

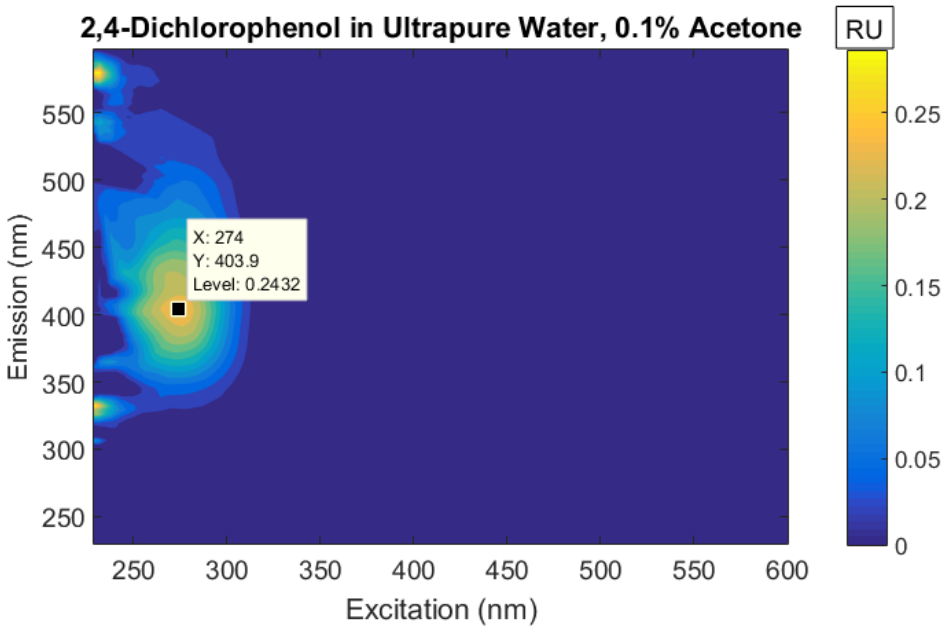

Figure 3: Individual EEMs TCC and 2-4 DCP in 0.1% acetone and high purity water.

Figure 4: Fluorescence Quenching EEM of Lime Treated (LT) Little Patuxent (LLP) DOM and Triclocarban (TCC). EEMs from left to right: A) individual EEMs TCC in 0.1% acetone and high purity water, and LLP-DOM in 0.1% acetone. B) Theoretically constructed and experimental mixture EEMs pf TCC and LLP (all blanked with acetone), followed by residual. C) Experimental mixtures blanked against TCC, first residual of theoretical and experimental mixtures, and 2nd residual of mixtures and TCC spectra

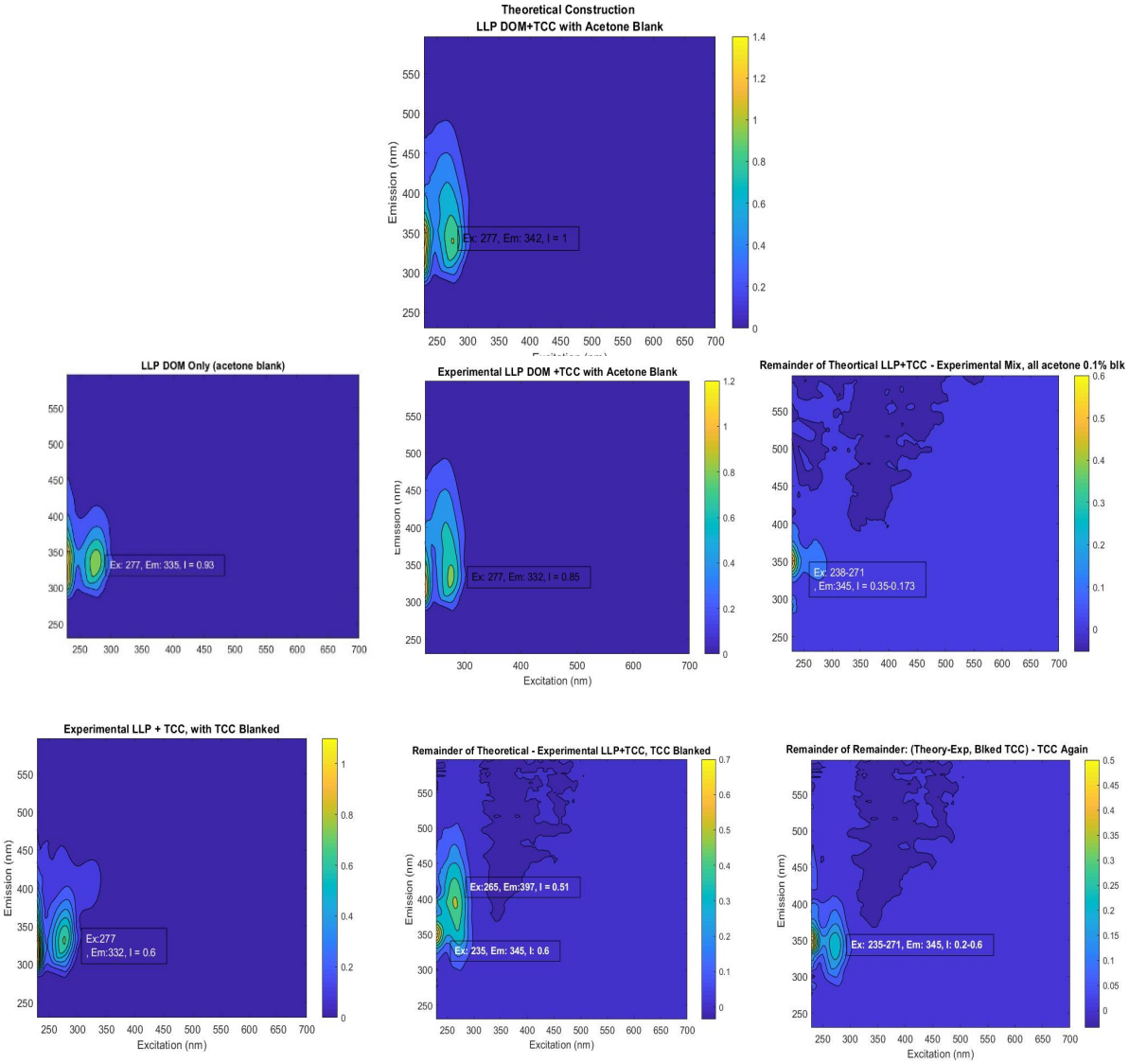

Figure 5: EEMs of LT Laurel Biosolids DOM. Theoretical construction of TCC and LT Laurel DOM is not shown. A) LLaurel DOM only (0.1% acetone), b) 1st residual of theoretical and experimental mixture (blanked against TCC) indicating combined quenching of TCC and and DOM and c) 2nd residual removing quenching of TCC, indicating quenching of DOM only.

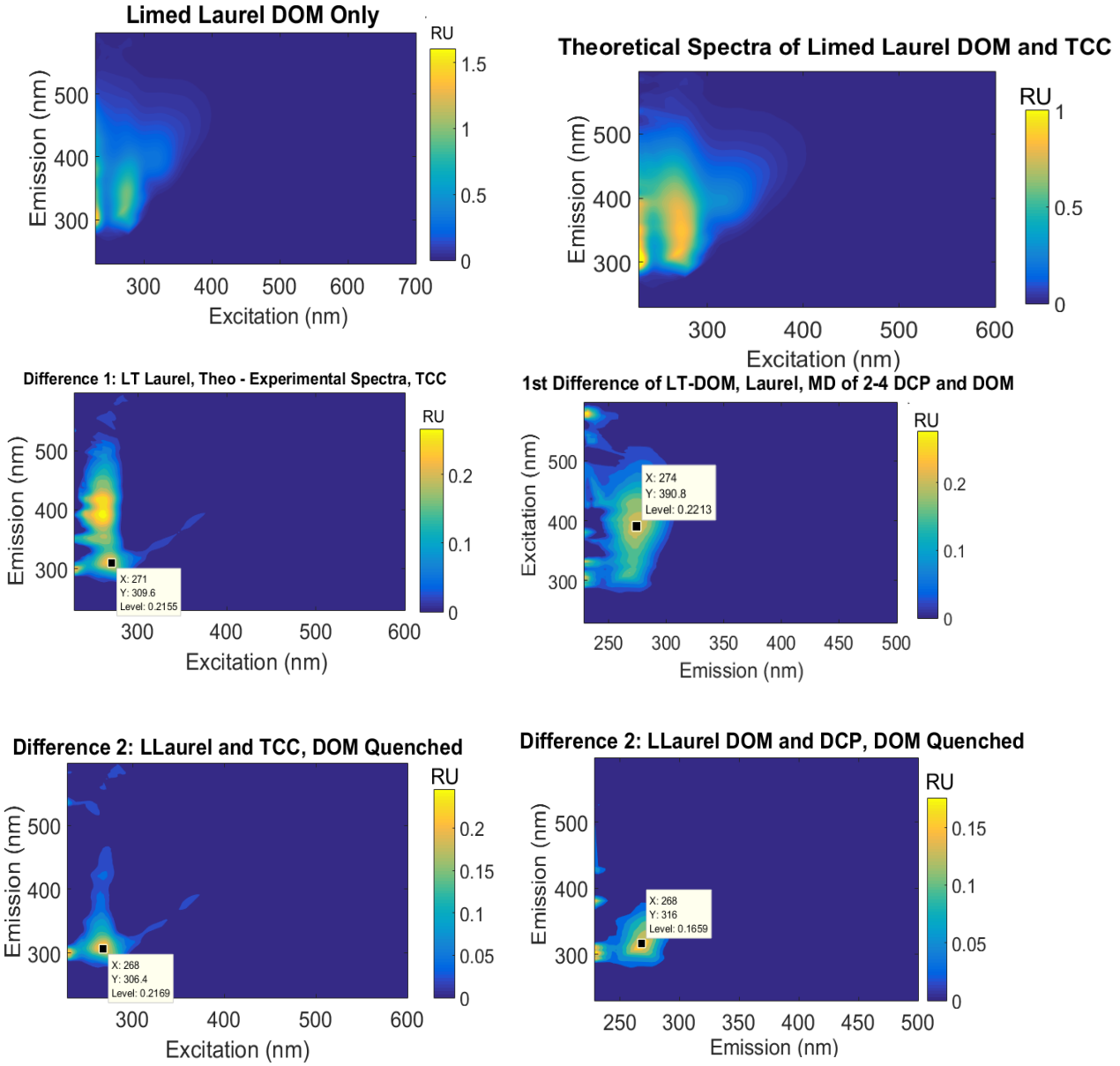

Figure 6: EEMs of AnD DCW (THP-AD) biosolids-DOM and quenching from triclocarban and 2-4 dichlorophenol.

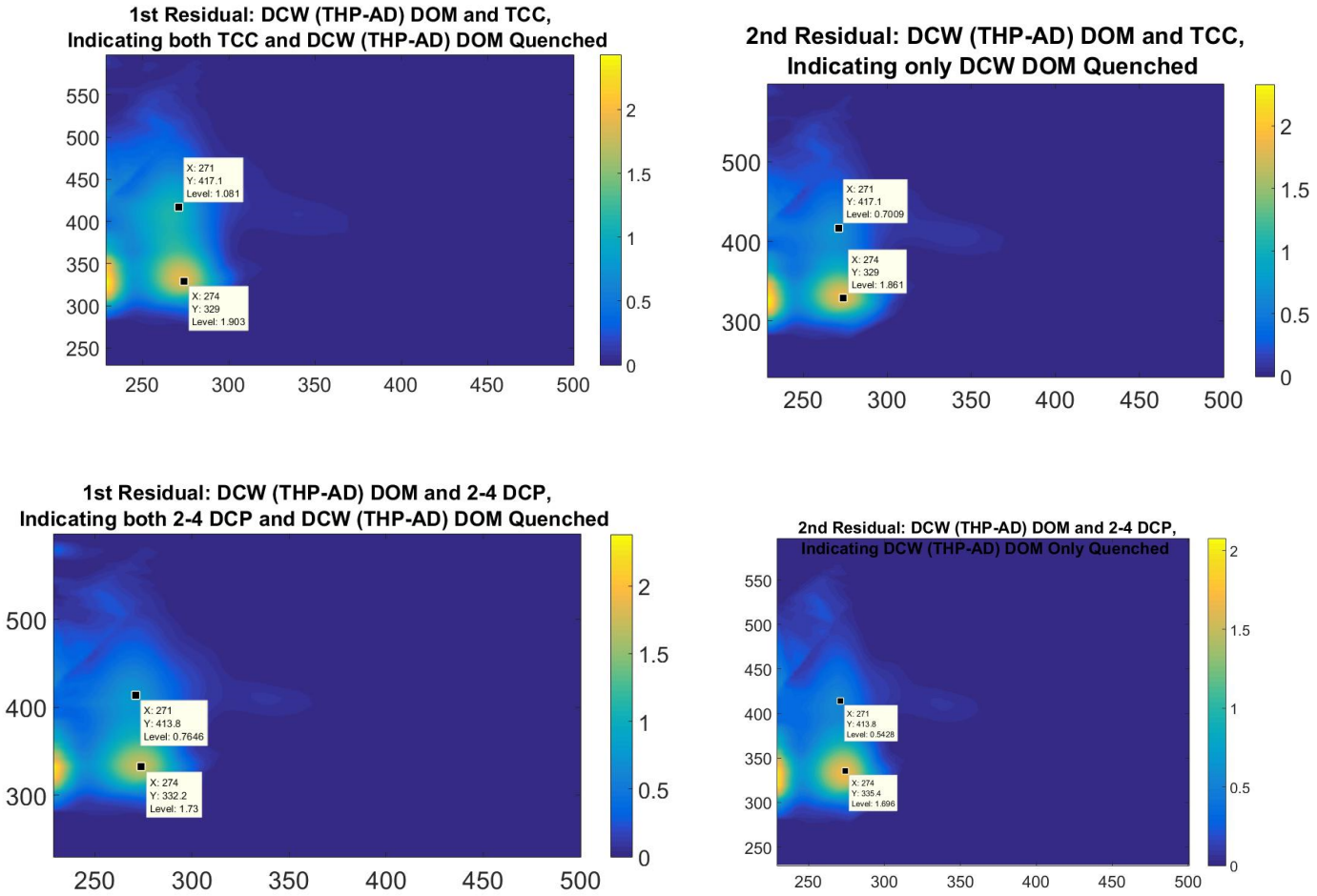

Figure 7: EEMs of AnD Sod Run biosolids-DOM Quenching. a) Theoretical Construction of Sod Run DOM with TCC and 2-4 DCP Only. 2nd Residual Plots indicating only TCC and 2-4 DCP Quenched.

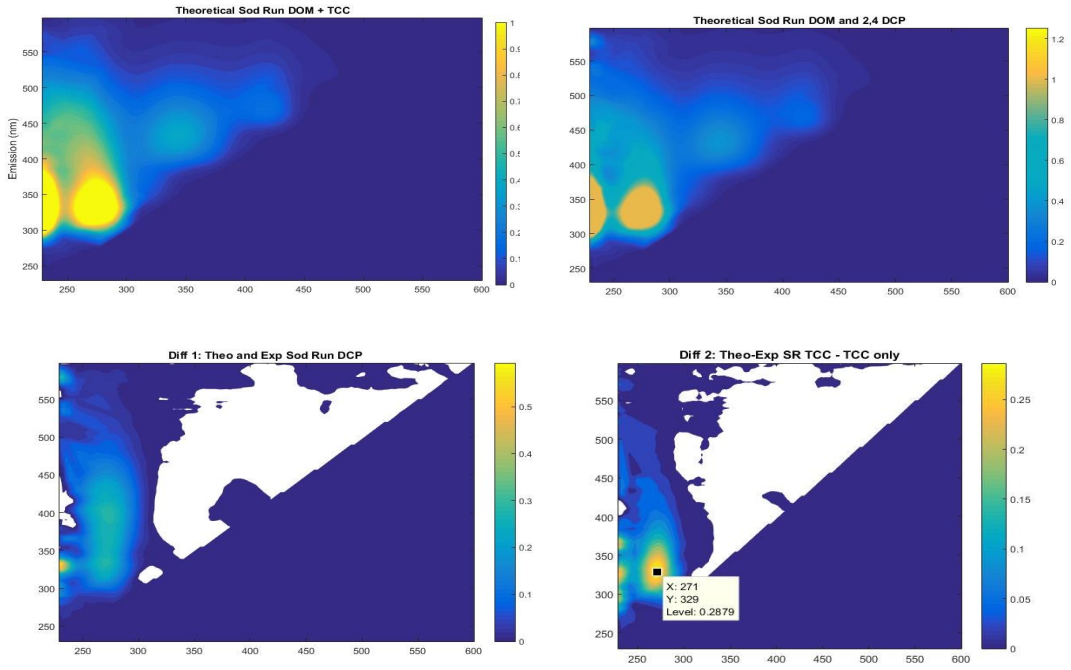

Figure 8: Excitation Emission Matrices of AeD Tolchester -DOM Quenching from TCC and 2-4 DCP.

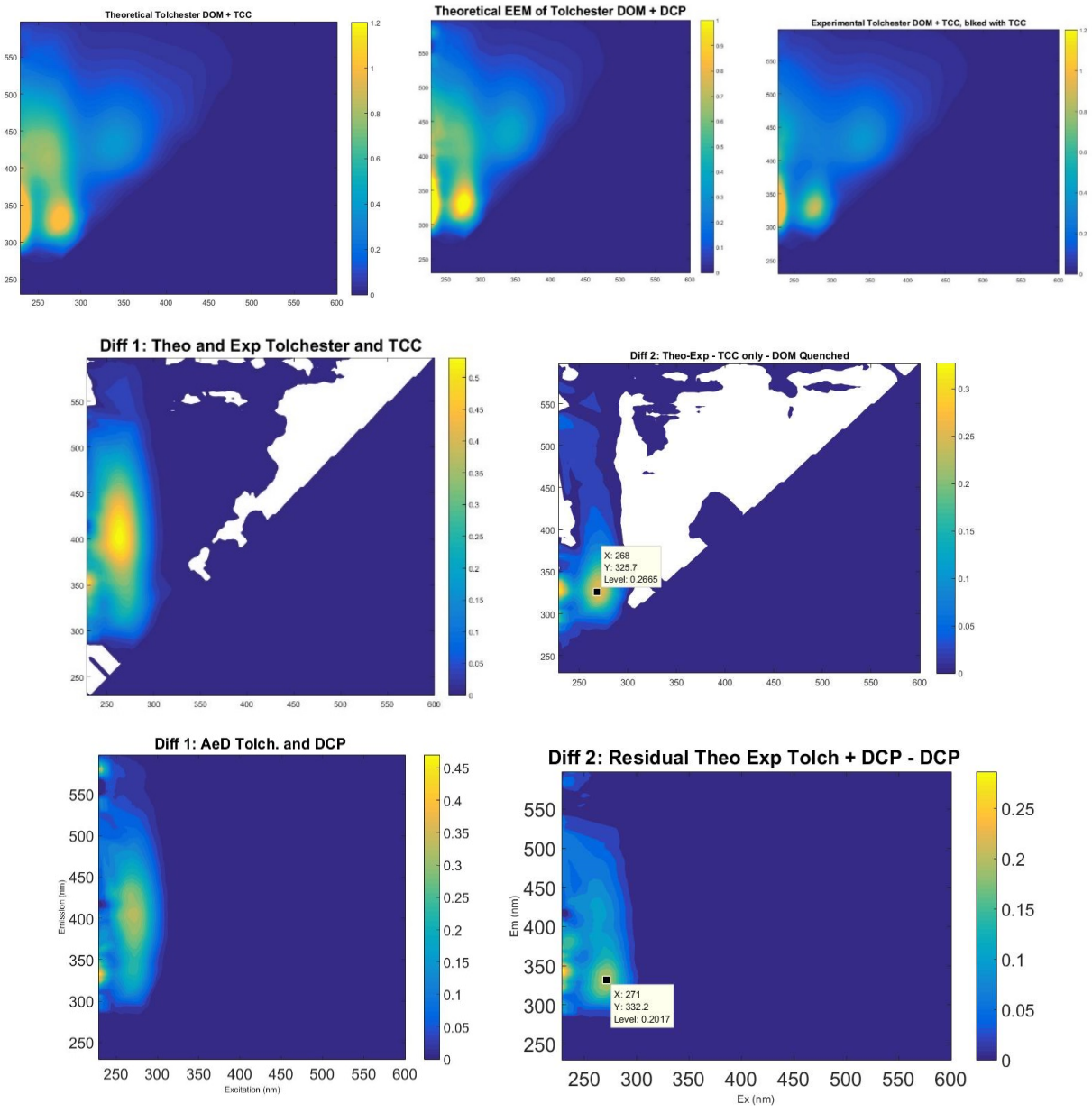

Figure 9: EEMs of AeD Wicomico Shores -DOM Quenching from TCC and 2-4 DCP.

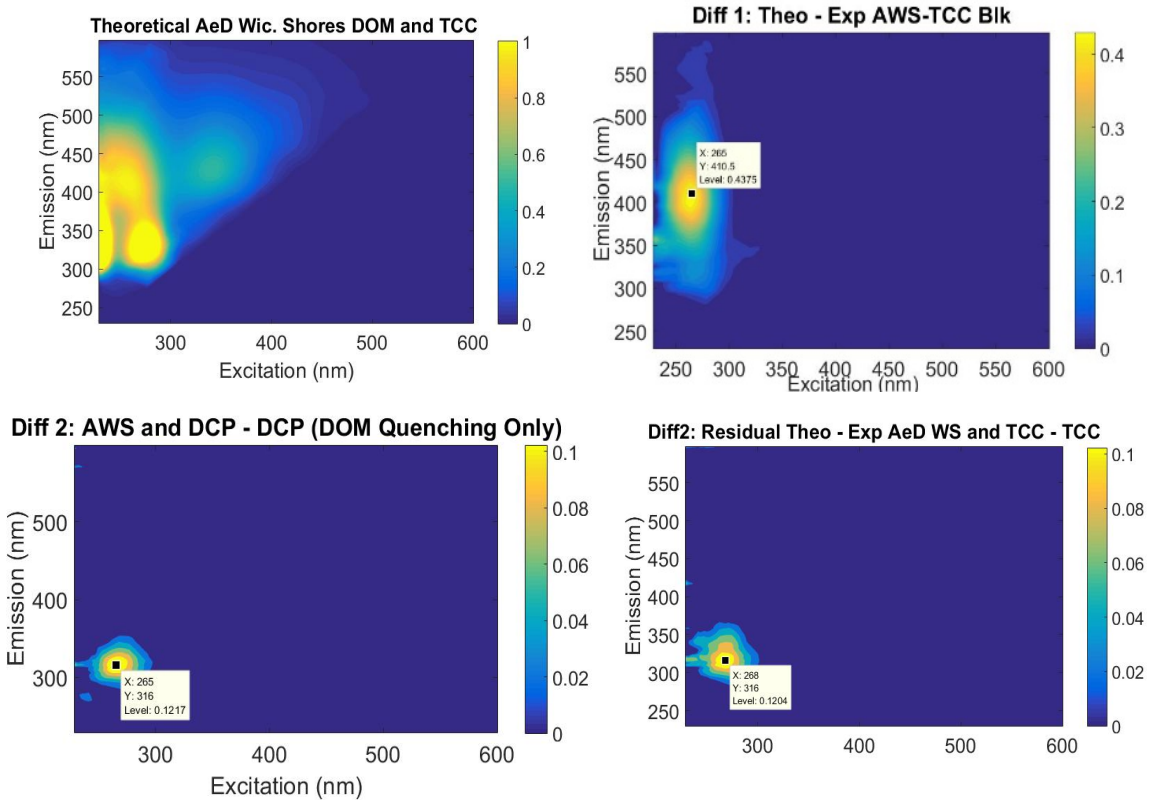

Figure 10: EEMs of Suwannee River Natural Organic Matter and 2-4 DCP and TCC Quenching. Residual computations are indicated.

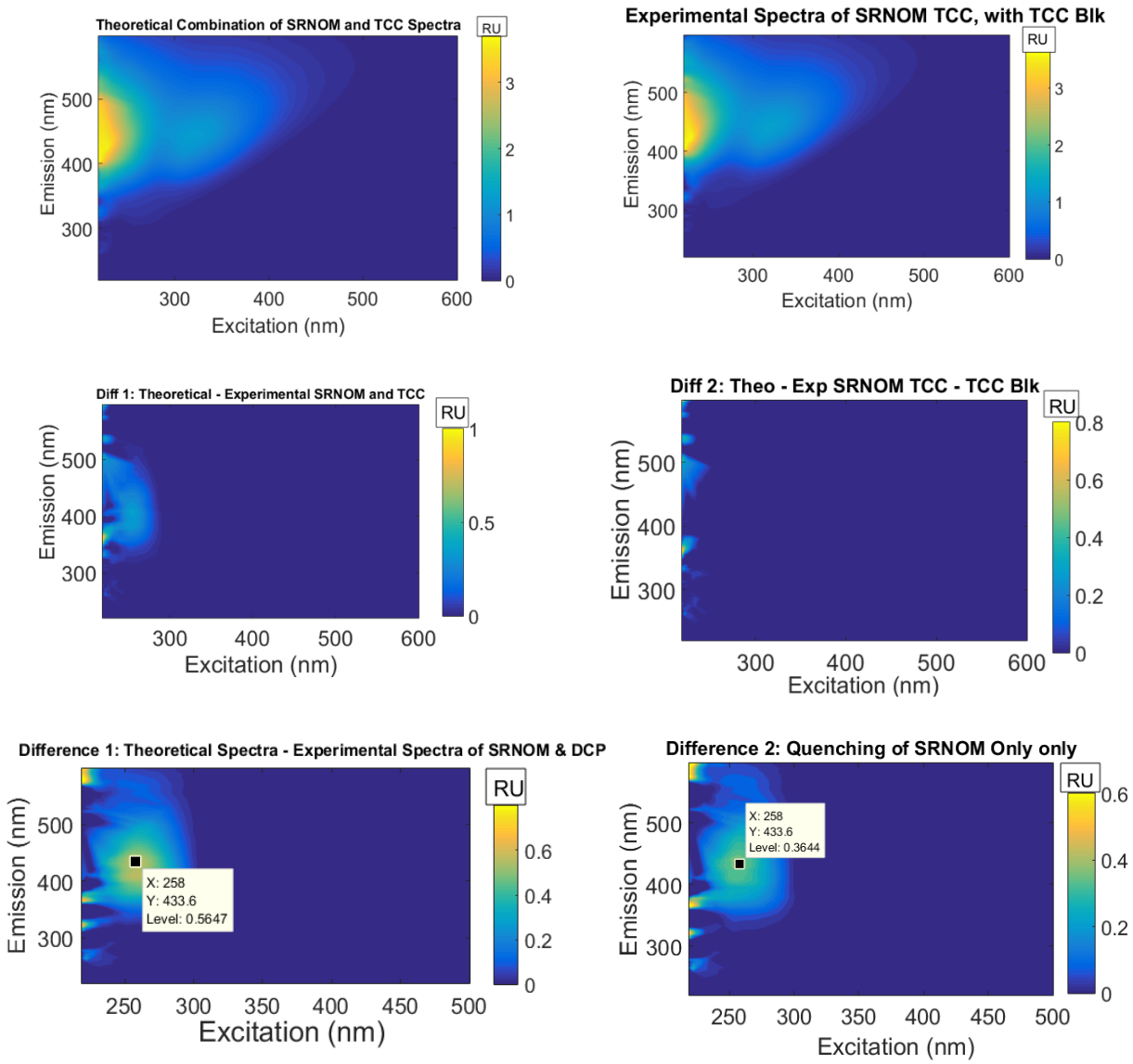

Table 2: Summary of 2nd residual computation results with the Ex_{max}:Em_{max} and peak intensity of quenching of DOM are indicated. Quenching of the contaminant was removed from the 1st residual.

	2-4 DCP Ex_{max}:Em_{max} Max Intensity of DOM Quenched (RU)	**TCC Ex_{max}:Em_{max} Max Intensity of DOM Quenched (RU)**
LT DOM Little Patuxent, MD	No DOM quenched	238-271 nm: 354 nm RU = 0.35
LT DOM, Laurel, MD	268 nm: 316 nm RU = 0.17	268 nm: 307 nm RU = 0.22
AnD-DOM DC Water, Washington DC	274 nm:336 RU = 1.70 Additional quenching at 271 nm:414 nm	271 nm: 332 nm RU = 1.86 Additional quenching at 271 nm:417 nm
AnD-DOM Sod Run, MD	269 nm:326 nm RU = 0.29	271 nm:329 nm RU = 0.27
AeD-DOM, Tolchester, MD	271 nm:332 nm RU = 0.20	271 nm:326 nm RU = 0.23
AeD-DOM, Wicomico Shores	265 nm: 316 nm RU = 0.12	268 nm:316nm RU = 0.12
SRNOM	258 nm:434 nm RU=0.37	Minimal quenching of DOM occurred

Chapter 5: Dehalogenating microbes and anaerobic community structure across thermal hydrolysis and anaerobic digestion systems

Results from this chapter will contribute to two publications lead by other graduate students on halogenated emerging contaminants triclosan (TCS), triclocarban (TCC), and polybrominated diphenyl ethers (PBDEs).

Abstract

Full-scale thermal hydrolysis pretreated anaerobic sludge digesters (Washington, DC) were sampled for the presence 12 dehaloginating phylotypes. Three obligate dehalogentating strains of *D. mccartyii*, *Chloroflexi Dehalogenimonas*, and *Chloroflexi Dehalobacter* and several facultative strains including *Desulfomonile* and *Sulfurospirillum* were present in the digesters. An average of 10^{10} gene copies of *Chloroflexi Dehalogenimonas*/g dry weight sludge was then quantified in unit processes across DC Water, including the water treatment side and solids treatment, across two summer and winter sampling events. The anaerobic digesters contained 10^{2}-10^{3} fold higher *Chloroflexi Dehalogenimonas* gene copies than the water treatment processes at DC Water and Sewer Authority. This suggests that dehalogenating microbes within the anaerobic digesters of DC Water have greater potential to dehalogenate emerging contaminants. The anaerobic community structure of thermal hydrolysis pretreated (THP) sludge and non-THP treated sludge in 22-day incubated mesocosms was assessed with NextGen Sequencing of the 16S rRNA. Bioinformatic analyses confirmed the presence of similar relative abundances of methanogenic and fermenting community structures in both treatments. Various computations of alpha diversity and dissimilarity statistics indicated that the treatments of THP or without THP substrate resulted in similar community richness. This suggests that both THP and non-THP AD systems may have

similar anaerobic microbial communities capable of contaminant degradation. Results from this chapter contributes to on-going studies investigated degradation of halogenated emerging contaminants across wastewater treatment systems.

1. Introduction

Organic contaminants in biosolids pose a risk for recycling the organic nutrient source in agricultural settings. Halogenated emerging contaminants (ECs) can persistent in biosolids and soil, and later bioaccumulate (Andrade et al. 2010). In the 2001 EPA National Sewage Sludge Survey for PPCPs in biosolids, of 110 biosolids samples collected nationally, halogenated antimicrobials triclocarban (TCC) and triclosan (TCS) were the most abundant analytes of thirty-eight pharmaceutical and personal care products (PPCPs) detected, accounting for 65% of the total PPCP mass (McClellan et al. 2010). Halogenated ECs have also been detected in runoff from land receiving biosolid (Topp et al., 2008; Edwards et al., 2009; Sabourin et al., 2009). Brominated flame retardants such as polybrominated diphenyl ethers (PBDEs) are also an example of detected in biosolids distributed to agricultural lands (Andrade et al. 2010).

These compounds are considered “contaminants of emerging concern”, or CECs, due to their prevalence in society and mounting evidence for human and ecological risk (Ogunyoku et al. 2014). The compounds demonstrate endocrine disrupting activity in mammals (Zorrilla et al. 2009). Halogenated ECs are also toxic to aquatic organisms at environmentally relevant concentrations (Brausch and Rand 2011). Due to the consumer use and relative stability, the compounds have been detected in wastewater treatment facility (WWTF) effluent and receiving waters and sediments (Halden et al. 2005, Zhao et al. 2011). Because halogenated compounds such as PBDEs and antimicrobials are

relatively hydrophobic, however (logKow > 2), a significant fraction of halogenated ECs compounds partition to the treated solids at WWTF, resulting in their accumulation in the final biosolids (Lozano et al. 2010).

While halogenated ECs can persist in the environment, certain biological settings have the capacity to degrade ECs. This chapter seeks to identify the presence of microbial communities wastewater treatment technologies that support the growth of with microorganisms and have the potential to reduce halogenated EC fate in biosolids. Wastewater treatment anaerobic digesters are sludge treatment units that stabilize raw material, reduce pathogens, and produce methane that can be utilized for energy production (EPA Process Design Manual, 1995). Anaerobic digesters contain complex microbial communities that break down sludge in several steps the absence of oxygen, through fermentation, acidogenesis, acetogenesis, and fermentation to producing biogas. Halogenated compounds such as PBDEs, TCS, TCC are not typically degraded by aerobic bacteria that largely lack the enzymes needed to extract energy from chlorinated functional groups or degrade the compounds co-metabolically (Chang and Alvarez-Cohen 1995, Tran et al. 2013). As microbial reductive dehalorespiration is a metabolism yields low free energy to bacteria, environments that lack energy more rich electron donors (such as oxygen) may be more suitable to support populations of microorganisms that could degrade halogenated contaminants, such as anoxic sediments, groundwater, or anaerobic digesters (Kjellerup et al. 2008, Kzmarzick and Novak, 2014). Several microbial metabolisms exist for dehalogenation: facultative, cometabolic, or by obligate - utilizing only metabolic pathway (Löffler et al. 2013, Krzmarzick and Novak, 2014). Our goal was to survey sludge digesters for obligate dehalorespirers that are most likely to

live exclusively on low concentrations halogenated ECs, and study variations in anaerobic community structure with mesocosms fed different substrates.

In 2015, DC Water installed the thermal hydrolysis processing (THP) system prior to mesophilic anaerobic digestion (AD) for the enhanced stabilization of final wastewater residuals. The THP pre-treatment heats sludge up to 165ºC and pressurizes the material to 55 - 138 PSI at a solids retention of 30 minutes, similar to to autoclaving solids before digestion (Wang et al. 2018). The THP pre-treatment enhances hydrolysis of macromolecular compounds such as proteins, lipids, and polysaccrides in sludge (Wilson and Novak 2009) to enhance downstream methane production during anaerobic digestion (Xue et al. 2015). The effect of this THP-pretreatment on dehalorespiring communities and community structures that could support dehalogenation is currently unknown.

The three goals of this chapter were to:

1) Survey full-scale DC Water anaerobic digester sludge for the presence or absence of 12 dehaloginating phylotypes
2) Quantify the abundance of obligate dehalorespiring *Chloroflexi Dehalogenimona*s across the water and solids treatment of DC Water
3) Assess complimentary microbial community structure in anaerobic mesocosms designed to test the effects of THP treated substrate versus non-THP treated substrate.

This work compliments and contributes to on-going studies quantifying ECs across wastewater treatment systems in the Torrents & Kjellerup labs.

2. Material and Methods

2.1 Sludge Collection and DNA Extraction

Sludge was collected in sterile plastic centrifuge tubes or acid-washed plastic containers and frozen at -20°C the day of collection. Sludge was then thawed overnight at 4°C prior DNA extraction. DNA was extracted from DC Water and Sewer Authority (DC WASA) wastewater treatment sludge collected across facility unit processes July 2016-December 2017 to screen sludge for a range of targeted PCR/qPCR primers for dehalogenating microorganisms. Genomic DNA was also extracted in duplicate from a THP-AD mesocosm experiment for selected timepoints on days 0, 10, and 22 days for bioinformatic analysis. Further details of the mesocosm experimental set-up of that experiment are available in the dissertation of Armstrong (2018). Genomic DNA was extracted from ~ 0.25 grams (wet weight) of sludge using the PowerSoil® DNA Isolation kit (MoBio Laboratories, Inc., Carlsbad, CA, USA) according to manufacturer's guidelines. The quantity and quality of the extracted DNA was assessed with a Nanodrop 2000c (Thermo Scientific, Wilmington, DE, USA).

2.2 Polymerase Chain Reaction (PCR) and Quantitative Polymerase Chain Reaction (qPCR) for dehalorespirating bacteria in full-scale digesters

Polymerase chain reaction (PCR) and quantitative Polymerase Chain Reaction (qPCR) was performed on extracted genomic DNA organohalide respiring bacteria (Smith et al. 2015). Twelve primers were selected to target various organohalide respiring phylogenies spanning the extended V3-V6 region of the 16s rRNA gene (Smith et al. 2015). Primer sequences and reaction conditions are summarized in Smith et al. (2015).

Primers were purchased from Integrated DNA Technologies. Polymerase chain reaction was carried out with BioRad DreamTaq polymerase on a BioRad PCR Thermocycler. Gel electrophoresis confirmed the presence or absence of amplified genes. Obligate dehalogenating phylotype *Chloroflexi Dehalogenimonas* was targeted for quantitative polymerase chain reaction (qPCR) with a BioRad Sybr Green chemistry. Reaction conditions were optimized for qPCR as well, all qPCR analyses were conducted on a CFX Connect Real Time System with CFX Manager software (Bio-Rad Laboratories).

2.2 THP-AD Mesocosm Experiment Amplicon sequencing and sequence processing

Microbial community analysis on extracted DNA from THP-AD versus non-THP-AD sludge was carried out by means of high-throughput amplicon sequencing using 300 bp paired-end sequencing chemistry (MiSeq Illumina), at the University of Maryland, Biological Services Laboratory (BSL) (Baltimore, Maryland). The V3-V4 region of the 16S rRNA gene was targeted for sequencing with the primers described by Klindworth et al. (2013) for both bacterial and archaeal populations. The preparation of libraries for barcode sequencing following manufacturer Illumina's MiSeq V3-V4 protocol. Data-set was demultiplexed and barcodes & adapters trimmed before paired-end fastq file reads were further filtered, denoised, and merged via the *Dada2 1.8* pipeline for R version 3.4.2, generating final amplicon sequence variants (ASV), a higher-resolution version of the traditional OTUs (R Development Core Team, 2013, Callahan et al. 2016). Briefly, primers were trimmed, and unpaired reads were filtered to maintain a minimum Phred score quality of 10 across the read. Samples were dereplicated, then forward and reverse reads were merged to maintain a minimum 25

base pair overlap. Chimeras were removed, and the taxonomy was assigned via the SILVA, 16S rRNA database, version 128 (Quast et al. 2012).

2.3. Statistical Community Analysis

The phylotype-assigned dataset was analyzed with R software packages of 'vegan' version 2.5-3 (Oksanen et al. 2011) and 'phyloseq' version 1.24.2 (McMurdie and Homes, 2013) packages for microbial diversity, statistical, and consensus analysis. Sampling depth was assessed by generating rarefaction curves for each sample with vegan, function rarecurve. Relative abundance was computed by normalizing each ASV count to the sum of ASVs per sample, with the user-defined function of transform_sample_counts for phyloseq. The top 20 most dominant taxonomies per phylogenetic level were assessed with phyloseq's plotbar -function. Alpha diversity, or the representative per-sample diversity, was assessed by all standard measures on non-normalized count data with the plot_richness of phyloseq. Statistical differences of alpha diversity as a function of treatment was further assessed by an analysis of variance (function aov) modeling richness estimates (estimate_richness) against treatment or day. Community differences as a function of i) substrate treatment ("With THP", "Without THP", AD Inoculumn only) or ii) time (days) was also assessed by several ordination methods applying Bray-Curtis dissimilarity estimates within the function options for ordinate in phyloseq. Ordination of treatment and time effects were also appraised utilizing envfit {vegan} and metaMDS {phyloseq} assignment.

3. Results and Discussion

3.3 Targeted Halorespiring Primer Survey

The presence of several obligate dehalogenating organisms was confirmed in anaerobic digester sludge sampled in June 2016. These phylotypes included *D. mccartyii*, *Chloroflexi Dehalogenimonas*, and *Chloroflexi Dehalobacter* (Table 1). These organisms are most likely to dehalogenate low concentrations of halogenated compounds in anaerobic digesters (Smith et al. 2016, Kzmarzick and Novak, 2014). Several facultative dehalorespiring organisms were also detected, including *Desulfomonile* and *Sulfurospirillum.* Facultative bacteria are considered generalists with multiple electron-accepting capacities that do not out-compete specific pathways. These organisms may contribute to some degree of incidental dehalogenation in anaerobic digesters.

3.3 Abundance of *Chloroflexi Dehalogenimonas* across DC Water Blue Plains

The abundance of obligate dehalorespirer *Chloroflexi Dehalogenimonas* was measured from unit processes of the water treatment side and solids treatment side across DC Water, Blue Plains wastewater treatment facility. Quantitative polymerase chain reaction indicated *Dehalogenimonas* was present at up to 10^{10} gene copies/g d.w. These levels were 10^2 to 10^3 fold greater gene copy abundance of in anaerobic digesters than the water treatment side of wastewater treatment, indicating greater potential for dehalogenation of halogenated contaminants (Figure 1, Chapter 5). Anaerobic digesters have solids retention times (SRT) of 22-26 days and represent unit processes with the longest SRT at DC Water and Sewer Authority. Water treatment side processes have HRT of 2-8 days maximum (personal correspondence). This is consistent opportunity for

slower growth of dehalorespiring microorganisms with low concentrations of halogenated contaminants in anaerobic digesters (Kzmarzick and Novak, 2014).

3.3 THP-AD versus non-THP-AD substrate Mesocosm Community Analysis

An average of 206,693 ± 64, 936 raw reads per sample were entered the Dada 1.8 pipeline. After filtering, denoising, merging, and chimera removal, an average of 45,470 ± 19138 reads where kept for taxonomic assignment and analysis. Rarefaction curves confirmed that complete coverage of the microbial community was sampled in the mesocosm experiment, including anaerobic digester sludge inoculum incubations, WithTHP substrate incubations, and WithoutTHP substrate incubations (Figure 2). Rarefaction results also indicated that direct sequencing and processing of THP influent and THP effluent sludge samples indicated that sufficient sampling depth however. Results were extremely limited for THP Effluent samples, with only 26,208 raw reads entering the Dada 2 processing pipeline and only high quality 6,377 reads remaining. This suggests that the TH pretreatment is effective at hydrolyzing and damaging significant DNA during sterilization, resulting in a lack of quality DNA able to successfully amplify during Illumina sequencing chemistry. DNA quality in mesocosms were likely improved by the addition of the AD inoculum that was sampled during steady-state and functioning full-scale AD operation.

Anaerobic digestion is driven by a complex microbial community carrying out sequential and related steps of decomposition, leading to methanogenesis. As digesters are operated to ensure maximum biogas production, the methogenic population is often the target of AD microbial community analysis research (Amani et al. 2010, De Vrieze et al. 2016). In this study, it was hypothesized that the THP-treated substrate would

stimulate more biogas production and a greater relative abundance of methanogens. The archaeal methanogenic population was dominated by the Euryarcheota Methanomicrobia class. The relative abundance of this group increased to 4.3 ± 0.2 % for AD Inoculum, 2.6 ± 0.8% for WithOutTHP, and 5.0 ±1.0% for WithTHP treatments by the end of the 22 day experiment (Figure 3, Chapter 5). Both the AD inoculum and WithTHP treatments contain THP treated substrate that could have resulted in the ~2% greater abundance of methanogens. The Euryarcheota Methanomicrobia class was dominated by genus Methanosaeta, previously identified in AD communities (De Vrieze et al. 2011). The bacterial phyla of Firmicutes, Bacteroidetes, and Chloroflexi dominated, consistent with the core anaerobic phyla previously identified in a meta-analysis of 16s rRNA gene sequences from anaerobic digester study deposited to GenBank and RPD genomic databases (Figure 3, Chapter 5, http://www.ncbi.nlm.nih.gov, http://rdp.cme.msu.edu, Nelson et al. 2010). The dominate Firmicutes were represented by genus Ruminococcaceae Fastidiosipila, obligate anaerobic fermenting bacteria associated with cellulosic hydrolysis and H2 production (Morrison and Miron, 2000, Ziganshin et al. 2013).

Various computations of alpha diversity or mean diversity per sample indicated that the treatments of THP, without THP substrate, or AD inoculum resulted in similar levels of community richness (Figure 4, Chapter 5). The richness of THP Influent was greater than incubated samples, but lower total reads comprised that result. Incubated mesocosm richness also did not change as a function of time (Figure 5, Chapter 5). Analysis of variance of alpha diversity as a function of mesocosm treatment confirmed a lack of statistical difference between mesocosm treatments ($p = 0.726$, SI Figure 8).

Ordination of community differences indicated that only the THP Influent and Effluent samples were dissimilar from mesocosm experiments (Figure 6, Chapter 5)". With these samples removed, non-metric multidimensional scaling (NDMS) ordination indicated that "WithTHP" or "WithOut" treatment substrates did not drive dissimilarity between the mesocosms (Figure "MultiPanel Ordination b"). More clustering was observed as a function of time, indicating that mesocosm communities established in similar ways, such as in methanogen growth. Similar results were seen with Additional Principle Component Analysis (PCoA) (SI Figure 9). Ordination onto the vectors of time and treatment did not result in significant correlation to either variable (SI Figure 10).

Physical measurements (VFAs, CH_4%) did not seem to indicate a significant difference in activity between the THP or non-THP treated mesocosms. Similarly, microbial community analysis and statistical treatment of bioinformatic results did not point to significant differences between the treatments applied, but change in the established community over the 22 day batch experiments. The decrease in total VFAs over time is consistent with methanogenic *Methanomicrobia Methanosaeta* growth observed. These results suggest that while the THP pretreatment has full-scale benefits of enhancing biogas production, this batch mesocosm design may have not supported establishment of a steady-state methanogenic community. CSTR designs may have supported a more stable methanogenic populations to develop, where differences in abundance or activity due to substrate quality could be observed with DNA-based sequencing, VFA, and biogas production. De Vrieze et al. (2016) also demonstrate that RNA-based sequencing methods more strongly correlate to anaerobic digester activity measurements than DNA-based sequence analysis. Future work to elucidate that

community metabolism effects on EDC degradation during AD could focus on coupling an RNA-based analysis.

4. Conclusions

Several obligate and facultative dehalorespiring phylotype. The high abundance of obligate respirer *C. Dehalogenimonas* in the digesters compared with parts of DC Water Blue plains indicates the potential for EC degradation in AD. The anaerobic digesters have a solids retention time of 22-25 days and represent some of the longest retention time of any wastewater treatment process. Longer retention times support reductive dehalogenation communities in metabolisms with lower free energy yields and slower growth (Kjellerup et al. 2008). Bioinformatics results from the THP-AD treated and non-THP-AD treated mesocosms indicated that both anaerobic treatments contained similar methanogenic and fermenting microbial community structures that could support reductive dehalogenation, as confirmed by 16s rRNA Illumina sequencing.

5. Figures for Chapter:

Table 1: Results of 16S rRNA Dehalorespirer Primer Survey on sludge.

Bacteria Name & Primers	Presence ++/Absence -- in Anaerobic Digester Inoculum	Presence ++/Absence -- in SDC-9	*E. Coli* (control)	Obligate, facultative or cometabolic dechlorination
***D. mccartyii* 582F 728R yas**	++	+	--	**Obligate**
***D. chloroflexi* 1150F 1286R no**	Inconclusive			**Obligate**
***Dehalobium chlorocoercia* 866F 1265R**	-	++	--	**Obligate**
***Dehalogenimonas* 634F 799R**	+	++	--	**Obligate**
***Dehalobacter* 447F 647R yes**	+	++	+	**Obligate**
***Desulfitobacteria* 406F 619R yes**	+	+	--	**Facultative**
***Geobacter lovleyi* 564F 840R**	-	+	--	**Facultative**
***Desulfomonile* 205F 628R (almost)**	+	++	--	**Facultative**
***Desulfovibrio* 691F 826R**	-	-	--	**Facultative**
***Sulfurospirillum* 114F 421R**	+	-	--	**Facultative**
Gopher Group 163F 441R	++	-	--	**Facultative**
Bacteria 341F 534R	-	++	++	---

Figure 2: Abundance of obligate dehalorespirer Chloroflexi Dehalogenimonas in sludge across DC Water, Blue Plains wastewater treatment facility. Quantitative polymerase chain reaction indicated log(2) to log (3) fold greater abundance of Dehalogenimonas in anaerobic digesters for two sampling events.

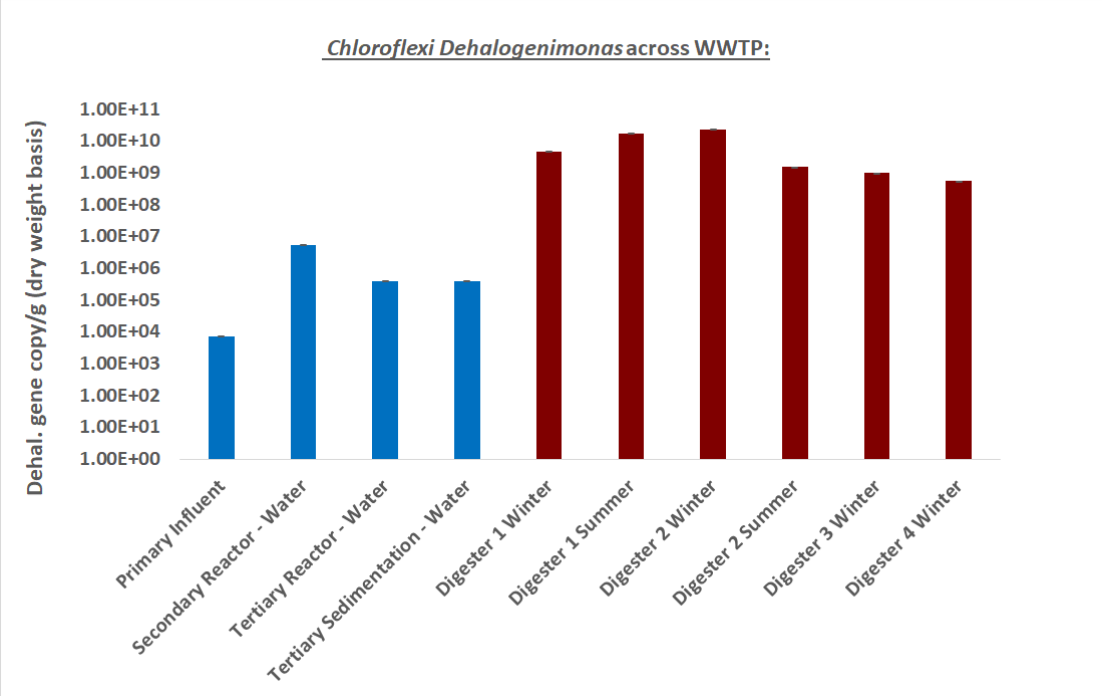

Figure 2: Rarefaction analysis confirm sufficient sampling depth for bioinformatic analyese on selected mesocosm sequenced timepoints. Sufficient sampling depth was marginally achieved for “THP Sludge Influent” and not achieved for “THP Effluent” samples, likely due to poor DNA quality. These samples were excluded from select statistical analyses.

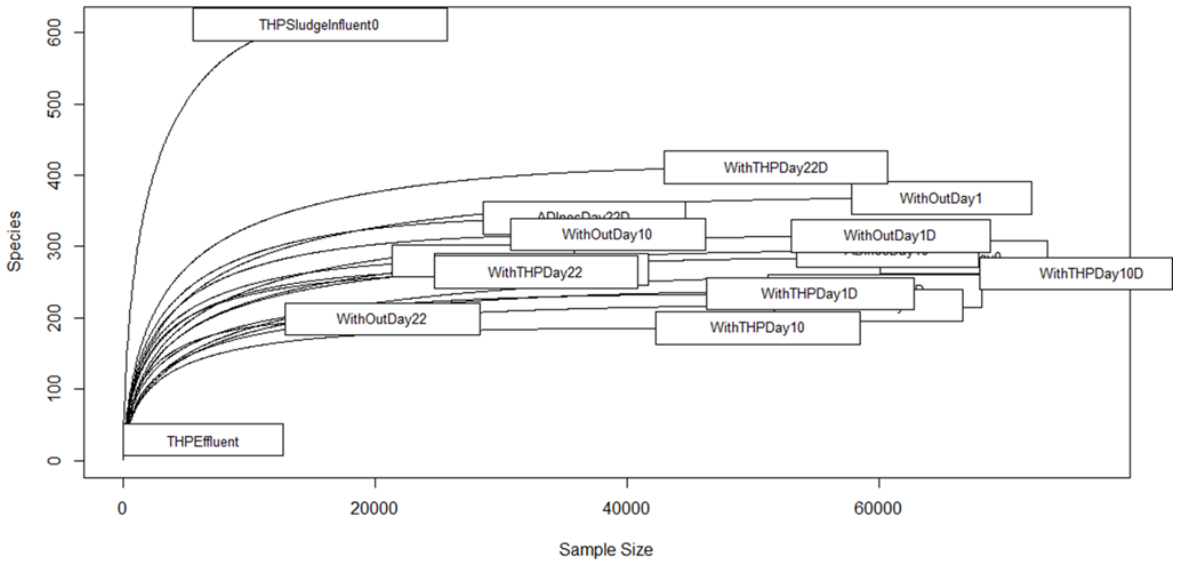

Figure 3: Relative Abundance and Taxonomic Assignment for Community structure at different Phylogenetic levels across anaerobic mesocosm with THP substrate and without THP substrate.

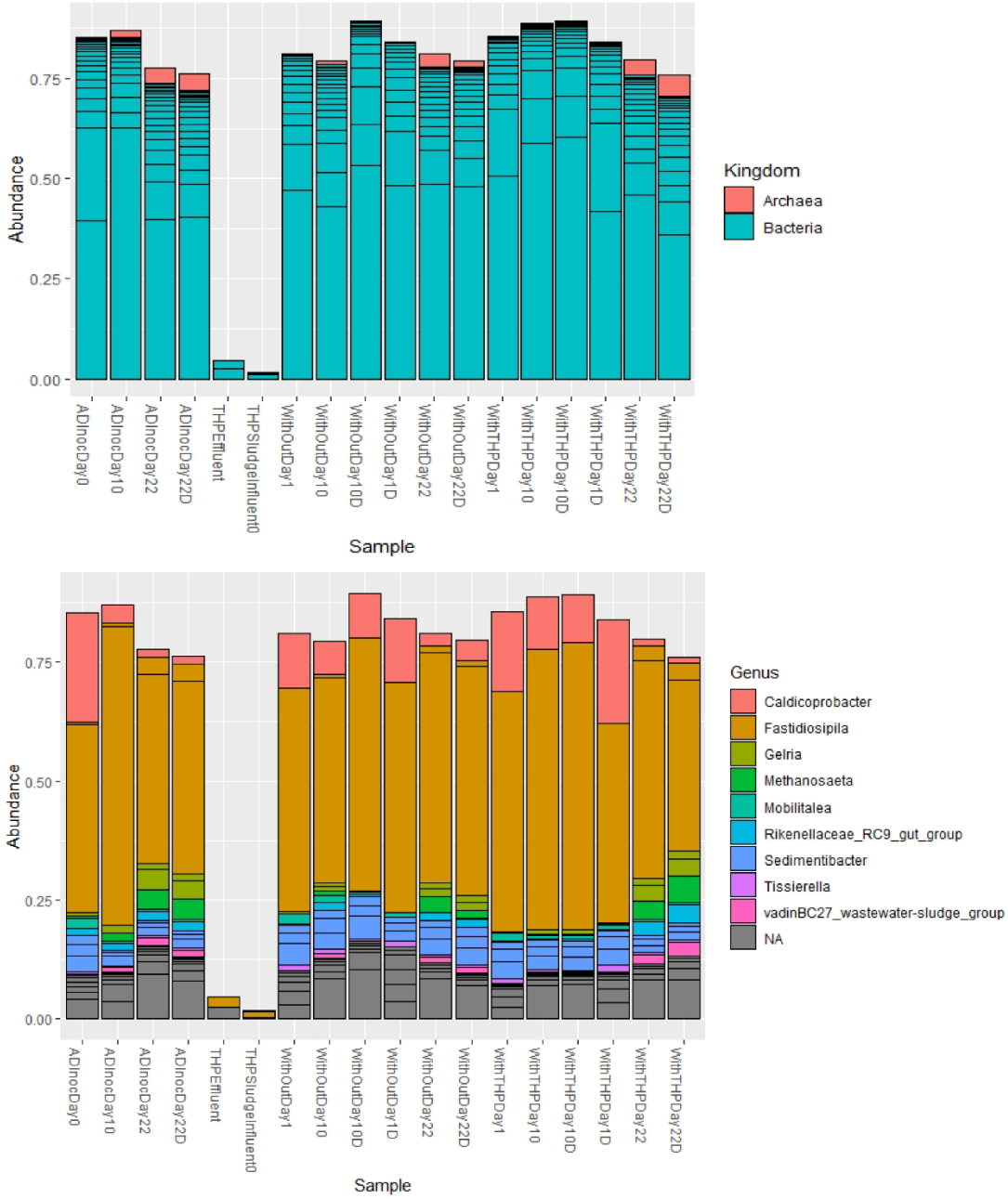

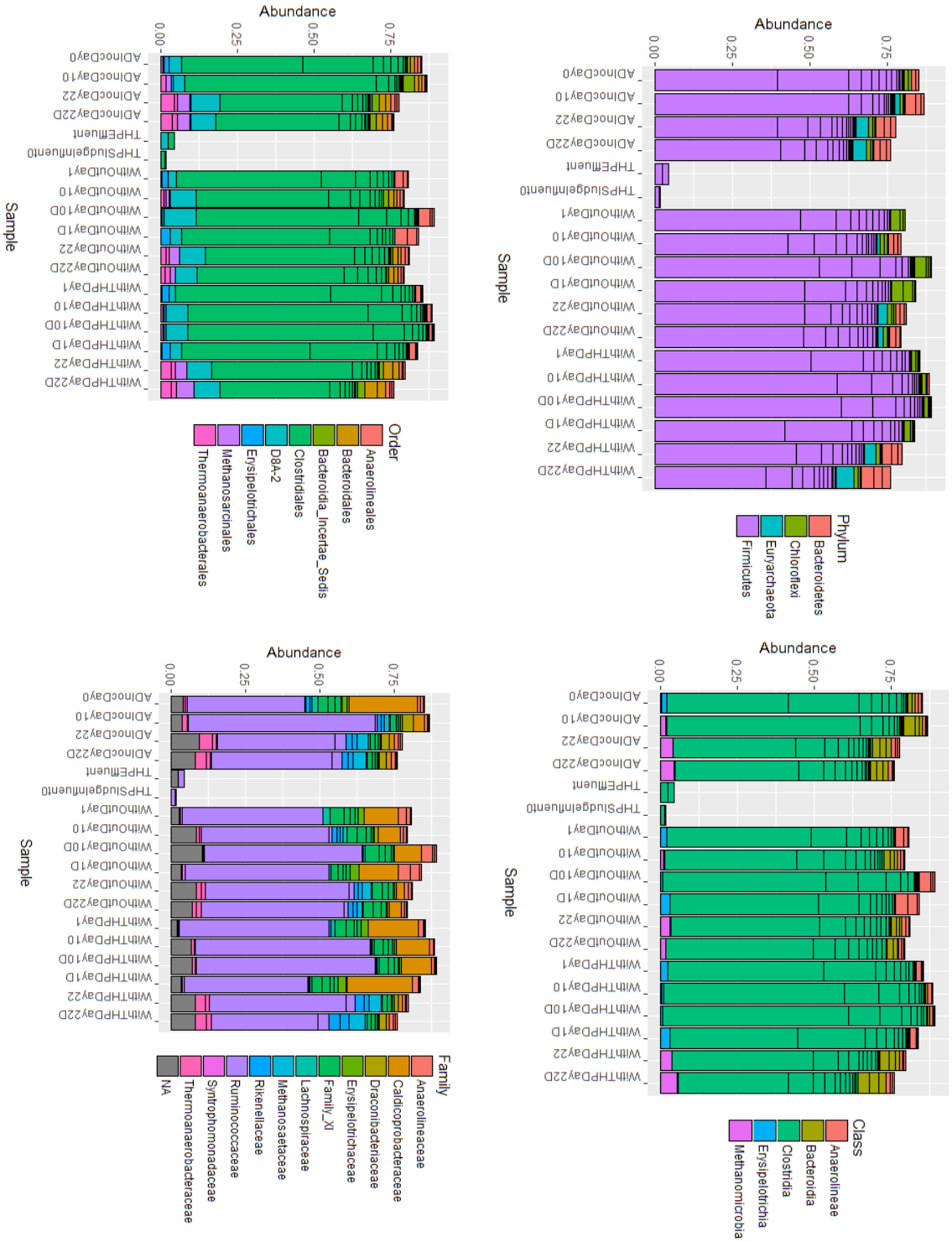
Abundance
0.00
0.25
0.50
0.75
Sample
ADinocDay0
ADinocDay10
ADinocDay22
ADinocDay22D
THPEffluent
THPSludgeInfluent0
WithOutDay1
WithOutDay10
WithOutDay10D
WithOutDay1D
WithOutDay22
WithOutDay22D
WithTHPDay1
WithTHPDay10
WithTHPDay10D
WithTHPDay1D
WithTHPDay22
WithTHPDay22D
Phylum
Bacteroidetes
Chloroflexi
Euryarchaeota
Firmicutes
Order
Anaerolineales
Bacteroidales
Bacteroidia_Incertae_Sedis
Clostridiales
D8A-2
Erysipelotrichales
Methanosarcinales
Thermoanaerobacterales
Class
Anaerolineae
Bacteroidia
Clostridia
Erysipelotrichia
Methanomicrobia
Family
Anaerolineaceae
Caldicoprobacteraceae
Draconibacteriaceae
Erysipelotrichaceae
Family_XI
Lachnospiraceae
Methanosaetaceae
Rikenellaceae
Ruminococcaceae
Syntrophomonadaceae
Thermoanaerobacteraceae
NA

Figure 4: Alpha Diversity analysis across mesocosm experiment with THP substrate and without. Computation of alpha diversity by several sub-tests are indicated. A) Limited differences in alpha diversity as a function of treatment type or b) time.

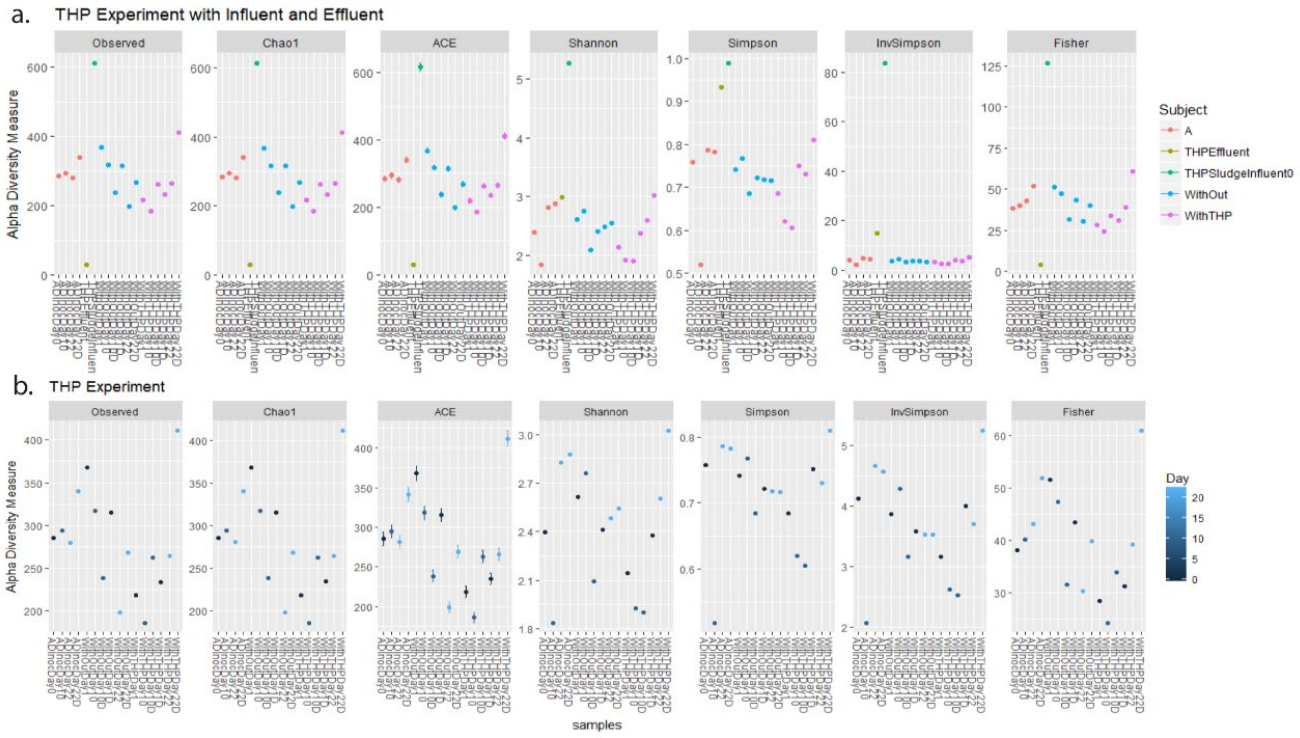

Figure 5: Statistical Community Differences as a function of i) substrate treatment ("With THP", "Without THP", AD Inoculum only) or ii) time (days) was assessed by several ordination methods applying Bray-Curtis dissimilarity estimates within the function options for ordinate in phyloseq. THP Influent and Effluent samples were removed for additional ordinations.

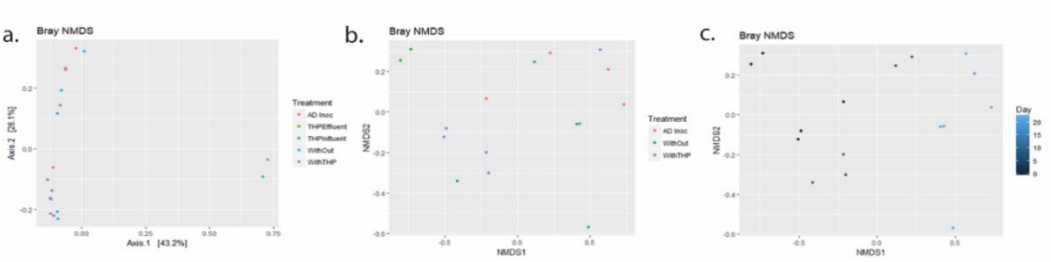

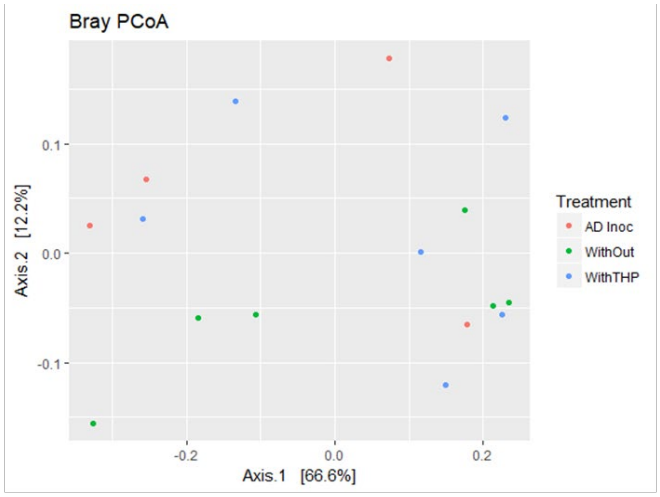

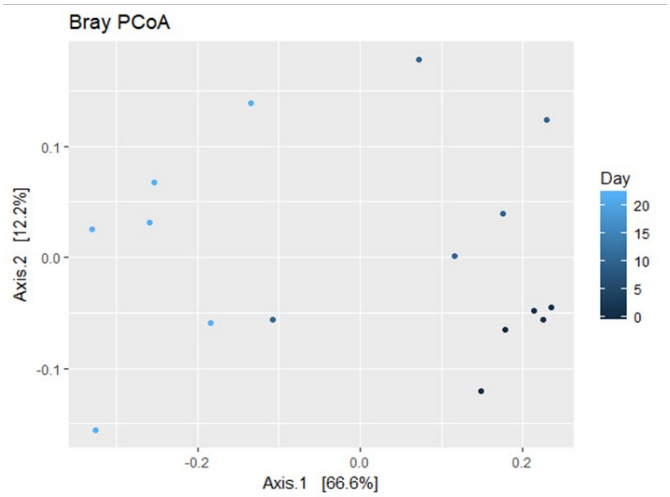

Figure 6: Ordination of treatment and time effects were also appraised utilizing envfit {vegan} and metaMDS {phyloseq} assignment.

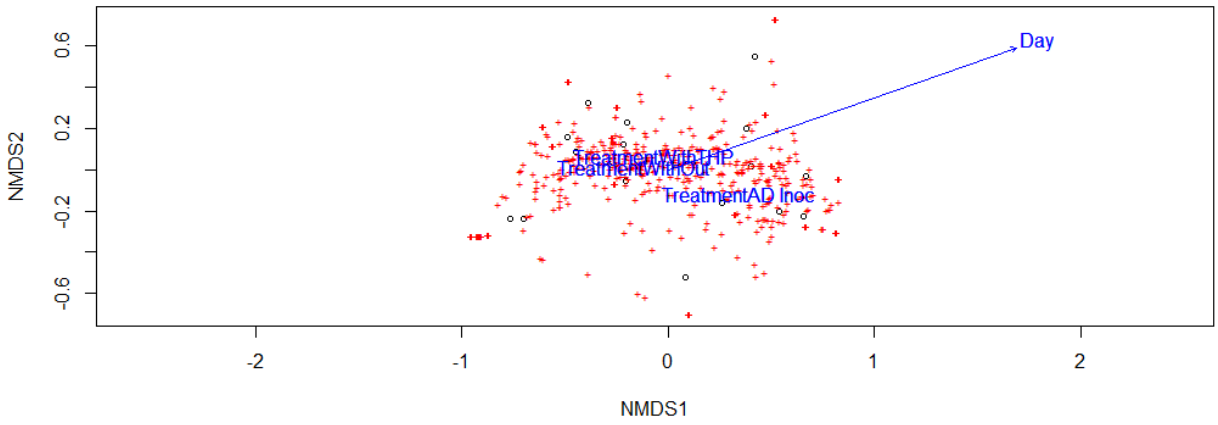

Chapter 6: Dissertation Conclusions

In this dissertation, I examined several challenges in biosolids research: targeting nutrient-based application rates, advancing leachate characterization, emerging contaminant interactions, and the influence of upstream microbial populations in the THP-AD system that could degrade contaminants before land application. Findings from this thesis range from immediate applicability in biosolids decision-making (Chapter 2 and Chapter 3) to theoretical and the ideas will advance when coupled to on-going or future study (Chapter 4 and 5). In this conclusion, I will highlight my key findings from each chapter and emphasize opportunities for future research.

The first contribution of this thesis characterized DOM and nitrogen mineralization rates of anaerobically digested (AnD) biosolids with variable pre-treatments, such as the thermal hydrolysis pretreatment coupled to anaerobic digestion (THP-AnD). Different pre-treatments did not significantly alter the overall inorganic nitrogen release when applied to a sandy loam soil. Low energy stimulated or fluorescent "humic-acid" like signatures of AD-DOM were the first to decay in the aerobic sandy loam soil. This data supports the Lehmann and Kleber (2015) view that biosolids organic matter is a complex, decomposing mixture that continues to degrade to mineral forms in soil, in contrast to the "humification" concept that continues to be discussed in biosolids stabilization literature. The DOM characterization in this chapter supports interpretation of DOM transformations of future composting or stabilization studies under the 'organic matter decomposition' paradigm rather than the 'humification' paradigm. Additional research to build on these results can measure N mineralization rates of THP-AD and other AD solids in field simulations, bulk incubations, or contrasting soil types for a

consensus on difference in mineral N produced in different circumstances (Chapter 2 Discussion). The fraction of mineral N produced by biosolids in a given season, or the EPA designated 'K_{min}' is assumed to be 20% of AD biosolids organic nitrogen in all circumstances. Before application rates are changed for THP-AD biosolids, additional study under different conditions should confirm the results we described.

Water extractable leachates from sludge and biosolids are increasingly studied with three-dimensional fluorescence spectroscopy to examine effects of reactor or composing technologies on soluble matter quality. In chapter 3, I demonstrate that several disconnects exists, however, between advances in aquatic and marine DOM chemistry versus leachate DOM characterization in waste treatment. Therefore, biosolids-DOM was characterized for multiple full-scale stabilization processes including (i) limed stabilization (LT), (ii) aerobic digestion (AeD), and (iii) anaerobic stabilization (AnD) with n=3 RRFs sampled per stabilization. These different stabilization processes produced substantially different leachates characterized by organic carbon content, size-exclusion chromatography, and fluorescence spectroscopy. Digested leachates contained higher molecular weight material (1360 Da) and additional red-shifted fluorophores not present in limed biosolids leachates. Traditional optical metrics previously defined for aquatic DOM did not consistently capture fluorescence maxima of anthropogenic material. Therefore, Peak A:C and T:C ratios and fluorescence regional integration (FRI) were adapted for EEMs of biosolids-DOM. Targeting calculations to anthropogenic fluorescence maxima results in up to a 20% difference from metrics defined for aquatic DOM. Novel application of parallel factor analysis (PARAFAC) and spectral database comparisons confirmed that biosolids-DOM contain both common blue-shifted (high

energy stimulated) components and red-shifted (low energy stimulated) components that are unique to digested leachates. DC Water and Sewer Authority is currently producing a cured 'Bloom' product (https://bloomsoil.com/about-bloom/) that is marketed for commercial sales. The material is cured in open air piles and measured for stability by CO_2 respiration rates and a cucumber bioassay. These assays rely on biological activity that introduces variability and uncertainty. It'd be exciting to couple fluorescence measurement of leachates to these parameters with a more rigorous framework we developed in Chapter 3. Experiments could be designed to measure rapid curing practices under a variety of conditions, so a stable and reliable product is consistently produced for sales.

In the third chapter, I discuss fluorescence suppression experiments to measure interactions of halogenated ECs with contrasting biosolids-DOM types. Emerging contaminants can be consistently measured in biosolid matrices, but the US EPA (2018) identified that a lack of data exists for risk assessment, bioavailability, and mobility assessment of 352 pollutants deriving from biosolids. We consider molecular scale interactions of DOM with contaminants TCC and 2-4 DCP. We built on previous quenching experimental designs by proposing a theoretical superposition model to isolate suppression of the "quencher" and DOM. My *hypothesis* was that differently characterized DOM from major waste stabilizations (Chapter 3) would cause contrasting interactions with biosolids DOM. Despite digested biosolids-DOM containing different humic acid-like or fulvic acid-like signatures, antimicrobial TCC and industrial compound 2-4 DCP suppressed similar high energy fluorescent signatures in all biosolids-DOM. This suggested that TCC and 2-4 DCP electronically interacts with

smaller aromatic compounds, such as amino acids, and this interaction is not unique to DOM from different waste stabilizations. Additional research can measure quenching effects as a function of temperature, and varying concentrations of contaminants (or DOC). Future work can build on these studies by connecting quenching experiments to K_{DOM} measurements (LC-MS/MS, dialysis tubing) or bioavailability assays (such as bacterial luminescence tests) with leachates from biosolids-DOM. Although many quenching experiments have been conducted with DOM and organic chemicals, no known work as scaled quenching measurements to other experimental designs where the influence of DOM quality has been shown to influence the bioavailability of organic contaminants.

This thesis also confirmed the presence of dehalogenating microbes in the anaerobic microbial community structure of a THP-AD system (Chapter 5). Three obligate dehalogentating strains of *D. mccartyii*, *Chloroflexi Dehalogenimonas*, and *Chloroflexi Dehalobacter* and several facultative strains including *Desulfomonile* and *Sulfurospirillum* were present in full-scale digester (Washington, DC). An average of 10^{10} gene copies of *Chloroflexi Dehalogenimonas*/g dry weight sludge were present in the digesters across two summer and winter sampling events, and 10^{2}-10^{3} fold higher than water treatment processes at DC Water and Sewer Authority. This suggests that dehalogenating microbes within the anaerobic digesters of DC Water have the potential to dehalogenate emerging contaminants. The anaerobic community structure of thermal hydrolysis pretreated (THP) sludge and non-THP treated sludge in 22-day incubated mesocosms was assessed with NextGen Sequencing of the 16S rRNA. Bioinformatic analyses confirmed the presence of similar relative abundances of methanogenic and

fermenting community structures in both treatments. Various computations of alpha diversity and dissimilarity statistics indicated that the treatments of THP or without THP substrate resulted in similar community richness. This suggests that both THP and non-THP AD systems may have similar anaerobic microbial communities capable of contaminant degradation. Results from this chapter contributes to on-going studies investigated degradation of halogenated emerging contaminants across wastewater treatment systems. I can't to see what Taylor finds. There's a promising trend that PBDEs are debrominating in the full-scale AD system. Further qPCR could be conducted for additional dehalogenating strains *D. mccartyii* and *Chloroflexi Dehalobacter* across DC Water, in addition to *C. Dehalogenimonas.* Archived incubated mesocosm experiments may be useful assessing PBDE degradation rates.

This dissertation advances understanding of biosolids DOM leachates, modeling EEM data, and fate of ECs in full-scale solids treatment processes.

Bibliography

Chapter 1:

Gilmour, J.T. and Skinner, V., 1999. Predicting plant available nitrogen in land-applied biosolids. Journal of environmental quality, 28(4), pp.1122-1126.

He, X.T., S.T. Traina, and T.J. Logan. 1992. Chemical properties of municipal solid waste composts. J. Environ. Qual. 21:318–329. doi:10.2134/jeq1992.00472425002100030003x

Leenheer, J.A. and Croué, J.P., 2003. Peer reviewed: characterizing aquatic dissolved organic matter.

Lu, Q., He, Z.L. and Stoffella, P.J., 2012. Land application of biosolids in the USA: a review. Applied and Environmental Soil Science, 2012.

Olk, D.C., Bloom, P.R., Perdue, E.M., McKnight, D.M., Chen, Y., Farenhorst, A., Senesi, N., Chin, Y.P., Schmitt-Kopplin, P., Hertkorn, N. and Harir, M., 2019. Environmental and agricultural relevance of humic fractions extracted by alkali from soils and natural waters. Journal of Environmental Quality, 48(2), pp.217-232.

U.S. EPA, 1995. A guide to the biosolids risk assessments for the EPA Part 503 Rule. Tech. Rep. EPA/832-B-93-005, Office of Wastewater Management, Washington, DC, USA.

U.S. EPA, 2018. EPA Unable to Assess the Impact of Hundreds of Unregulated Pollutants in Land-Applied Biosolids on Human Health and the Environment. Technical Report No. 19-P-0002, Office Inspector General, Washington, DC, USA.

Romero-Flores, A., McConnell, L.L., Hapeman, C.J., Ramirez, M. and Torrents, A., 2017. Evaluation of an electronic nose for odorant and process monitoring of alkaline-stabilized biosolids production. Chemosphere, 186, pp.151-159.

Romero, A., Ramirez, M. and Torrents, A., 2018. Impact of biosolids treatment and storage conditions on odor production: Thermal Hydrolysis-Anaerobic Digestion vs Alkaline Stabilization. Proceedings of the Water Environment Federation, 2018(4), pp.543-546.

Piterina, A., Barlett, J. and Pembroke, J.T., 2009. ^{13}C-NMR assessment of the pattern of organic matter transformation during domestic wastewater treatment by Autothermal Aerobic Digestion (ATAD). International journal of environmental research and public health, 6(8), pp.2288-2306.

Purusottam, R.N., 2015. Towards improved sensitivity of solid-state NMR experiments in biosolids (Doctoral dissertation, Université Pierre et Marie Curie-Paris VI).

Sharpless, C.M. and Blough, N.V., 2014. The importance of charge-transfer interactions in determining chromophoric dissolved organic matter (CDOM) optical and photochemical properties. Environmental Science: Processes & Impacts, 16(4), pp.654-671.

Sun, J., Guo, L., Li, Q., Zhao, Y., Gao, M., She, Z. and Jin, C., 2016. Three-dimensional fluorescence excitation–emission matrix (EEM) spectroscopy with regional integration analysis for assessing waste sludge hydrolysis at different pretreated temperatures. Environmental Science and Pollution Research, 23(23), pp.24061-24067.

Thomas, O., Junqua, G. and Thomas, M.F., 2017. Leachates and Organic Extracts From Solids. In UV-Visible Spectrophotometry of Water and Wastewater (pp. 349-378). Elsevier.

Wang, K., He, C., You, S., Liu, W., Wang, W., Zhang, R., Qi, H. and Ren, N., 2015. Transformation of organic matters in animal wastes during composting. Journal of hazardous materials, 300, pp.745-753.

Vrkoslavová, J., Demnerová, K., Macková, M., Zemanová, T., Macek, T., Hajšlová, J., Pulkrabová, J., Hrádková, P. and Stiborová, H., 2010. Absorption and translocation of polybrominated diphenyl ethers (PBDEs) by plants from contaminated sewage sludge. Chemosphere, 81(3), pp.381-386.

Chapter 2:

Barber, W.P.F., Lancaster, R. and Kleiven, H., 2012. Thermal hydrolysis: the missing ingredient for better biosolids. WaterWorld, West Chester, PA, p.A4.

Bremner, J. and Mulvaney, C., 1982. Nitrogen total. Methods of soil analysis. Part 2. Chemical and microbiological properties Soil Sci. Soc. Am.

Cabaniss, S.E., Zhou, Q., Maurice, P.A., Chin, Y.P. and Aiken, G.R., 2000. A log-normal distribution model for the molecular weight of aquatic fulvic acids. Environmental Science & Technology, 34(6), pp.1103-1109.

Cabrera, M.L., Kissel, D.E. and Vigil, M.F., 2005. Nitrogen mineralization from organic residues. Journal of environmental quality, 34(1), pp.75-79.

Coble, P.G., Green, S.A., Blough, N.V. and Gagosian, R.B., 1990. Characterization of dissolved organic matter in the Black Sea by fluorescence spectroscopy. Nature, 348(6300), p.432.

Carballo, T., Gil, M.V., Gómez, X., González-Andrés, F. and Morán, A., 2008. Characterization of different compost extracts using Fourier-transform infrared spectroscopy (FTIR) and thermal analysis. Biodegradation, 19(6), pp.815-830.

Chauzy, J., Dimassimo, R., Kline, M. and Howell, G., 2014. First Full-scale Digestion-THP-Digestion (DLD) Plant at Lille-France (620 000 PE): Presentation of a Success Story. Proceedings of the Water Environment Federation, 2014(15), pp.6717-6730.

Chen, W., Westerhoff, P., Leenheer, J.A. and Booksh, K., 2003. Fluorescence excitation− emission matrix regional integration to quantify spectra for dissolved organic matter. Environmental science & technology, 37(24), pp.5701-5710.

Cogger, C.G., Bary, A.I., Sullivan, D.M. and Myhre, E.A., 2004. Biosolids processing effects on first-and second-year available nitrogen. Soil Science Society of America Journal, 68(1), pp.162-167.

Cook, B.D. and Allan, D.L., 1992. Dissolved organic carbon in old field soils: total amounts as a measure of available resources for soil mineralization. Soil Biology and Biochemistry, 24(6), pp.585-594.

Daigger, G.T., 2009. Evolving urban water and residuals management paradigms: Water reclamation and reuse, decentralization, and resource recovery. Water environment research, 81(8), pp.809-823.

El Fels, L., Zamama, M., El Asli, A. and Hafidi, M., 2014. Assessment of biotransformation of organic matter during co-composting of sewage sludge-lignocelullosic waste by chemical, FTIR analyses, and phytotoxicity tests. International Biodeterioration & Biodegradation, 87, pp.128-137.

EPA Method 9045D: https://www.epa.gov/sites/production/files/2015-12/documents/9045d.pdf

Fischer, S.J., York, J.K., Voynova, Y.G. and Ullman, W.J., 2017. Distance-based mixing models of δ18NNO3− and δ18ONO3− in a marsh-lined estuary with multiple, distinct NO3− sources (Murderkill Estuary, Delaware, USA). Limnology and Oceanography, 62(2), pp.408-420.

Gigliotti, G., Kaiser, K., Guggenberger, G. and Haumaier, L., 2002. Differences in the chemical composition of dissolved organic matter from waste material of different sources. Biology and Fertility of Soils, 36(5), pp.321-329.

Gilmour, J.T., Cogger, C.G., Jacobs, L.W., Evanylo, G.K. and Sullivan, D.M., 2003. Decomposition and plant-available nitrogen in biosolids. Journal of Environmental Quality, 32(4), pp.1498-1507.

Hanselman, T.A., Graetz, D.A. and Obreza, T.A., 2004. A comparison of in situ methods for measuring net nitrogen mineralization rates of organic soil amendments. Journal of environmental quality, 33(3), pp.1098-1105.

Hernandez-Ruiz, S., Abrell, L., Wickramasekara, S., Chefetz, B. and Chorover, J., 2012. Quantifying PPCP interaction with dissolved organic matter in aqueous solution: combined use of fluorescence quenching and tandem mass spectrometry. water research, 46(4), pp.943-954.

Hudson, N., Baker, A. and Reynolds, D., 2007. Fluorescence analysis of dissolved organic matter in natural, waste and polluted waters—a review. River Research and Applications, 23(6), pp.631-649.

Huo, S., Xi, B., Yu, H., He, L., Fan, S. and Liu, H., 2008. Characteristics of dissolved organic matter (DOM) in leachate with different landfill ages. Journal of Environmental Sciences, 20(4), pp.492-498.

Jednak, T., Avdalović, J., Miletić, S., Slavković-Beškoski, L., Stanković, D., Milić, J., Ilić, M., Beškoski, V., Gojgić-Cvijović, G. and Vrvić, M.M., 2017. Transformation and synthesis of humic substances during bioremediation of petroleum hydrocarbons. International Biodeterioration & Biodegradation, 122, pp.47-52.

Lehmann, J. and Kleber, M., 2015. The contentious nature of soil organic matter. Nature, 528(7580), p.60.

Kalbitz, K., Schmerwitz, J., Schwesig, D. and Matzner, E., 2003. Biodegradation of soil-derived dissolved organic matter as related to its properties. Geoderma, 113(3-4), pp.273-291.

Klute, A., 1986. Water retention: laboratory methods. Methods of soil analysis: part 1—physical and mineralogical methods, (Agronomy Monograph No. 9), pp.635-662.

Kumar, K., Hundal, L.S., Cox, A.E. and Granato, T., 2014. Nitrogen Mineralization from Anaerobically Digested Centrifuge Cake and Aged Air-Dried Biosolids. Water Environment Research, 86(9), pp.828-834.

Kumar, K. and Goh, K.M., 2000. Biological nitrogen fixation, accumulation of soil nitrogen and nitrogen balance for white clover (Trifolium repens L.) and field pea (Pisum sativum L.) grown for seed. Field Crops Research, 68(1), pp.49-59.

Lagae, H.J., Langemeier, M., Lybecker, D. and Barbarick, K., 2009. Economic value of biosolids in a semiarid agroecosystem. Agronomy journal, 101(4), pp.933-939.

Lapen, D.R., Topp, E., Edwards, M., Sabourin, L., Curnoe, W., Gottschall, N., Bolton, P., Rahman, S., Ball-Coelho, B., Payne, M. and Kleywegt, S., 2008. Effect of liquid municipal biosolid application method on tile and ground water quality. Journal of environmental quality, 37(3), pp.925-936.

Leenheer, J.A., 1981. Comprehensive approach to preparative isolation and fractionation of dissolved organic carbon from natural waters and wastewaters. Environmental science & technology, 15(5), pp.578-587.

Li, X., Dai, X., Takahashi, J., Li, N., Jin, J., Dai, L. and Dong, B., 2014. New insight into chemical changes of dissolved organic matter during anaerobic digestion of dewatered sewage sludge using EEM-PARAFAC and two-dimensional FTIR correlation spectroscopy. Bioresource technology, 159, pp.412-420.

Marcato, C.E., Mohtar, R., Revel, J.C., Pouech, P., Hafidi, M. and Guiresse, M., 2009. Impact of anaerobic digestion on organic matter quality in pig slurry. International Biodeterioration & Biodegradation, 63(3), pp.260-266.

Marschner, B. and Kalbitz, K., 2003. Controls of bioavailability and biodegradability of dissolved organic matter in soils. Geoderma, 113(3-4), pp.211-235.

Meyer, V.F., Redente, E.F., Barbarick, K.A. and Brobst, R., 2001. Biosolids applications affect runoff water quality following forest fire. Journal of Environmental Quality, 30(5), pp.1528-1532.

Morris, R., Smith, S.R., Bellett-Travers, D.M. and Bell, J.N.B., 2003, November. Reproducibility of the nitrogen response and residual fertiliser value of conventional and enhanced-treated biosolids. In Proceedings of the Joint CIWEM Aqua Enviro Technology Transfer 8th European Biosolids and Organic Residuals Conference (pp. 24-26).

Mulbry, W., Westhead, E.K., Pizarro, C. and Sikora, L., 2005. Recycling of manure nutrients: use of algal biomass from dairy manure treatment as a slow release fertilizer. Bioresource technology, 96(4), pp.451-458.

Omoike, A. and Chorover, J., 2006. Adsorption to goethite of extracellular polymeric substances from Bacillus subtilis. Geochimica et Cosmochimica Acta, 70(4), pp.827-838.

Pacific Northwest Extension 0511e: Worksheet for Calculating Biosolids Application Rates in Agriculture

Rigby, H., Clarke, B.O., Pritchard, D.L., Meehan, B., Beshah, F., Smith, S.R. and Porter, N.A., 2016. A critical review of nitrogen mineralization in biosolids-amended soil, the associated fertilizer value for crop production and potential for emissions to the environment. Science of the Total Environment, 541, pp.1310-1338.

Said-Pullicino, D., Kaiser, K., Guggenberger, G. and Gigliotti, G., 2007. Changes in the chemical composition of water-extractable organic matter during composting: Distribution between stable and labile organic matter pools. Chemosphere, 66(11), pp.2166-2176.

Smidt, E. and Meissl, K., 2007. The applicability of Fourier transform infrared (FT-IR) spectroscopy in waste management. Waste management, 27(2), pp.268-276.

Singh, R.P. and Agrawal, M., 2008. Potential benefits and risks of land application of sewage sludge. Waste management, 28(2), pp.347-358.

Sommers, L.E., Parker, C.F. and Meyers, G.J., 1981. Volatilization, plant uptake and mineralization of nitrogen in soils treated with sewage sludge. IWRRC Technical Reports. Paper 133.

Song, C., Li, M., Xi, B., Wei, Z., Zhao, Y., Jia, X., Qi, H. and Zhu, C., 2015. Characterization of dissolved organic matter extracted from the bio-oxidative phase of co-composting of biogas residues and livestock manure using spectroscopic techniques. International Biodeterioration & Biodegradation, 103, pp.38-50.

Sutton, R. and Sposito, G., 2005. Molecular structure in soil humic substances: the new view. Environmental science & technology, 39(23), pp. 9009-9015.

Stedmon, C.A., Markager, S. and Bro, R., 2003. Tracing dissolved organic matter in aquatic environments using a new approach to fluorescence spectroscopy. Marine Chemistry, 82(3-4), pp.239-254.

Tian, W., Li, L.Z., Liu, F., 2012. Assessment of the maturity and biological parameters of compost produced from dairy manure and rice chaff by excitation-emission matrix fluorescence spectroscopy. Bioresource Technology 110, 330-337.

Timko, S.A., Gonsior, M. and Cooper, W.J., 2015. Influence of pH on fluorescent dissolved organic matter photo-degradation. Water research, 85, pp.266-274.

EPA (Environmental Protection Agency), 1994. Land application of sewage sludge. A guide for land appliers on the requirements of the federal standards for the use of disposal of sewage sludge, 40 CFR Part 503.; https://www3.epa.gov/npdes/pubs/sludge.pdf (accessed June 3, 2018).

Wang, K., Li, W., Gong, X., Li, Y., Wu, C. and Ren, N., 2013. Spectral study of dissolved organic matter in biosolid during the composting process using inorganic bulking agent: UV–vis, GPC, FTIR and EEM. International Biodeterioration & Biodegradation, 85, pp.617-623.

Wang, X., Andrade, N., Shekarchi, J., Fischer, S.J., Torrents, A. and Ramirez, M., 2018. Full scale study of Class A biosolids produced by thermal hydrolysis pretreatment and anaerobic digestion. Waste Management, 78, pp.43-50.

Wang, H., Kimberley, M.O. and Schlegelmilch, M., 2003a. Biosolids-derived nitrogen mineralization and transformation in forest soils. Journal of environmental quality, 32(5), pp.1851-1856.

Wang, W.J., Smith, C.J. and Chen, D., 2003b. Towards a standardised procedure for determining the potentially mineralisable nitrogen of soil. Biology and Fertility of Soils, 37(6), pp.362-374.

Wei, Z., Wang, X., Zhao, X., Xi, B., Wei, Y., Zhang, X. and Zhao, Y., 2016. Fluorescence characteristics of molecular weight fractions of dissolved organic matter derived from composts. International Biodeterioration & Biodegradation, 113, pp.187-194.

Wilson, C.A. and Novak, J.T., 2009. Hydrolysis of macromolecular components of primary and secondary wastewater sludge by thermal hydrolytic pretreatment. Water research, 43(18), pp.4489-4498.

Xue, Y., Liu, H., Chen, S., Dichtl, N., Dai, X. and Li, N., 2015. Effects of thermal hydrolysis on organic matter solubilization and anaerobic digestion of high solid sludge. Chemical Engineering Journal, 264, pp.174-180.

Zarabi, M. and Jalali, M., 2013. Nitrogen mineralization in two calcareous soils treated with raw organic amendments. Clean Technologies and Environmental Policy, 15(2), pp.317-331.

Zhang, X., Zhao, Y., Zhu, L., Cui, H., Jia, L., Xie, X., Li, J. and Wei, Z., 2017. Assessing the use of composts from multiple sources based on the characteristics of carbon mineralization in soil. Waste management, 70, pp.30-36.

Zepp, R.G., Sheldon, W.M. and Moran, M.A., 2004. Dissolved organic fluorophores in southeastern US coastal waters: correction method for eliminating Rayleigh and Raman scattering peaks in excitation–emission matrices. Marine chemistry, 89(1-4), pp.15-36.

Zsolnay, A., 1996. Dissolved humus in soil waters. Humic substances in terrestrial ecosystems (pp. 171-223).

Chapter 3:

Baker, A. (2001). Fluorescence excitation emission matrix characterization of some sewage-
impacted rivers. Environ. Sci. Technol., 35(5), 948–953.

Baker, A., 2002. Fluorescence properties of some farm wastes: implications for water quality monitoring. Water Research, 36(1), pp.189-195.

Cabaniss, S. E., Zhou, Q., Maurice, P. A., Chin, Y. P., & Aiken, G. R. (2000). A log-normal distribution model for the molecular weight of aquatic fulvic acids. Environmental Science & Technology, 34(6), 1103-1109.

Cawley, K.M., Butler, K.D., Aiken, G.R., Larsen, L.G., Huntington, T.G. and McKnight, D.M., 2012. Identifying fluorescent pulp mill effluent in the Gulf of Maine and its watershed. Marine pollution bulletin, 64(8), pp.1678-1687.

Chen, Z., Zhang, Y., Gao, Y., Boyd, S. A., Zhu, D., & Li, H. (2015). Influence of dissolved organic matter on tetracycline bioavailability to an antibiotic-resistant bacterium. Environmental science & technology, 49(18), 10903-10910.

Chen, W., Westerhoff, P., Leenheer, J. A., & Booksh, K. (2003). Fluorescence excitation− emission matrix regional integration to quantify spectra for dissolved organic matter. Environmental science & technology, 37(24), 5701-5710.

Chefetz, B., Mualem, T. and Ben-Ari, J., 2008. Sorption and mobility of pharmaceutical compounds in soil irrigated with reclaimed wastewater. Chemosphere, 73(8), pp.1335-1343.

Cory, R.M. and McKnight, D.M., 2005. Fluorescence spectroscopy reveals ubiquitous presence of oxidized and reduced quinones in dissolved organic matter. Environmental science & technology, 39(21), pp.8142-8149.

Delgado-Moreno, L., Wu, L. and Gan, J., 2010. Effect of dissolved organic carbon on sorption of pyrethroids to sediments. Environmental science & technology, 44(22), pp.8473-8478.

Del Vecchio, R. and Blough, N.V., 2004. On the origin of the optical properties of humic substances. Environmental Science & Technology, 38(14), pp.3885-3891.

El Fels, L., Zamama, M., El Asli, A. and Hafidi, M., 2014. Assessment of biotransformation of organic matter during co-composting of sewage sludge-lignocelullosic waste by chemical, FTIR analyses, and phytotoxicity tests. International Biodeterioration & Biodegradation, 87, pp.128-137.

Gabor, R.S., Baker, A., McKnight, D.M. and Miller, M.P., 2014. Fluorescence indices and their interpretation. Aquatic Organic Matter Fluorescence, 303.

Gabor, R.S., Burns, M.A., Lee, R.H., Elg, J.B., Kemper, C.J., Barnard, H.R. and McKnight, D.M., 2015. Influence of leaching solution and catchment location on the fluorescence of water-soluble organic matter. Environmental science & technology, 49(7), pp.4425-4432.

Garcia, R.D., Diéguez, M.D.C., Gerea, M., Garcia, P.E. and Reissig, M., 2018. Characterisation and reactivity continuum of dissolved organic matter in forested headwater catchments of Andean Patagonia. Freshwater Biology, 63(9), pp.1049-1062.

Fischer, S., McCarty, G., Ramirez, M., and Torrents, A. (2019) Dissolved Organic Matter (DOM) Profiles and Nutrient Mineralization Rates of Anaerobically Digested Biosolids with variable pre-treatments (Manuscript – In Review).

Gendebien, A. et al. 2008 Environmental, economic and social impacts of the use of sewage sludge on land, Part I: Overview Report. Report prepared by Milieu Ltd, WRc and RPA for the European Commission, DG Environment under Study Contract DG ENV.G.4/ETU/2008/0076r.
http://ec.europa.eu/environment/archives/waste/sludge/pdf/part_i_report.pdf

Hambly, A.C., Arvin, E., Pedersen, L.F., Pedersen, P.B., Seredyńska-Sobecka, B. and Stedmon, C.A., 2015. Characterising organic matter in recirculating aquaculture systems with fluorescence EEM spectroscopy. Water research, 83, pp.112-120.

He, X.S., Xi, B.D., Li, X., Pan, H.W., An, D., Bai, S.G., Li, D. and Cui, D.Y., 2013. Fluorescence excitation–emission matrix spectra coupled with parallel factor and regional integration analysis to characterize organic matter humification. Chemosphere, 93(9), pp.2208-2215.
He, W. and Hur, J., 2015. Conservative behavior of fluorescence EEM-PARAFAC components in resin fractionation processes and its applicability for characterizing dissolved organic matter. Water research, 83, pp.217-226.

Hebting, Y., Adam, P. and Albrecht, P., 2003. Reductive desulfurization of allylic thiols by HS-/H2S in water gives clue to chemical reactions widespread in natural environments. Organic letters, 5(9), pp.1571-1574.

Henderson, R.K., Baker, A., Murphy, K.R., Hambly, A., Stuetz, R.M. and Khan, S.J., 2009. Fluorescence as a potential monitoring tool for recycled water systems: a review. Water research, 43(4), pp.863-881.

Hernandez-Ruiz, S., Abrell, L., Wickramasekara, S., Chefetz, B. and Chorover, J., 2012. Quantifying PPCP interaction with dissolved organic matter in aqueous solution: combined use of fluorescence quenching and tandem mass spectrometry. water research, 46(4), pp.943-954.

Helms, J. R.; Stubbins, A.; Ritchie, J. D.; Minor, E. C.; Kieber, D. J.; Mopper, K. Absorption spectral slopes and slope ratios as indicators of molecular weight, source, and photobleaching of chromophoric dissolved organic matter. Limnol. Oceanogr. 2008, 53 (3), 955−969.

Hudson, N., Baker, A. and Reynolds, D., 2007. Fluorescence analysis of dissolved organic matter in natural, waste and polluted waters—a review. River Research and Applications, 23(6), pp.631-649.

Hudson et al 2009 (Gabor et al. 2007)

Huguet, A., Vacher, L., Relexans, S., Saubusse, S., Froidefond, J.M. and Parlanti, E., 2009. Properties of fluorescent dissolved organic matter in the Gironde Estuary. Organic Geochemistry, 40(6), pp.706-719.

Hunt, J.F. and Ohno, T., 2007. Characterization of fresh and decomposed dissolved organic matter using excitation− emission matrix fluorescence spectroscopy and multiway analysis. Journal of Agricultural and Food Chemistry, 55(6), pp.2121-2128.

Kalbitz, K. and Wennrich, R., 1998. Mobilization of heavy metals and arsenic in polluted wetland soils and its dependence on dissolved organic matter. Science of the Total Environment, 209(1), pp.27-39.

Kleber, M. and Lehmann, J., 2019. Humic substances extracted by alkali are invalid proxies for the dynamics and functions of organic matter in terrestrial and aquatic ecosystems. Journal of Environmental Quality, 48(2), pp.207-216.

Kowalczuk, P., Durako, M.J., Young, H., Kahn, A.E., Cooper, W.J. and Gonsior, M., 2009. Characterization of dissolved organic matter fluorescence in the South Atlantic Bight with use of PARAFAC model: interannual variability. Marine Chemistry, 113(3-4), pp.182-196.

Korak, J.A., Dotson, A.D., Summers, R.S. and Rosario-Ortiz, F.L., 2014. Critical analysis of commonly used fluorescence metrics to characterize dissolved organic matter. Water research, 49, pp.327-338.

Lagae, H.J., Langemeier, M., Lybecker, D. and Barbarick, K., 2009. Economic value of biosolids in a semiarid agroecosystem. Agronomy journal, 101(4), pp.933-939.

Luo, K., Yang, Q., Li, X.M., Chen, H.B., Liu, X., Yang, G.J. and Zeng, G.M., 2013. Novel insights into enzymatic-enhanced anaerobic digestion of waste activated sludge by three-dimensional excitation and emission matrix fluorescence spectroscopy. Chemosphere, 91(5), pp.579-585.

Lu, Q., He, Z.L. and Stoffella, P.J., 2012. Land application of biosolids in the USA: a review. Applied and Environmental Soil Science, 2012.

Maie, N., Scully, N.M., Pisani, O. and Jaffé, R., 2007. Composition of a protein-like fluorophore of dissolved organic matter in coastal wetland and estuarine ecosystems. Water Research, 41(3), pp.563-570.

Mangalgiri, K., Timko, S., Gonsior, M., and Blaney, L. "PARAFAC modeling of irradiation-and oxidation-induced changes in fluorescent dissolved organic matter extracted from poultry litter." Environmental Science & Technology 51, no. 14 (2017): 8036-8047.

McAdams, B.C., Aiken, G.R., McKnight, D.M., Arnold, W.A. and Chin, Y.P., 2017. High Pressure Size Exclusion Chromatography (HPSEC) Determination of Dissolved Organic Matter Molecular Weight Revisited: Accounting for Changes in Stationary Phases, Analytical Standards, and Isolation Methods. Environmental science & technology, 52(2), pp.722-730.

McKnight, D.M., Boyer, E.W., Westerhoff, P.K., Doran, P.T., Kulbe, T. and Andersen, D.T., 2001. Spectrofluorometric characterization of dissolved organic matter for indication of precursor organic material and aromaticity. Limnology and Oceanography, 46(1), pp.38-48.

Minor, E.C., Swenson, M.M., Mattson, B.M. and Oyler, A.R., 2014. Structural characterization of dissolved organic matter: a review of current techniques for isolation and analysis. Environmental Science: Processes & Impacts, 16(9), pp.2064-2079.

Mostofa, K.M., Jie, Y., Sakugawa, H. and Liu, C.Q., 2018. Equal Treatment of Different EEM Data on PARAFAC Modeling Produces Artifact Fluorescent Components That Have Misleading Biogeochemical Consequences.

Murphy, K.R., Hambly, A., Singh, S., Henderson, R.K., Baker, A., Stuetz, R. and Khan, S.J., 2011. Organic matter fluorescence in municipal water recycling schemes: toward a unified PARAFAC model. Environmental Science & Technology, 45(7), pp.2909-2916.

Murphy, K.R., Stedmon, C.A., Graeber, D. and Bro, R., 2013. Fluorescence spectroscopy and multi-way techniques. PARAFAC. Analytical Methods, 5(23), pp.6557-6566.

Murphy, K. R.; Bro, R.; Stedmon, C. A., 2014. Chemometric analysis of organic matter fluorescence. In Aquatic Organic Matter Fluorescence; Coble, P., Baker, A., Lead, J., Reynolds, D., Spencer, R., Eds.; Cambridge University Press: New York; pp 339−375.

Murphy, K.R., Stedmon, C.A., Wenig, P. and Bro, R., 2014. OpenFluor–an online spectral library of auto-fluorescence by organic compounds in the environment. Analytical Methods, 6(3), pp.658-661.

Navon, R., Hernandez-Ruiz, S., Chorover, J. and Chefetz, B., 2011. Interactions of carbamazepine in soil: effects of dissolved organic matter. Journal of environmental quality, 40(3), pp.942-948.

Nimptsch, J., Woelfl, S., Osorio, S., Valenzuela, J., Ebersbach, P., von Tuempling, W., Palma, R., Encina, F., Figueroa, D., Kamjunke, N. and Graeber, D., 2015. Tracing dissolved organic matter (DOM) from land-based aquaculture systems in North Patagonian streams. Science of the Total Environment, 537, pp.129-138.

NEBRA: North East Biosolids and Residuals Association, 2007. A National Biosolids Regulation, Quality, End Use and Disposal Survey, Tamworth, New Hampshire

NSW EPA, 1997. Environmental Guidelines: Use and Disposal of Biosolids Products. New South Wales Environment Protection Authority, Sydney, Australia.

Ohno, T. (2002). Fluorescence inner-filtering correction for determining the humification index of dissolved organic matter. Environmental science & technology, 36(4), 742-746.

Olk, D.C., Bloom, P.R., Perdue, E.M., McKnight, D.M., Chen, Y., Farenhorst, A., Senesi, N., Chin, Y.P., Schmitt-Kopplin, P., Hertkorn, N. and Harir, M., 2019. Environmental and agricultural relevance of humic fractions extracted by alkali from soils and natural waters. Journal of Environmental Quality, 48(2), pp.217-232.

Omoike, A., Chorover, J., Kwon, K. D., & Kubicki, J. D. (2004). Adhesion of bacterial exopolymers to α-FeOOH: Inner-sphere complexation of phosphodiester groups. Langmuir, 20(25), 11108-11114.

Parlanti, E., Wörz, K., Geoffroy, L. and Lamotte, M., 2000. Dissolved organic matter fluorescence spectroscopy as a tool to estimate biological activity in a coastal zone submitted to anthropogenic inputs. Organic geochemistry, 31(12), pp.1765-1781.

Peuravuori, J., Bursáková, P., & Pihlaja, K. (2007). ESI-MS analyses of lake dissolved organic matter in light of supramolecular assembly. Analytical and bioanalytical chemistry, 389(5), 1559-1568.

Piccolo, A., 2002. The supramolecular structure of humic substances: a novel understanding of humus chemistry and implications in soil science.

Rosario-Ortiz, F.L. and Korak, J.A., 2016. Oversimplification of dissolved organic matter fluorescence analysis: potential pitfalls of current methods.

Stedmon, C.A., Markager, S. and Bro, R., 2003. Tracing dissolved organic matter in aquatic environments using a new approach to fluorescence spectroscopy. Marine Chemistry, 82(3-4), pp.239-254.

Sharpless, C.M. and Blough, N.V., 2014. The importance of charge-transfer interactions in determining chromophoric dissolved organic matter (CDOM) optical and photochemical properties. Environmental Science: Processes & Impacts, 16(4), pp.654-671.

Sutton, R., and Sposito, G. (2005). Molecular structure in soil humic substances: the new view. Environmental science & technology, 39(23), 9009-9015.

Tian, W., Li, L., Liu, F., Zhang, Z., Yu, G., Shen, Q. and Shen, B., 2012. Assessment of the maturity and biological parameters of compost produced from dairy manure and rice chaff by excitation–emission matrix fluorescence spectroscopy. Bioresource technology, 110, pp.330-337.

Zhou, J., Wang, J.J., Baudon, A. and Chow, A.T., 2013. Improved fluorescence excitation-emission matrix regional integration to quantify spectra for fluorescent dissolved organic matter. Journal of environmental quality, 42(3), pp.925-930.

US EPA, 1994. United States Environmental Protection Agency: Land application of sewage sludge. A guide for land appliers on the requirements of the federal standards for the use of disposal of sewage sludge, 40 CFR Part 503.; https://www3.epa.gov/npdes/pubs/sludge.pdf (accessed June 3, 2018).

Wang, K., Li, W., Gong, X., Li, Y., Wu, C. and Ren, N., 2013. Spectral study of dissolved organic matter in biosolid during the composting process using inorganic

bulking agent: UV–vis, GPC, FTIR and EEM. International Biodeterioration & Biodegradation, 85, pp.617-623.

Wang, B., Cai, C., Li, G. and Liu, H., 2017. Assessing the stability in dry mycelial fertilizer of Penicillium chrysogenum as soil amendment via fluorescence excitation-emission matrix spectra: organic matter's transformation and maturity. Environmental Science and Pollution Research, 24(36), pp.28258-28267

Wilson, C.A. and Novak, J.T., 2009. Hydrolysis of macromolecular components of primary and secondary wastewater sludge by thermal hydrolytic pretreatment. Water research, 43(18), pp.4489-4498.

Wünsch, U.J., Murphy, K.R. and Stedmon, C.A., 2017. The one-sample PARAFAC approach reveals molecular size distributions of fluorescent components in dissolved organic matter. Environmental science & technology, 51(20), pp.11900-11908.

Wünsch, U.J., Murphy, K.R. and Stedmon, C.A., 2015. Fluorescence quantum yields of natural organic matter and organic compounds: Implications for the fluorescence-based interpretation of organic matter composition. Frontiers in Marine Science, 2, p.98.

Yu, G.H., Luo, Y.H., Wu, M.J., Tang, Z., Liu, D.Y., Yang, X.M. and Shen, Q.R., 2010. PARAFAC modeling of fluorescence excitation− emission spectra for rapid assessment of compost maturity. Bioresource technology, 101(21), pp.8244-8251.

Zhang, J., Lv, B., Xing, M. and Yang, J., 2015. Tracking the composition and transformation of humic and fulvic acids during vermicomposting of sewage sludge by elemental analysis and fluorescence excitation–emission matrix. Waste management, 39, pp.111-118.

Zmora-Nahum, S., Markovitch, O., Tarchitzky, J. and Chen, Y., 2005. Dissolved organic carbon (DOC) as a parameter of compost maturity. Soil Biology and Biochemistry, 37(11), pp.2109-2116.

Zsolnay, A., Baigar, E., Jimenez, M., Steinweg, B. and Saccomandi, F., 1999. Differentiating with fluorescence spectroscopy the sources of dissolved organic matter in soils subjected to drying. Chemosphere, 38(1), pp.45-50.

Chapter 4:

Boyle, E.S., Guerriero, N., Thiallet, A., Vecchio, R.D. and Blough, N.V., 2009. Optical properties of humic substances and CDOM: relation to structure. Environmental science & technology, 43(7), pp.2262-2268.

Bright, D.A. and Healey, N., 2003. Contaminant risks from biosolids land application: contemporary organic contaminant levels in digested sewage sludge from five treatment

plants in Greater Vancouver, British Columbia. Environmental Pollution, 126(1), pp.39-49.

Chen, Z., Zhang, Y., Gao, Y., Boyd, S. A., Zhu, D., & Li, H. 2015. Influence of Dissolved Organic Matter on Tetracycline Bioavailability to an Antibiotic-Resistant Bacterium. Environmental science & technology, 49(18), 10903-10910.

Del Vecchio, R. and Blough, N.V., 2004. On the origin of the optical properties of humic substances. Environmental Science & Technology, 38(14), pp.3885-3891.

Gu, C., Karthikeyan, K. G., Sibley, S. D., & Pedersen, J. A. 2007. Complexation of the antibiotic tetracycline with humic acid. Chemosphere, 66(8), 1494-1501.

Hsieh, C.Y., Tsai, M.H., Ryan, D.K. and Pancorbo, O.C., 2004. Toxicity of the 13 priority pollutant metals to Vibrio fisheri in the Microtox® chronic toxicity test. Science of the total environment, 320(1), pp.37-50.

Holbrook, R.D., Breidenich, J. and DeRose, P.C., 2005. Impact of reclaimed water on select organic matter properties of a receiving stream fluorescence and perylene sorption behavior. Environmental science & technology, 39(17), pp.6453-6460.

Lakowicz, J.R. ed., 2013. Principles of fluorescence spectroscopy. Springer Science & Business Media.

Pan, B., Liu, Y., Xiao, D., Wu, F., Wu, M., Zhang, D. and Xing, B., 2012. Quantitative identification of dynamic and static quenching of ofloxacin by dissolved organic matter using temperature-dependent kinetic approach. Environmental pollution, 161, pp.192-198.

Wang, H.B. and Zhang, Y.J., 2014. Mechanisms of interaction between polycyclic aromatic hydrocarbons and dissolved organic matters. Journal of Environmental Science and Health, Part A, 49(1), pp.78-84.

Wang, Z., Cao, J. and Meng, F., 2015. Interactions between protein-like and humic-like components in dissolved organic matter revealed by fluorescence quenching. Water Research, 68, pp.404-413.

Wang, L., Li, H., Yang, Y., Zhang, D., Wu, M., Pan, B. and Xing, B., 2017. Identifying structural characteristics of humic acid to static and dynamic fluorescence quenching of phenanthrene, 9-phenanthrol, and naphthalene. Water research, 122, pp.337-344.

Villa, S., Vighi, M. and Finizio, A., 2014. Experimental and predicted acute toxicity of antibacterial compounds and their mixtures using the luminescent bacterium Vibrio fischeri. Chemosphere, 108, pp.239-244.

Wei-Haas, M.L., Hageman, K.J. and Chin, Y.P., 2014. Partitioning of polybrominated diphenyl ethers to dissolved organic matter isolated from arctic surface waters. Environmental science & technology, 48(9), pp.4852-4859.

Chapter 5:

Adrian, L., Rahnenführer, J., Gobom, J., & Hölscher, T. (2007). Identification of a chlorobenzene reductive dehalogenase in Dehalococcoides sp. strain CBDB1. Applied and environmental microbiology, 73(23), 7717-7724.

Andrade, N. A., McConnell, L. L., Torrents, A., & Ramirez, M. (2010). Persistence of Polybrominated Diphenyl Ethers in Agricultural Soils after Biosolids Applications. Journal of Agricultural and Food Chemistry, 58(5), 3077–3084.

Azzouz, A., & Ballesteros, E. (2012). Combined microwave-assisted extraction and continuous solid-phase extraction prior to gas chromatography–mass spectrometry determination of pharmaceuticals, personal care products and hormones in soils, sediments and sludge. Science of the Total Environment, 419, 208-215.

Aydin, S. (2016). Enhancement of microbial diversity and methane yield by bacterial bioaugmentation through the anaerobic digestion of Haematococcus pluvialis. Applied Microbiology and Biotechnology, 1-7.

Bo, Z, Wei-min, C.A.I. and Pin-jing, H.E. (2007). Influence of lactic acid on the two-phase anaerobic digestion of kitchen wastes. Journal of Environmental Sciences, 19(2), pp.244-249.

Brausch, J. M., & Rand, G. M. (2011). A review of personal care products in the aquatic environment: environmental concentrations and toxicity. Chemosphere, 82(11), 41518-1532.

Carey, Daniel E., Daniel H. Zitomer, Krassimira R. Hristova, Anthony D. Kappell, and Patrick J. Mcnamara (2016). Triclocarban Influences Antibiotic Resistance and Alters Anaerobic Digester Microbial Community Structure. Environmental Science & Technology Environ. Sci. Technol. 50, no. 1: 126-34.

Chang HL, Alvarez-Cohen L (1995) Transformation capacities of chlorinated organics by mixed cultures enriched on methane, propane, toluene, or phenol. Biotech Bioeng 45:440–449.

Daughton, C.G., Ternes, T.A. (1999). Pharmaceuticals and personal care products in the environment: agents of subtle change? Environ. Health Perspect. 107 (Suppl. 6), 907–938

Duhamel M, Mo K, Edwards EA (2004) Characterization of a highly enriched Dehalococcoides-containing culture that grows on vinyl chloride and trichloroethene. Appl Environ Microbiol.;70:5538–5545.

EPA Pesticide Registrations (2010). https://archive.epa.gov/pesticides/reregistration/web/html/triclosan_fs.html

Fite A, Macfarlane GT, Cummings JH, et al (2004) Identification and quantitation of mucosal and faecel Desulfovibrios using real time polymerase chain reaction. Gut 53:523–529.

Fotidis, I. A., Karakashev, D., & Angelidaki, I. (2013). Bioaugmentation with an acetate-oxidising consortium as a tool to tackle ammonia inhibition of anaerobic digestion. Bioresource technology, 146, 57-62.

Fricker AD, LaRoe SL, Shea ME, Bedard DL (2014) Dehalococcoides mccartyi strain JNA dechlorinates multiple chlorinated phenols including pentachlorophenol and harbors at least 19 reductive dehalogenase homologous genes. Environ Sci Technol 48(24):14300–14308

Grostern, A., Duhamel, M., Dworatzek, S., & Edwards, E. A. (2010). Chloroform respiration to dichloromethane by a Dehalobacter population. Environmental microbiology, 12(4), 1053-1060.

Halden, R. U., & Paull, D. H. (2005). Co-occurrence of triclocarban and triclosan in US water resources. Environmental Science & Technology,39(6), 1420-1426.

He, J., Holmes, V. F., Lee, P. K., & Alvarez-Cohen, L. (2007). Influence of vitamin B12 and cocultures on the growth of Dehalococcoides isolates in defined medium. Applied and environmental microbiology, 73(9), 2847-2853.

Keymer, P., Ruffell, I., Pratt, S., & Lant, P. (2013). High pressure thermal hydrolysis as pre-treatment to increase the methane yield during anaerobic digestion of microalgae. Bioresource technology, 131, 128-133.
Kjellerup, B.V., Sun, X., Ghosh, U., May, H.D. and Sowers, K.R., 2008. Site-specific microbial communities in three PCB-impacted sediments are associated with different in situ dechlorinating activities. Environmental Microbiology, 10(5), pp.1296-1309.

Krzmarzick, M. and Novak, P. (2014) Removal of chlorinated organic compounds during wastewater treatment: achievements and limits. Applied microbiology and biotechnology 98, no. 14 6233-6242.

Löffler, F. E., Yan, J., Ritalahti, K. M., Adrian, L., Edwards, E. A., Konstantinidis, K. T., ... & Spormann, A. M. (2012 & 2013). Dehalococcoides mccartyi gen. nov., sp. nov., obligately organohalide-respiring anaerobic bacteria relevant to halogen cycling and bioremediation, belong to a novel bacterial class, Dehalococcoidia classis nov., order

Dehalococcoidales ord. nov. and family Dehalococcoidaceae fam. nov., within the phylum Chloroflexi. International journal of systematic and evolutionary microbiology, 63(2), 625-635.

Lozano, N., Rice, C. P., Ramirez, M., & Torrents, A. (2010). Fate of triclosan in agricultural soils after biosolid applications. Chemosphere, 78(6), 760–766.

McMurdie, P. J., Behrens, S. F., Müller, J. A., Göke, J., Ritalahti, K. M., Wagner, R., ... & Spormann, A. M. (2009). Localized plasticity in the streamlined genomes of vinyl chloride respiring Dehalococcoides. PLoS Genet, 5(11), 1-13.

McClellan, K., & Halden, R. U. (2010). Pharmaceuticals and personal care products in archived US biosolids from the 2001 EPA national sewage sludge survey. Water research, 44(2), 658-668.

McNamara, Patrick J., and Mark J. Krzmarzick (2013). Triclosan Enriches for Dehalococcoides -like Chloroflexi in Anaerobic Soil at Environmentally Relevant Concentrations.FEMS Microbiol Lett FEMS Microbiology Letters 344, no. 1 48-52

Miller, Todd R., Jochen Heidler, Steven N. Chillrud, Amelia Delaquil, Jerry C. Ritchie, Jana N. Mihalic, Richard Bopp, and Rolf U. Halden (2008). Fate of Triclosan and Evidence for Reductive Dechlorination of Triclocarban in Estuarine Sediments." Environmental Science & Technology Environ. Sci. Technol. 42, no. 12, 4570-576.

Narumiya, M.; Nakada, N.; Yamashita, N.; Tanaka, H. Phase distribution and removal of pharmaceuticals and personal care products during anaerobic sludge digestion. J. Hazard. Mater. 2013, 260, 305−312.

Ogunyoku, Temitope A., and Thomas M. Young. "Removal of Triclocarban and Triclosan during Municipal Biosolid Production." *Water Environment Research Water Environ Res* 86, no. 3 (2014): 197-203.

Pycke BFG, Roll IB, Brownawell BJ (2014). Transformation products and human metabolites of triclocarban and triclosan in sewage sludge across the United States. Environ Science and Technol.48:7881–7890.

Schaefer, C. E., Condee, C. W., Vainberg, S., & Steffan, R. J. (2009). Bioaugmentation for chlorinated ethenes using Dehalococcoides sp.: Comparison between batch and column experiments. Chemosphere, 75(2), 141-148.

Schaefer, C.E., D. R. Lippincott, and R. J. Steffan. (2010). Field-scale evaluation of bioaugmentation dosage for treating Chlorinatedethenes. Ground Water Monitoring Remediation. 30:113-124.

Schauer-Gimenez, A. E., Zitomer, D. H., Maki, J. S., & Struble, C. A. (2010). Bioaugmentation for improved recovery of anaerobic digesters after toxicant exposure. Water research, 44(12), 3555-3564.

Seshadri, R., Adrian, L., Fouts, D. E., Eisen, J. A., Phillippy, A. M., Methe, B. A., ... & Kolonay, J. F. (2005). Genome sequence of the PCE-dechlorinating bacterium Dehalococcoides ethenogenes. Science, 307(5706), 105-108.

Shelton D. and Tiedje J. (1984) General method for determining anaerobic biodegradation potential. Appl Environ Microbiology 47:850–85

Singer, H., Muller, S., Tixier, C., Pillonel, L., 2002. Triclosan: occurrence and fate of a widely used biocide in the aquatic environment: field measurements in wastewater treatment plants, surface waters, and lake sediments. Environ.Sci. Technol. 36, 4998–5004.

Smith, B. J., Boothe, M. A., Fiddler, B. A., Lozano, T. M., Rahi, R. K., & Krzmarzick, M. J. (2015). Enumeration of Organohalide Respirers in Municipal Wastewater Anaerobic Digesters. Microbiology insights, 8(Suppl 2), 9.

Smits THM, Devenoges C, Szynalski K, Maillard J, Holliger C. (2004) Development of a real-time PCR method for quantification of the three genera Dehalobacter, Dehalococcoides, and Desulfitobacterium in microbial communities. J Microbiology Methods, 57:369–378.

Steffan, R. J., & Sewell, G. W. (2012). Advances in Bioremediation of Aquifers. In Clean Soil and Safe Water (pp. 143-151). Springer Netherlands.

Tale, V. P., Maki, J. S., Struble, C. A., & Zitomer, D. H. (2011). Methanogen community structure-activity relationship and bioaugmentation of overloaded anaerobic digesters. Water research, 45(16), 5249-5256.

Tran NH,Urase T, Ngo HH, Hu JY, Ong SL (2013) Insight intometabolic and cometabolic activities of autotrophic and heterotrophic microorganisms in the biodegradation of emerging trace organic contaminants. Biores Technol 146:721–731

Veldhoen, N., Skirrow, R.C., Osachoff, H., Wigmore, H., Clapson, D.J., Gunderson, M.P., Van Aggelen, G. and Helbing, C.C. (2006). The bactericidal agent triclosan modulates thyroid hormone-associated gene expression and disrupts postembryonic anuran development. Aquatic toxicology, 80(3), pp.217-227.

Vainberg, S., Condee, C. W., & Steffan, R. J. (2009). Large-scale production of bacterial consortia for remediation of chlorinated solvent-contaminated groundwater. Journal of industrial microbiology & biotechnology, 36(9), 1189-1197.

Wang, S., Chng, K. R., Wilm, A., Zhao, S., Yang, K. L., Nagarajan, N., & He, J. (2014). Genomic characterization of three unique Dehalococcoides that respire on persistent polychlorinated biphenyls. Proceedings of the National Academy of Sciences, 111(33), 12103-12108.

Wang, Shanquan, Kern Rei Chng, Chen Chen, Donna L. Bedard, and Jianzhong He. (2015). Genomic Characterization of Dehalococcoides mccartyi Strain JNA That Reductively Dechlorinates Tetrachloroethene and Polychlorinated Biphenyls." Environmental science & technology 49, no. 24. 14319-14325.

Yan, J., Ritalahti, K. M., Wagner, D. D., & Löffler, F. E. (2012). Unexpected specificity of interspecies cobamide transfer from Geobacter spp. to organohalide-respiring Dehalococcoides mccartyi strains. Applied and environmental microbiology, 78(18), 6630-6636.

Zhao, J. L., Ying, G. G., Liu, Y. S., Chen, F., Yang, J. F., & Wang, L. (2010). Occurrence and risks of triclosan and triclocarban in the Pearl River system, South China: from source to the receiving environment. Journal of Hazardous Materials, 179(1), 215-222.

Zorrilla, L. M., Gibson, E. K., Jeffay, S. C., Crofton, K. M., Setzer, W. R., Cooper, R. L., & Stoker, T. E. (2009). The effects of triclosan on puberty and thyroid hormones in male Wistar rats. *Toxicological Sciences*, *107*(1), 56-64.